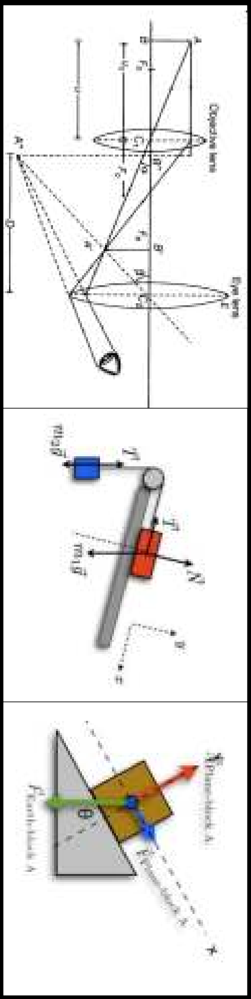

KADA
Journal of Physics

Vol. 2 (1)   August, 2018   ISSN: 2579-1168

**A Publication of
Department of Physics,
Faculty of Science,
Kaduna State University, Kaduna.**

KADA JOURNAL OF PHYSICS

Vol. 2 (1)   August, 2018   ISSN: 2579-1168

August, 2018

All rights reserved: No part of this publication may be reproduced
or transmitted in any way or form by any means without the
permission and express acknowledgment of the source.

Published By
DEPARTMENT OF PHYSICS, FACULTY OF SCIENCE,
KADUNA STATE UNIVERSITY,
P. M. B 2339, KADUNA - NIGERIA.
Email: kadajournphys@gmail.com
kadajournphys@kasu.edu.ng

DEPARTMENT OF PHYSICS,
FACULTY OF SCIENCE,
KADUNA STATE UNIVERSITY, KADUNA - NIGERIA

Editor-in-Chief
H. O. Aboh, Ph.D, FNIP

Deputy Editor
M. S Abubakar, Ph.D, FNIP

Journal Editorial Committee
Dr. M. D. Dogara, MNIP
Dr. P. M. Gyuk, MNIP
Dr. S. G. Abdu, MNIP

Business Editor
Mr. Jerry Aba

Editorial Board Members
Prof B. J. Kwaha, FNIP
Department of Physics,
University of Jos.
Prof S. B. Elegba, FNIP
Department of Physics,
University of Abuja.
Prof K. M. Lawal, MNIP
Department of Physics,
Ahmadu Bello University, Zaria.
Prof I. Okunade, MNIP
Centre for Energy Research and Training,
Ahmadu Bello University, Zaria.
Prof G. Babaji, MNIP
Department of Physics,
Bayero University Kano
Dr. A. Mayere
University of Nottingham,
University Park, Nottingham,
United Kingdom.

Introduction:

Kada Journal of Physics (KJP) is published bi-annually by the Department of Physics, Kaduna State University, Nigeria. The KJP is a peer-review on-line international journal which is aimed at fast but standard publication of cutting edge research in all areas of physics and their applications.

AUTHOR'S GUIDELINE

Authors are expected to adhere to the following while submitting their manuscripts for assessment for possible publication in the Kada Journal of Physics.

FORMAT

All headings are flush left. The beginning of every paragraph must flush to the left margin. All paragraphs must be blocked and separated with an extra line space between them. All pages must be numbered.

ARRANGEMENTS

The contents of the articles must be presented in the following sequence: Title Names(s) of author(s), Abstract, Keywords, Introduction, Materials and Methods, Results, Discussions, Acknowledgments, and References.

TITLE

This should be on a separate page and contain the name(s) of the author(s), their addresses and e-mail addresses. In case of more than one author, indicate who correspondences should be addressed to. The title of the paper should, if possible, be short, but must contain enough information to reflect what is contained in the text.

ABSTRACT

This should be in on the same page with the title of the work. The abstract should convey the essential account concisely, in not more than 200 words all in one paragraph.

INTRODUCTION

It is the background information and therefore should include the theory behind the work. The goals of the research or hypothesis explaining clearly what you are investigating and why you choose to investigate it should be comprehensively addressed. The introduction should be motivation for the work.

MATERIALS AND METHODS

Procedures and materials used should be described in sufficient detail to allow repetition of the work. Protocols already described elsewhere can be quoted.

RESULTS

Describe the data generated from the experiments using statements, tables and figures. Any data already presented in a table should not be repeated in a figure and vice versa. Also results described in the text must not be repeated in tables and figures again. Present the statistics you calculated, the sample size for the statistical test, and the P-value for the statistics. All tables and figures must be numbered in the order in which they are cited in the text.

DISCUSSIONS

Discuss and refer to the results obtained in the experiments and link the results to your original goal or idea. Compare the results obtained to other published studies. Since the objective is to make a contribution to the literature on this particular topic, you are expected to relate your work to the studies already done in this field. If your results are not what you expected, try to explain why they differ.

ACKNOWLEDGMENT

Where applicable, acknowledgment(s) should be concise.

CITATION OF REFERENCES IN THE TEXT

References by different authors should be arranged chronologically, e.g. (Ado 1965; James 1973; Kelvin 1977). No comma between name and year. References from the same year should be listed alphabetically, e.g. (Ali 1966; Chukwu 1966; Jude 1966) without comma between name and year. When the name of the author and the year of publication do not form part of a sentence, they should be written in parentheses and separated only by a single space without comma, e.g. (Gambo 1931). However, an author's name, and sometimes the year of publication, may form part of a sentence as follows: "Gambo (1931) showed that..." or "In 1931 Gambo published this report..." . In the case of two authors the two names should be linked by an ampersand

(&)., E.g. Hassan & Umma (2005). For more than two authors, quote only the name of the first author followed by et al., Typed in italics, e.g. (Aboh, Smith & James (1931) become (Aboh et al. 1931). The quotation of multiple papers published by one author in the same year should be distinguished by the suffixes a, b, c, etc., inserted after the year of publication. For a series of papers, their arrangements should obey ascendant chronological order with each paper separated from the next by a semicolon (Garba 2005; Daniel 2006). If the papers are published the same year, use alphabetical orders (e.g. Daniel 2006; Garba 2006; Haruna 2006). Quotation of papers that are still in the press should be done only for those papers that have actually gone to the press by inserting the words "in press" in the text instead of the year of publication. When an unseen paper is being quoted from another publication, only the latter should be included in the reference list. The example only Garba (2000) would be included in the reference list. Authors must check to ensure accuracy that all references mentions in the text are listed at the end of the paper and vice versa.

LISTING REFERENCES AT THE END OF THE PAPER

References must be listed out according to the Harvard reference method. When one author has several publications they must be listed out chronologically. When two or more papers have the same author and published in the same year, the letters a, b, c, should be added after the year. When the publication carries the name of an editor and not the author of the article, insert "(Eds.)" between the name and the date of publication. If there is more than one editor, use the abbreviation "(Eds)". When the reference includes both authors and editors, insert the phrase "edited by" after the title of the book. The title of a journal must be given in full and italicized, using Arabic numerals to indicate the volume number, e.g. Geophysics, 7:4-32. When the reference consists of a single page only, just insert a colon before the page number. Papers that are still in press should carry the word "in press" after the name of the journal, the correct volume and page numbers. Titles of books must be italicized. Use the abbreviation "ed." for edition and only an Arabic numeral to indicate the volume(s) cited. No page numbers are given for books, e.g. Godwin, A.S. 2006. Concepts in Physics, 3rd ed. 1. London; Churchill. When it is only the abstract of an article that had been seen, indicate this as follows: Jonah, T. N. 2005. Rural water development in Nigeria. Nigerian Journal of Physics, 2:200-210. Articles and book chapters should be written as follows: King, O. D. 1963. Briqquette making in: Small scale business, edited by F. Smith & B. Timothy. Kaduna: Nura, B.A. 2003. Groundwater contamination of Narayi village. Proceedings of the 30th Summit of Science Association of Nigeria, Abuja, Nigeria 2013: 423-459. Individual articles from Annual Reports should be listed as follows: Esther, S A. A. 2003. Radiation Report of the Nigeria Nuclear Regulatory Agency, Nigeria, for 1999:62. Publications without the name of the author or editor should carry the name of the organization issuing the work, e.g. NNRA 1999. NNRA Year book for 1999. Unpublished theses and dissertations should be listed as follows: Halima, T. H. 2016. Solar Radiation Effects in Kachia town, Nigeria. B.Sc. Thesis, Kaduna State University, Kaduna 45 pp. Note that the title of an unpublished work is not italicized. For citations of journals from the web, follow the example below: Abu, M.S. 2005. A new method of digitization. Science World Journal [on line] 32-40. Available in http://www.scienceworldjournal.com (date and time retrieved).

For articles accessed in the net authors and the date of publication, use the example below: Solar flux over the Equatorial Axis. Retrieved 2nd January, 2016 from www.cc.geosci.edu

Other relevant information

TABLES

Each table must be typed using table menu for easy retrieval and editing. It should contain a brief heading with enough information to enable the reader to understand the table without consulting the text. The approximate positions of all tables must be indicated in the main text. Duplication in the text of information given in the tables must be avoided. They are to be numbered with Roman numerals.

FIGURES

Illustrations are referred to as figures (abbreviated as "Fig."). The approximate position of all figures must be indicated in the main text. Repetition in the text of information given in the figures must be avoided. They are to be numbered with Arabic numerals. Authors are encouraged to supply the original spreadsheet data used to produce the graph to enable us maintain a uniform look for all graphs in the journal.

PHOTOGRAPHS AND DIAGRAMS

Production of colour figures are free. They should be saved in JPEG format

PAGE CHARGES

Twenty Thousand Nigerian Naira (N20, 000:00) or US $100.00 will be charged per article after the paper might have been accepted for publication, while Five thousand naira (N5,000.00) will be charged for Assessment fee.

Manuscripts that do not comply with the editorial requirements will be returned for amendment before they are considered by the Editorial Committee.

BANKER:

FCMB

Kada Journal of Physics
Acct. No. 4358627011

FONT SIZE:

All test must be in Times Roman with Text Size of 10 and Numbers of pages must not exceed 15 pages per article.

All Correspondence to:

H.O. Aboh, Ph.D, FNIP
Editor-in-Chief
Department of Physics, Kaduna State University, P.M.B. 2339, Kaduna, Kaduna State, Nigeria.
✉ : kadajournphys@gmail.com
copy: kadajournphys@kasu.edu.ng
☎: +234 813 612 4134, +234 802 334 8334

X-RAY FLUORESCENT SPECTROMETRY ANALYSIS TO DETERMINE THE CHEMICAL COMPOSITION OF SOME ROCK SAMPLES FROM RIMA AND BUGAI MINING SITES AT BIRNIN GWARI AREA OF KADUNA STATE NIGERIA.

Namadi, A. Z, Aboh, H. O, and Dogara, M. D
Department of Physics, Kaduna State University, Kaduna.
e-mail: abdoulnamady336@gmail.com

ABSTRACT

An elemental analysis research work was carried out Using X-ray Fluorescent Spectrometer to determine the chemical composition of Rock samples collected from Rima and Bugai mining sites which are located 10 and 16km away from Birnin Gwari town in Birnin Gwari Local Government area of Kaduna State, Nigeria respectively. The analysis was carried out to detect the presence of elements and their composition. At the first mining site Rima. 26 elements were found, which are Si, Al, S, Na, Ca, Ti, Cr, Mn, Fe, N, Cu, As, Se, Ba, V, Ru, Eu, Pb, Os, Pr, Hg, Au, Ge, Tl, Bi and Ag. At the second mining site (BUGAI) 37 elements were found, which are Si, Al, S, Yb, Ca, Ti, Sr, Mn, Fe, Ni, Cu, As, Se, Ba, V, Cr, Ge, Pr, Sm, Ru, Eu, Zn, Pb, Os, Y, Ir, Hg, Tl, In, Zr, Au, Ce, Ga, Sb, Bi and Ag respectively. The elements with their quantities found from the analysis were tabulated.

Introduction

The chemical compositions of rocks are used to solve numerous geological problems, including crystallization history of igneous bodies such as granite or basalt, processes of formation of the sea floor, nature of chemical weathering in various climates, stratigraphic correlation of sedimentary and volcanic rocks, processes of ore generation, and many others. Most rocks are composed primarily of silicate minerals, and over 90% of the composition of most silicate rocks can be characterized by oxides of Si, Ti, Al, Fe, Mg, Ca, Na and K. Minor and trace elements present in rocks include practically every other element, many of which are especially useful for geochemical modeling of geological processes (Timothy 1989).

X-ray fluorescence spectrometry (XRF) is the technique of choice of most petrologists and geochemists to obtain rock analyses. The XRF analytical technique is far superior to older wet-chemical or atomic absorption because it is rapid and does not require extensive training or experience on the part of the analyst (Timothy 1989).

Study Area

The study area is at Rima and Bugai Villages which are 10 and 16km away from Birnin Gwari town in Birnin Gwari local government area of Kaduna state, in the North-western geological zone of Nigeria. Birnin Gwari is on the Geographical coordinates of 11^0 1' 33” N to 6^0 47' 22” with the total land area of about 16220 hectres. The image below shows Birnin Gwari from Google

Map.

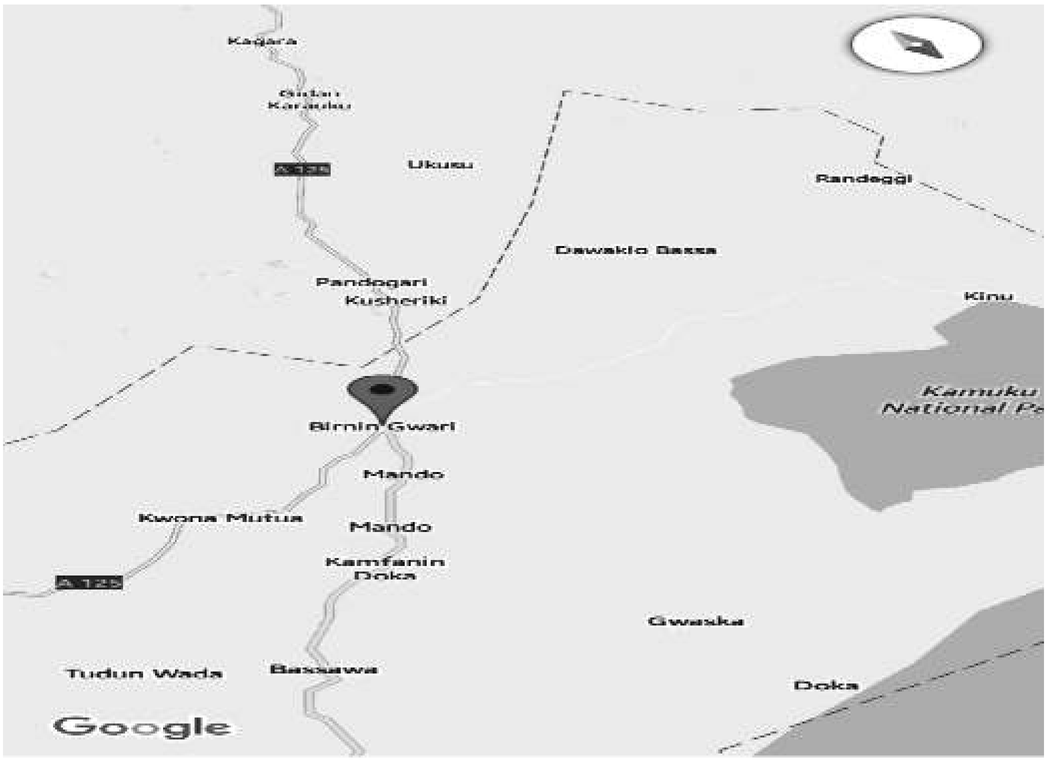

Fig 1. Birnin Gwari on Google Map.

The Satellite map below shows the locations of the study area (villages) obtained from google map.

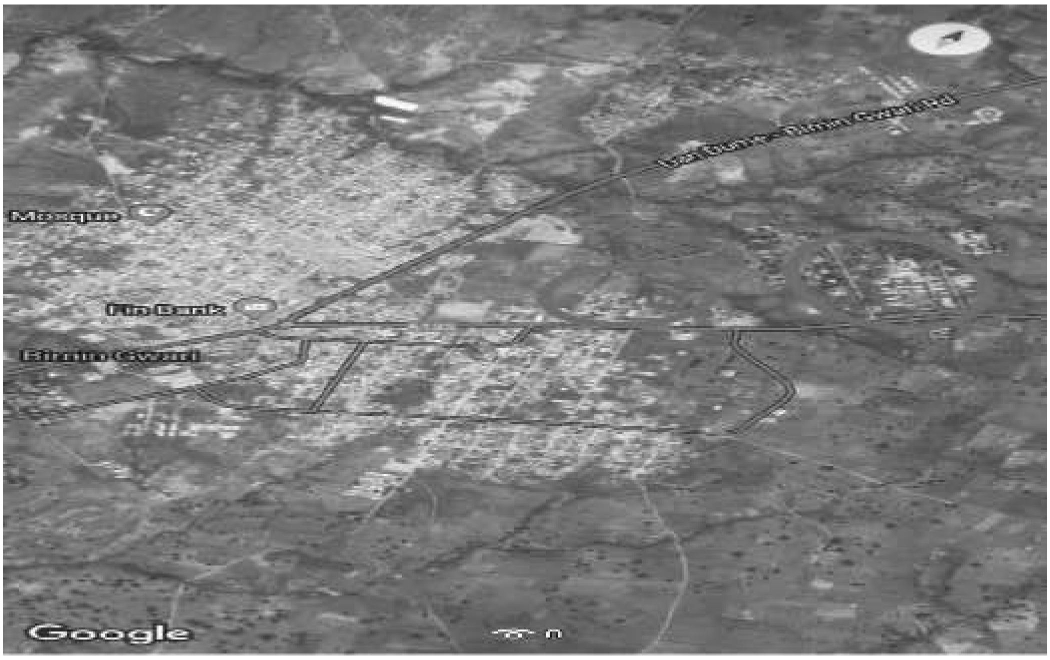

Fig 2. Satellite Image of the mining villages (Rima and Bugai)

Sample Collection and Preparation

Rock samples were collected from Rema and Bugai mining sites in Birnin Gwari local government area of Kaduna State, Northwest-Nigeria for analysis. The ten field samples (of about 1 kg of rocks) five from each mining sites (Rima and Bugai), labeled R1, R2, R3, R4 and R5 for REMA. B1, B2, B3, B4 and B5 for BUGAI were collected at random. The samples were taken to the laboratory and left open for slightly over twenty-four (24) hours under ambient temperature after which the analysis was carried out. The picture below shows the labelled samples.

Plate 1. Labeled Image of the collected samples before the analysis

Ten samples (of about 1 kg) five each from a mining village to a depth of about 10 cm, within the area of consideration were collected at random, initially filled into polyethylene bags separately for respective points in equal measures and labeled accordingly. The rock samples were packed in plastic containers from the areas of surveillance, properly sealed and labeled for easy identification and then transported to the National Geosciences Laboratory Research, Barnawa Kaduna.

Analysis

X-Ray Fluorescent Spectrometry

X-ray fluorescence spectrometry is a method of quantitative analysis that uses x-ray energy. The x-rays obey the law of electromagnetic radiation which states that a body surface can absorb incident radiation and reflect the incident radiation as a mirror with spherical symmetry which can transmit incident radiation and emit the radiations (NGRL 2017).

The origin of X-rays is from the loss associated with the interaction of high energy election with atoms. The electrons coming from the x-ray tub moves towards the electronic field of the electrons in the various shells of the atoms of the targeted material. The incident electrons are decelerated and lose energy. Incident high-energy electrons penetrate the outer orbital of the atoms and collide with an electron in the inner orbital. These inner electrons may be completely removed, leaving the atom in an unstable state. Electron rearrangement to restores stability takes place, leading to the release of energy in form of x-rays. X-rays generated in this way have discrete wave length which is related to the atomic number of the atoms producing them. They are called 'CHARACTERISTIC X-RAYS'. The detection and measurement of the Characteristic X-rays are the basis of X-ray spectrometry.

Sample Preparation

Pulverization:

The samples were pulverized (grind to fine powder) using arget pulverizing machine (planetary micro mill pulverisette7). The ground samples were ensured to pass 150 micro mesh sieves. This was to ensure homogeneity of the samples.

Palletization:

5g of the pulverized sample was weighed into a beaker, 1g of binding aid (Starch soluble). The mixture was thoroughly mixed to ensure homogeneity, which was pressed under high pressure (6 “tone”) to produced pellets; labeled and package ready for the analysis.

Procedure of the analysis:

Energy Dispersive x-ray fluorescence (EDXRF) spectrometer of model “Minipal 4” was used for the analysis. The pellets were carefully placed in the respective measuring positions on a sample changer of the machine. The following condition sets were made as the machine was switched on.

Elemental composition determination

- Nature of the samples to analyzed as press powder (pellet)
- The current used as 14kv for major oxides, 20kv for the trace elements/rare earth metals.
- Selected filters were “kapton” for major oxides, Ag/Al-thin for the trace elements/rare earth metals.

The selection of filters was guided by a given periodic table used for elemental analysis. Time of measurement for each sample was 100 seconds and the medium used was air throughout.

The machine was then celebrated by the machines gain control, after which the respective samples were measured by clicking the respective positions of the sample changer.

LOI was determined gravimetrically by heating 1g of the powdered sample in a cleaned weighed crucible at 1000^{o}c. After which the crucible and the content was weighed to get the difference in weight before and after heating.

LOI = (a-b) x 100% = H_2O^+

Where a = weight of crucible + 1g of the sample before heating

b= weight of crucible + 1g of the sample after heating.

Results

Table 1. Result for X-Ray Fluorescent Spectrometry Analysis for Rima (RM1-RM5)

S/No	Element	Symbol	Atomic No	RM 1	RM 2	RM 3	RM 4	RM 5
1	Silicon	Si	14	96.00	97.80	96.00	97.30	94.10
2	Aluminum	Al	13	0.64	0.42	0.59	0.40	0.74
3	Potassium	K	19	1.05	0.30	0.12	0.403	0.52
4	Sulphur	S	16	N.D	N.D	0.2	N.D	N.D
5	Sodium	Na	11	N.D	N.D	N.D	N.D	N.D
6	Calcium	C	20	0.15	0.91	0.29	0.10	0.058

7	Titanium	Ti	22	0.21	0.052	0.11	0.071	0.12
8	Chromium	Cr	24	0.04	0.041	N.D	N.D	0.028
9	Manganese	Mn	25	0.048	0.056	N.D	0.048	0.05
10	Iron	Fe	26	0.76	0.18	0.14	0.23	2.77
11	Nickel	Ni	28	N.D	N.D	0.22	N.D	N.D
12	Copper	Cu	29	0.052	0.047	0.052	0.058	0.045
13	Arsenic	As	33	N.D	0.015	0.023	0.021	0.008
14	Selenium	Se	34	N.D	0.013	N.D	N.D	N.D
15	Barium	Ba	56	N.D	0.04	N.D	0.04	0.12
16	Vanadium	V	23	0.001	N.D	N.D	N.D	N.D
17	Ruthenium	Ru	44	0.47	0.18	0.67	0.60	0.53
18	Europium	Eu	63	0.06	0.15	0.061	0.16	N.D
19	Thorium	Th	90	N.D	N.D	N.D	N.D	N.D
20	Lead	Pb	82	N.D	0.032	0.01	0.038	0.058
21	Osmium	Us	76	0.065	N.D	N.D	N.D	0.037
22	Praseodymium	Pr	59	N.D	N.D	N.D	0.19	0.10
23	Mercury	Hg	80	N.D	N.D	N.D	0.055	N.D
24	Gold	Au	79	0.0056	0.0050	N.D	0.0046	0.042
25	Germanium	Ge	32	0.009	N.D	N.D	0.003	0.013
26	Uranium	U	92	N.D	N.D	N.D	N.D	N.D
27	Thallium	Tl	81	N.D	0.041	N.D	N.D	N.D
28	Bismuth	Bi	83	N.D	N.D	0.06	N.D	N.D
29	Silver	Ag	47	0.030	0.001	0.010	0.013	N.D

Table 2. Result for X-Ray Fluorescent Spectrometry Analysis for Bugai (BG1-BG5)

S/No	Element	Symbol	Atomic no	BG1	BG2	BG3	BG4	BG5
1	Silicon	Si	14	94.80	95.50	57.00	95.10	98.10
2	Aluminum	Al	13	0.56	N.D	20.00	0.83	0.64
3	Potassium	K	19	0.07	0.57	0.26	0.62	N.D
4	Sulphur	S	16	0.10	0.30	N.D	0.90	N.D
5	Ytterbium	Yb	70	0.037	N.D	N.D	N.D	N.D
6	Calcium	Ca	20	0.34	0.50	0.90	0.59	0.17
7	Titanium	Ti	22	0.24	0.18	0.34	0.30	0.807
8	Strontium	Sr	38	N.D	N.D	0.11	N.D	N.D
9	Manganese	Mn	25	0.053	0.17	0.11	0.54	0.024
10	Iron	Fe	26	1.07	0.69	15.63	0.86	0.12
11	Nickel	Ni	28	0.14	0.011	N.D	N.D	N.D
12	Copper	Cu	29	0.059	0.053	0.055	0.061	0.06
13	Arsenic	As	33	0.013	0.007	N.D	0.018	N.D
14	Selenium	Se	34	0.028	N.D	N.D	0.023	N.D

15	Barium	Ba	56	N.D	0.16	0.03	N.D	0.01
16	Vanadium	V	23	N.D	N.D	0.003	N.D	N.D
17	Chromium	Cr	24	N.D	N.D	N.D	N.D	0.036
18	Germanium	Ge	32	N.D	N.D	N.D	N.D	0.0071
19	Praseodymium	Pr	59	N.D	N.D	N.D	N.D	0.074
20	Samarium	Sm	62	N.D	N.D	N.D	N.D	0.056
21	Ruthenium	Ru	24	0.78	N.D	N.D	0.58	0.70
22	Europium	Eu	63	0.22	0.12	0.45	0.05	0.13
23	Zinc	Zn	60	N.D	N.D	0.11	0.031	N.D
24	Lead	Pb	82	0.055	0.051	0.11	0.02	N.D
25	Osmium	Os	76	N.D	0.03	N.D	N.D	0.038
26	Yttrium	Y	39	N.D	N.D	0.049	0.020	N.D
27	Iridium	Ir	77	N.D	N.D	0.04	N.D	0.055
28	Mercury	Hg	80	N.D	N.D	N.D	0.041	N.D
29	Thallium	Tl	81	N.D	N.D	N.D	0.030	N.D
30	Indium	In	49	N.D	N.D	N.D	0.93	0.19
31	Zirconium	Zr	40	N.D	N.D	0.034	N.D	N.D
32	Gold	Au	79	N.D	0.0065	N.D	N.D	0.0067
33	Cerium	Ce	58	N.D	0.050	N.D	0.069	N.D
34	Gallium	Ga	31	N.D	N.D	0.01	N.D	N.D
35	Antimony	Sb	51	N.D	N.D	0.41	N.D	N.D
36	Bismuth	Bi	83	0.059	N.D	N.D	0.046	0.079
37	Silver	Ag	47	0.016	0.050	N.D	N.D	N.D

Dicussion

X-ray spectrometer was adopted to carry out an elemental analysis to detect the presence of elements. At the first mining site (Rima) 27 elements were found, which are Si, Al, S, Na, Ca, Ti, Cr, Mn, Fe, N, Cu, As, Se, Ba, V, Ru, Eu, Pb, Os, Pr, Hg, Au, Ge, Tl, Bi and Ag. At the second mining site (Bugai) 37 elements were found, which are Si, Al, S, Yb, Ca, Ti, Sr, Mn, Fe, Ni, Cu, As, Se, Ba, V, Cr, Ge, Pr, Sm, Ru, Eu, Zn, Pb, Os, Y, Ir, Hg, Tl, In, Zr, Au, Ce, Ga, Sb, Bi and Ag respectively. Note that, the (N.D) in the tables stands for “Not Detected” which means the composition of that particular element from that sample is beyond detection level.

Conclusion

It has been confirmed that the mining sites (Rima and Bugai) are rich with so many elements that are very useful, although the mining activities are not done in a technical way. Gold is found in the two mining sites. It has been observed that, 4 out of the 5 samples collected from Rima contained a significant composition of Gold (Au) which indicates the presence of Gold in that mining site. Gold composition has been observed also from 2 out of the 5 samples collected from Bugai which indicates that, Gold (Au) is not very abundant there.

References

Abbey, S., (2001)**.** *Geological Survey of Canada Paper 5.* 83- 15.

Claisse, F., (2011). *Quebec Department of Mines* P.R. 327.

Heinrich, K. F. J., (1966). *The Electron Microprobe*, John Wiley and Sons, New York, p. 296.

Hutchison, C. S., (1974). *Laboratory Handbook of Petrographic Techniques*, John Wiley and Sons, New York, 527 p.

National Geosciences Research Laboratory (MANUAL 2017). Nigerian Geological Survey Agency.

Norrish, K. and Chappell, B. W., (1967). *Physical Methods in Determinative Mineralogy*, J. Zussman (Ed), Academic, London, p. 161.

Norrish, K. and Chappell, B. W., (1977). *Physical Methods in Determinative Mineralogy*, 2nd, ed., J. Zussman (Ed.), Academic, London, p. 201.

Norrish, K. and Hutton, J. T.,(1969). Geochemical et CosmochemaActa 33, p. 431.

Potts, P. J., (1987). *A Handbook of Silicate Rock Analysis*, Chapman and Hall, New York, 1987, 622 p.

Timothy E. La Tour (1989). Analysis of Rocks Using X-Ray Fluorescence Spectrometry. *The Rigaku Journal.* Vol. 6/ no. 1

ANALYSIS OF ALUMINA-DOPED WITH LOW DENSITY POLYETHYLENE (LDPE/ KANKARA ALUMINA) NANOCOMPOSITES USING X-RAY DIFFRACTION

A. Aliyu[1] , A. A. AbdelmaliK[1], U. Ahmadu[2] and U. Sadiq[1]

[1] *Physics Department, Ahmadu Bello University, Zaria, Nigeria*

[2] *Physics Department, Federal University of Technology, Minna, Nigeria*

Email - aliyuelokene@gmail.com

ABSTRACT

Nano-sized kaolin also known as alumina was synthesised from local kaolin and subsequently suspended in low density polyethylene (LDPE) to produce nano-polymer for application in electrical insulation. The alumina was prepared by acid leaching via digestion, precipitation, peptization and drying. It was subsequently used to dope the LDPE at varying compositions. The structural behaviour of the prepared polymeric insulation was studied to understand the structure of the nano-polymer. The structural properties of LDPE/γ-alumina with LDPE as a host matrix were investigated by X-ray diffraction. Intermediate LDPE/γ-alumina nanocomposites were confirmed by XRD with an increasing intensity as the alumina increases.

Keywords: *alumina, low density polyethylene (LDPE), structural properties, nanocomposites, X-ray diffraction*

Introduction

Low density Polyethylene has became very popular as power cable insulation when it was first introduced in 1960s, due to its low cost, better electrical properties compared to paper-oil insulation, processability, moisture and chemical resistance, and low temperature flexibility (Andrews, Hampton, Smedberg, 2006). Polymer/clay nanocomposites are an important class of organic- inorganic composites in which clay platelets are dispersed at a nanometric level in the polymer matrix, acting as a reinforcing phase (Silvia et al, 2013). With a very small addition of clay into the polymer matrix while achieving nanometric dispersion, the resulting nanocomposites exhibit substantial improvements in its physical properties (Grandjean 2006, Ray and Okamoto, 2003). This is because the properties of nano-composite materials depend not only on the properties of the parent constituent material or matrix but also on their morphology and interfacial characteristics (Rao Muller and Cheetham , 2004). There is therefore no doubt that inorganic mineral fillers has helped in increasing polymer performance properties, such as mechanical, structural and electrical. Priya and Jog(2002 & 2003) were the first to prepare Polymer–clay nanocomposites. They observed from the modified Cloisite used that the addition of organically modified clay resulted in the formation of the β-phase instead of the α-phase upon melt processing. Usually the general class of clay are hydrophilic in nature and are stacked together. In order to effectively disperse the clay into an organic polymer matrix and increase compatibility, it is usually necessary to modify the hydrophilic character of the silicate into organophilic character, so as to make it hydrophobic in order to ease its dispersion into the polymer matrix.

In general, the material properties of polymer nanocomposites are superior to the pure polymer matrix or composites with larger sized inclusions. The effects of the nanoparticles are dependent on many variables but especially upon the relative crystalline or amorphous nature of the polymer matrix as well as the interaction between the filler and matrix (Liqiang and Seong, 2008). Owing to the high need of enhancement of dielectric property of flexible polymeric materials with nano-ceramics, it will be imperative to look into how much of its structure has been altered during the course adding the nanoparticles. The structural analysis was necessary principally to evaluate the morphology and the extent of dispersion of the nano-particles to ascertain the microstructure of the alumina.

Materials and Methods

MATERIALS

Low density Polyethylene(LDPE) (commercial grade), Hydrochloric Acid (HCl) of M. W., 36.48 and purity 35.38% was supplied by BDH Chemical Ltd, Poole England. Ethanol (Absolute) of purity 99.7% was gotten from Johnson Solomom (Export) Ltd, London, England. NaOH of M. W. 40.0*g/mol* was also supplied by BDH. Polyvinyl Alcohol (PVA) of 98% purity was supplied by BDH Raw kaolintic clay sample. Toluene Analar-M.W. 92.14 and 0.86*g/mol*.

Preparation of Nanokaolin from Kaolin by Acid Leaching

Below is the schematic representation of how the doping leading to the samples were gotten

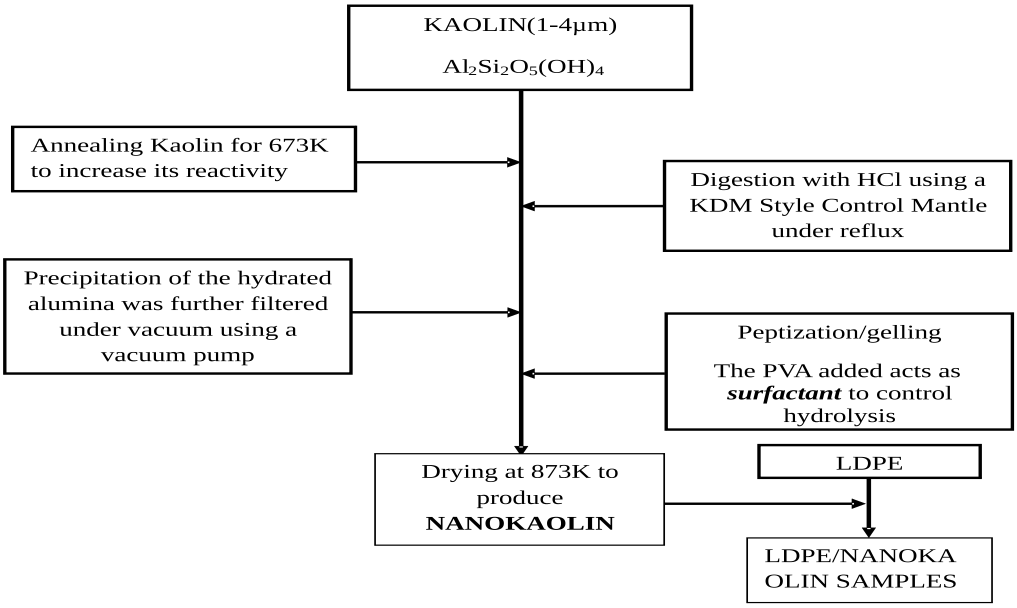
KAOLIN(1-4µm)
$Al_2Si_2O_5(OH)_4$
Annealing Kaolin for 673K to increase its reactivity
Digestion with HCl using a KDM Style Control Mantle under reflux
Precipitation of the hydrated alumina was further filtered under vacuum using a vacuum pump
Peptization/gelling
The PVA added acts as ***surfactant*** to control hydrolysis
Drying at 873K to produce **NANOKAOLIN**
LDPE
LDPE/NANOKAOLIN SAMPLES

Schematic diagram of preparation of samples

Methods of Morphological Investigation

X-RAY DIFFRACTION (XRD)

To investigate the effect of alumina on the intercalation of the LPDE layers XRD technique was employed. The modification of the LPDE is not intended to structurally change it flexibility and mode but rather to examine whether the samples so formed are exfoliated, intermediate or intercalated nanocomposites. XRD was carried out using a PANalytical XPERT-PRO diffractometer system with a Reflection-Transmission Spinner configuration on a PW3064/60 sample stage for powder diffraction. A Gonio scan axis with a start position of 5.0464 (2?) and end position of 99.9184 was employed using a step size (2?) and scan time (s) of 0.067 and 29.8450 respectively. The scan mode was continuous with a specimen length of 10mm ray-length and measurement was conducted at room temperature of 25℃. The generator setting employed was 30Ma and 40KV with K-Alpha 1 (?) wavelength of 1.54060 using Copper (Cu) as the anode material.

RESULTS AND DISCUSSIONS

X-RAY DIFFRACTION (XRD)

The XRD results obtained from PANalytical XPERT-PRO diffractometer system was with a view of deriving the structural phases from samples prepared. Before doping the low density polyethylene with the alumina that gives the various samples at varying composition, the nanosize of the alumina was confirmed by the use of the well-known Scherrer formula the average crystallite size, *L*, is:

$$L = \frac{K\lambda}{\beta Cos\theta} \qquad 1.0$$

Where λ is the X-ray wavelength in nanometer (nm), β is the peak width of the diffraction peak profile at half maximum height resulting from small crystallite size in radians and K is a constant related to crystallite shape, normally taken as 0.9 (**Cullity and Stock, 2001)**. The value of β in 2θ axis of diffraction profile must be in radians. The θ can be in degrees or radians, since the Cosθ corresponds to the same number. It can be taken as 0.89 or 0.9 for Full Width Half Maximum (FWHM) of spherical crystals with cubic unit cells (Ahmad, 2012).

The XRD result is expected to give the following: Lattice parameters, Phase identity, Phase purity, Crystallinity, Crystal structure and Percent phase composition about the samples.

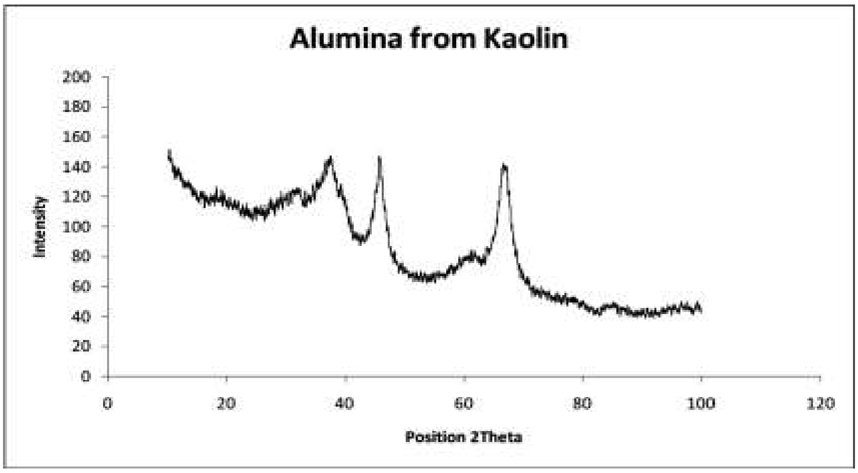

Fig 1: XRD of pure Nanokaolin (alumina) from Kaolin

The analysis of the diffractogram revealed a crystalline material though with relatively three average peaks which were quite pronounced of various intensities and that is characteristic of all γ- alumina. This in conformity with the work of (*Seyed, Aligholi, And Dariush, 2011)* where there 2θ peaks appeared on 37 46 and 67 respectively.

In this work, the 2θ peaks are visible at 36, 46 and 66 respectively. From fig 1, the pure alumina sample was matched with a reference code of 01 – 075 – 0921, scale factor of 0.666, score of 69% and compound formula and name of γ- $(Al_2O_3)1.33$ and aluminum oxide. The sample had a cubic crystal system, Fm-3m space group and 225 space group number. The [hkl] value was calculated to be [200] from ICDD using POWD-12++ (1997) and classified as an inorganic alloy with metal or intermetallic ICDD pattern. The nanosize of the alumina was calculated to be 24.91*nm* using the stated equation. This therefore confirms the nanoscale of the dopant.

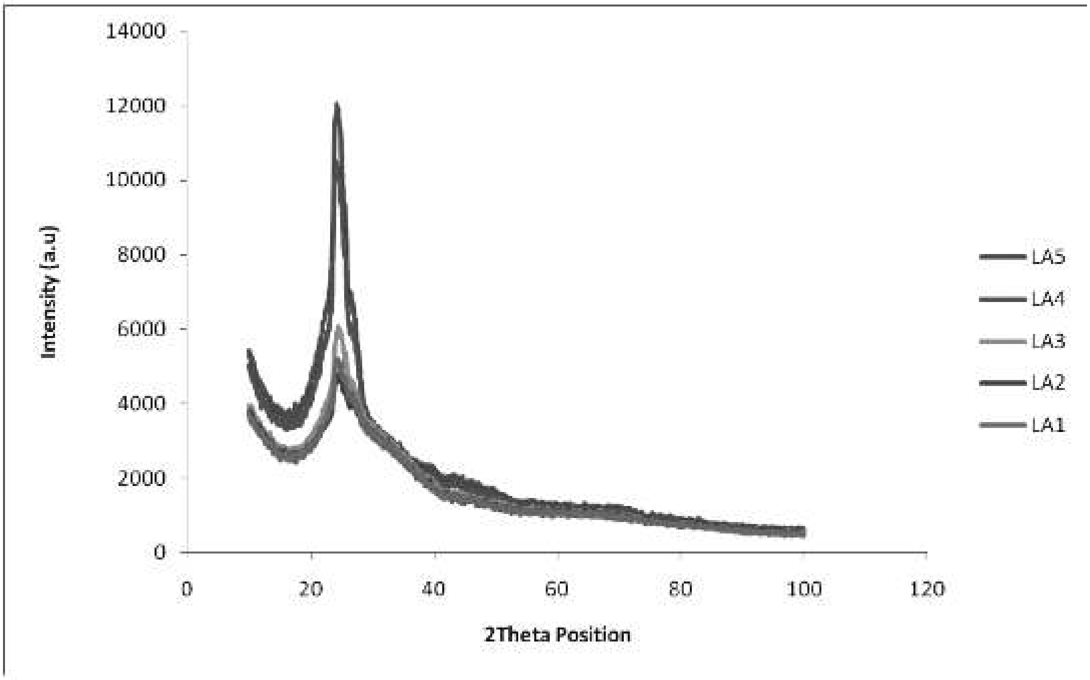

Fig 2: X-ray diffraction patterns of LDPE/alumina nanocomposites
LA⇒LDPE/Alumina, 1-5⇒Varying concentrations

Fig 2 shows that XRD results of LDPE doped with alumina at 1%wt, 2%wt, 3%wt 4%wt and 5%wt which is tagged as LA1,LA2 LA3, LA4 and LA5 respectively. LA1 and LA2 appears to overlap at the same intensity. As more alumina was added, the intensity increases which is characteristic of polymer behaviour as it came in the work of (*Chanmal and Jog, 2009*), where the intensity of XRD in PVDF increases with addition of montmorillonite in %wt. The XRD patterns of all the images shows peaks at about

21.9012[2θ], 23.8958[2?], and 25.7284[2?],

at various intensity. The appearance of peak

21.9012[2θ] clearly indicates that the matrix is

a semicrystalline material as stated by (Andrew, 2000). The diffraction peaks at 21.5 and 23.9 of [2 θ]reflection are assigned to the 110 and 200 reflections of polyethylene respectively. This makes this work in close agreement with the earlier ones. Also in the work of (Kieran *et al.*, 2013), three crystalline peaks were identified during their experiment, these were at 21.5°, 24.3° and 36.5°. The orthorhombic phase for the peak located at 21.5° is 110, for peak 24.3° is 200 and for peak 36.5° is 210. These phases represent the diffraction angle which corresponds to the orthorhombic crystallite plane.

The diffractogram of LA1 and LA2 from the measurements clearly indicated a semicrystalline material with broad peaks which was strongly unmatched with the PDF index files of the ICDD data-base. As more alumina was added, i.e LA3, LA4 and LA5,

more peaks were observed emerging at [2θ]

positions (40-60) showing the presence of certain impurity (alumina) which was not conspicuous at lower doping and that was also expected. The doping did not shift the peak position any farther from the initial values but caused an increase in intensity. The overall impression is that the alumina has interacted well with LDPE matrix

This shows the presence of certain impurity (alumina) which was not conspicuous at lower doping and that was also expected because the lower doping was too small to influence the matrix at that level. The doping did not shift the position of the peak any farther from the initial values. The width of the peaks did not also change with increase in doping but an increase in magnitude of the peak was observed. By doping the matrix, the LDPE is modified with the presence of nanoparticles. This implies a change in the mean atomic scattering factor on a given site (Paul, 2014). If the material is doped with a light atom, a small intensity is expected but if the atom is a heavy one like the case of alumina, there would be significant change in the magnitude of the intensity due to more scattering centres that could be created. This is because the intercalation of ions in the lattice surely leads to changes on scattering factors which will be reflected on different relative intensities. It is also possible that the change in the peak intensities is due increase in volume of nanoparticles which lead to change in the density of the crystallographic position of the samples (Paul, 2014). Generally, the [2θ] values of the peaks, for all concentrations fall virtually at the same point, except the vibrations emerging at higher [2θ] values showing the presence of alumina. This means that the alumina has interacted well with LDPE matrix and may have dispersed as isolated agglomerate rather than a network of linked particles (Maziyar and Hassan, 2014).

CONCLUSION

The morphology and microstructures of the samples have been examined by X-ray diffraction.. XRD patterns are very consistent with the previous works with all peaks having the same [2θ] position except for the broadness of some of the peaks and their increasing intensities. The significant change in broadness and the magnitude of the intensity is due to more scattering centres that were created from the addition of alumina. This is because the intercalation of ions in the lattice surely leads to changes on scattering factors which will be reflected on different relative intensities. Generally, the [2θ] values of the peaks, for all concentrations fall virtually at the same point, except the vibrations emerging at higher [2θ] values showing the presence of alumina. This implies that the alumina has interacted well with LDPE matrix and may have dispersed as isolated agglomerate rather than a network of linked particles.

References

Ahmad, Z.(Eds, **Marius A. S.**) (2012). *Dielectric Materials: Polymeric Dielectric Materials*, In Tech, Croatia

Andrew J. Peacock (2000). Handbook of Polyehtylene; Structures, properties and Applications, Marcel Dekker, inc, New York. pp. 67-113

Andrews, T. Hampton, R.N. Smedberg, A. ,(2006): “The role of degassing in XLPE power cable manufacture”, IEEE Electrical Insulation Magazine, Vol. 22, No. 6, pp. 5-16

Chanmal C.V and Jog J.P. (2009). A Study of Dielectric Behaviour of PVDF/clay Nanocomposites. e-Polymers, no. 112, http://www.e-polymers.org ISSN 1618-7229

Cullity B. D. and Stock S.R., (2001). Element of X-Ray Diffraction, 3rd Ed Prentice-Hall Inc, P 167-171

Grandjean, J. (2006): Solid-state NMR study of modified clays and polymer/clay nanocomposites. Clay Mater., 41 (2), 567- 586

Kieran A. M, James E. K, Brian M, Olivier V., Damien R., Richard C., Clement L. H.(2013): Characterisation of the Surface and Structural Properties of Gamma Ray and Electron Beam Irradiated Low Density Polyethylene, *International Journal of Material Science (IJMSCI) Volume 3 Issue 1*

Liqiang C. and Seong I. W (2008). Preparation and Characterization of Polyehtylene (PE)/Clay nanocomposites by in situ Polymerization with Vanadium-based Intercalation catalyst, *Polymer Bulletin* 61, 453-460

Maziyar S, Hassan S.(2014). Mechanical and electrical properties of low density polyethylene filled with carbon nanotubes, 2nd International Conference on Structural Nano Composites , IOP Conf. Series: Materials Science and Engineering 64, 012001

Liqiang C. and Seong I. W (2008). Preparation and Characterization of Polyehtylene (PE)/Clay nanocomposites by in situ Polymerization with Vanadium-based Intercalation catalyst, *Polymer Bulletin* 61, 453-460

Paul F. F.(2014). A new theory for X-ray diffraction, *Foundations and Advances,* Acta Crystallographica Section A, ISSN 2053-2733

Priya L and Jog J.(2002). *Journal of Polymer Science Part B Polymer Phys* ;40:1682–9

Priya L and Jog J.(2003). *Journal of Polymer Science Part B Polymer Phys* ;41:31–8.

Rao C. N. R. , A. Muller and A. K. Cheetham (Eds). (2004). The Chemistry of Nanomaterials. Synthesis, Properties and Applications., Copyright @ 2004 WILEY-VCH Verlag GmbH & Co. KGaA, Weinheim ISBN: 3-527-30686-2

Ray, S. S. And Okamoto, M. Polymer/layered silicate nanocomposites: a review from preparation to processing. Prog. Polym.Sci. 2003, 28, 1539- 1641

Seyed A. H., Aligholi N. & Dariush S (2011).

Production of γ-Alumina from Kaolin, Ope

Journal of Physical Chemistry, 1, 23-27

Ray, S. S. And Okamoto, M.(2003): Polymer/layered silicate nanocomposites: a review from preparation to processing. Prog. Polym.Sci., 28, 1539- 1641.

Silvia B. Umayal S., Marco G., Lucia R., Vincenzo L., and Giacomo R., (2013): Synthesis, Characterization, and Solid-State NMR Investigation of Organically Modified Bentonites and Their Composites with LDPE, Pubs.acs.org/Langmuir

GEOPHYSICAL INVESTIGATION OF GROUNDWATER POTENTIAL IN MILLENNIUM CITY HOUSING ESTATE KADUNA, NIGERIA USING ELECTRICAL RESISTIVITY METHOD

[1*]Shaibu, I.,[2]Udensi, E. E., [1]Chinwuko, A.I., [2]Usman, D. A., and [2]Adetona, A. A.Omale M.E.

[1]Department of Geology, Federal University Gusau, Zamfara State

[2]Department of Physics, Federal University of Technology, Minna, Niger State

Email: isahshaibu1982@gmail.com

ABSTRACT

Lack of potable drinking water supply remains one of the main challenges of residents of Millennium City Housing Estate, Kaduna, Nigeria. The groundwater potential of the area was investigated using vertical electrical sounding (VES) method. A total number of 36 vertical electrical sounding VES points were used for the entire investigation using Schlumberger array and the data obtained were analyzed using curve matching and computer iteration techniques. The data revealed both a 3-layer (KH and H Curve types) and 4-layer (H-curve type) only for the area. In the 3-layer system, the apparent resistivity of the first layer ranged from 31.0 ? m to 57.5 ? m with a corresponding thickness of 0.8 m to 1.6 m. The second layer has apparent resistivity value ranged from 13.6 ? m to 907.9 ? m with a corresponding thickness range of 4.4 m to 22.8 m while the third layer has resistivity values ranging from 1087.1 ? m to 1477.2 ? m with an infinite depth. For the four (4) layered model curves, first layers resistivity ranged from 131.7 ? m to 208.5 ? m, with a corresponding thickness ranged from 0.8 m to 1.0 m. The resistivity of the second layers ranged between 28.8 ? m to 29.9 ? m with a corresponding thickness ranged from 5.1 m to 16.3 m. The third layer resistivity ranged from 111.4 ? m to 287.2 ? m with a corresponding thickness ranged from 8.2 m to 22.6 m. The forth layer has a resistivity value ranging from 1044.3 ? m to 1833.6 ? m with an infinite depth. An integration of both isopach and iso-resistivity maps for both the 3- layer model curves and 4- layer model curves indicates that most of the north/west parts of the study area have low apparent resistivity values and thick overburden which implies good groundwater potential while the southern portion has a little higher resistivity values and shallow overburden, an indication of poor groundwater potential. Future boreholes in the area should reached an effective depth of 40 m to 55 m depth and the borehole be supervised by a certified hydrogeologist or geophysicist for optimum groundwater yields. Pumping test should be carried out in order to ascertain the size and type or quality of submersible pump to be installed for optimum yield.

Keywords: *Investigation, Groundwater Potentials, Millennium City Housing Estate, Kaduna, Nigeria.*

Introduction

The growth of any locality depends on availability of basic infrastructural needs such as roads, water, electricity and industries among others. A general case of northern Nigeria where the amount of rainfall is limited to very few months of the year with annual rainfall of about 1000-1500mm Eduvie, (1998). Surface water sources are often inadequate or non-existent.(Baimba,1978,Perez and Barber,1965).

There is need for scientific identification of parameters governing ground water resources, investigation of groundwater potential and management, particularly, if satisfactory living conditions of the inhabitants are to be catered for. This is paramount, due to the presence increase in groundwater demand for various human activities has placed great importance on water science and management. The Millennium City Housing Estate Kaduna, Nigeria was designed originally for 25,000 inhabitants but currently has population of over 50,000 people and basic amenities are over-stretched. This population and the daily influx of people into Kaduna, Nigerian's in search of greener pastures have resulted in acute water shortage in the area and the inhabitants now rely on water vendors for their daily water needs. Groundwater accounts for greater percentage of the world's fresh water and it is fairly distributed throughout the world. It is the world's greatest essential factor for sustainable development and the need to delineate the areas that would be suitable for groundwater potential and need to conduct hydrological and geophysical survey of the area in order to provide useful information on the possible sites for ground water exploration. Since the object of sound is to determine the variation of electric conductivity with depth, vertical electrical sounding (VES) has been the most important geophysical method of water prospecting in area of deep in situ weathering of fresh bedrock. The geo-electric resistivity method, particularly the (VES) method has been chosen for this particular work basically, because it has proven to be an economic, quick and effective means of solving most ground water problems in different parts of the world (Breusse,1963, Zohdy and Jackson, 1969 and Frohlich, 1974).

Materials and Methods

Materials

The equipment that will be used for the resistivity method is reasonably cheap and easy to use. The resistivity field data will be acquired with the aid of the following equipment:-

Terrameter (Geopulse campus Tiger)- This is the major power source of the whole set-up. It measures the resistance of the subsurface layers and can also measure the voltage of the power source. The equipment has an in-built system of reducing the effect of noise. The instrument is portable and fixed with a rechargeable battery. it has a maximum power of 18 watts, manual selection of current in steps up to 100mA, a choice of sample time/ signal length averaged three frequency settings.

Electrodes- These are steel rods of about 30cm with a base and a pointed end. The pointed end is use to penetrate the ground. The material makes it a good conductor. Four electrodes will be used; the first pair is the potential electrode while the second pair is the current electrode. Their basic function is to pass current into the ground and measure potential between two points. Two-third of the length of the electrodes will be driven below the earth surface.

Cables- They are made of conducting material (copper). There will be four reels of cables used during the geophysical survey. The cables will be connected to the terrameter on one end and the other is connected to the electrodes.

Clips- These are objects used for passing the currents from the cables to the electrodes by clipping the electrodes after wounding the cable on it. The mouth is made of conducting materials while the base (handle) is made of insulating material to prevent electrocution. The clips ensure good electrical contact

Hammer and Cutlass-These will be used to drive the electrodes into the ground. It consists of a relatively slim wooden cylindrical handle embedded into a metallic head. While the cutlass will be used to clear the path along which measurement are to be taken.

Tapes- These are used for making measurements of length on the field as they have been calibrated in metric units. The tapes used will be of 100m in length. They will be used in measuring electrode spacing on the field.

Global Positioning System and Compass-Clinometer- this equipment will be used for taking coordinates and bearing. GPS will be used for taking the longitudes, latitudes and elevation of various locations. It is portable and handy. The compass-clinometer will be used to take direction of the profiles.

Field Stationery- These are writing materials that will be used to record all observation and field data. The stationery consists of pencils, pens, recording sheets, rulers and so on.

Study Area Description

Kaduna state millennium city, was created in 1999, following the decision to expand the city in other to build more house for both federal and Kaduna state civil servants. The millennium city lies in the north-west part of Nigeria with latitude of $10^{O}31^{''}$ N and longitude 07^{O} $30^{''}$ E, with elevation of 619 m, (Fig. 1). The study area and it is accessibility through major and minor roads, while Fig .2 shows geological maps of Nigeria showing the study area and Fig .3 shows geological map of Kaduna State (NGSA 2007).

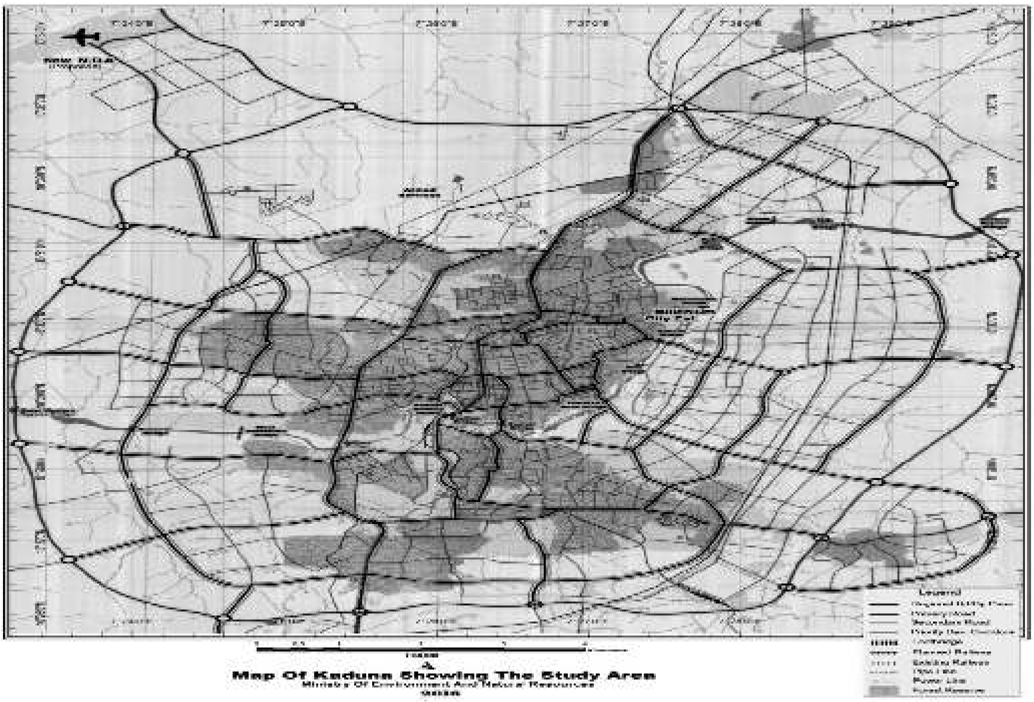

Fig. 1: Map of Kaduna showing the accessibility of the study areas

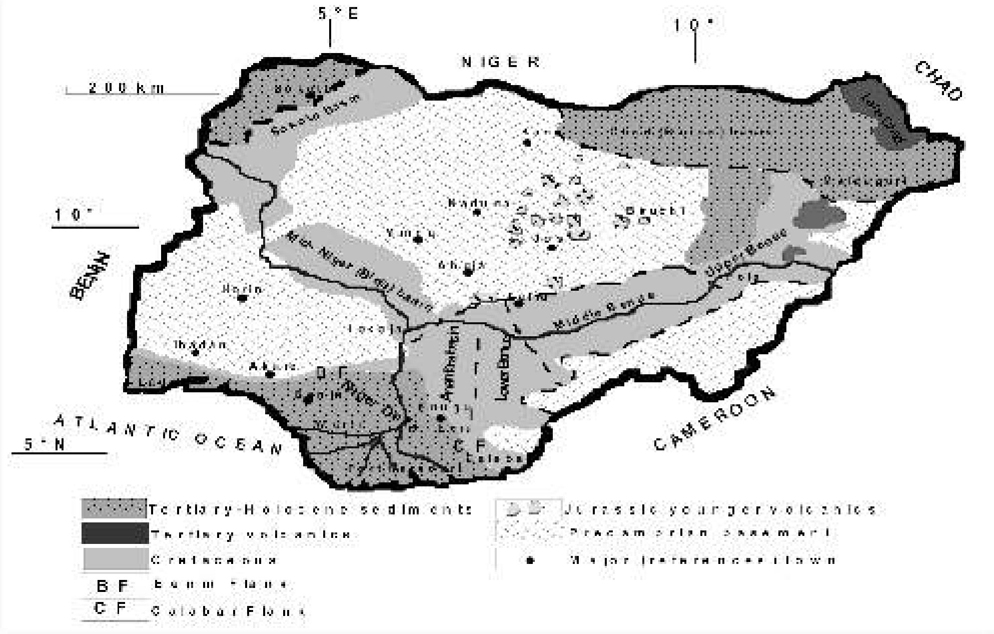

Fig. 2: Geologic map of Nigeria showing the Study Area (NGSA., 2000)

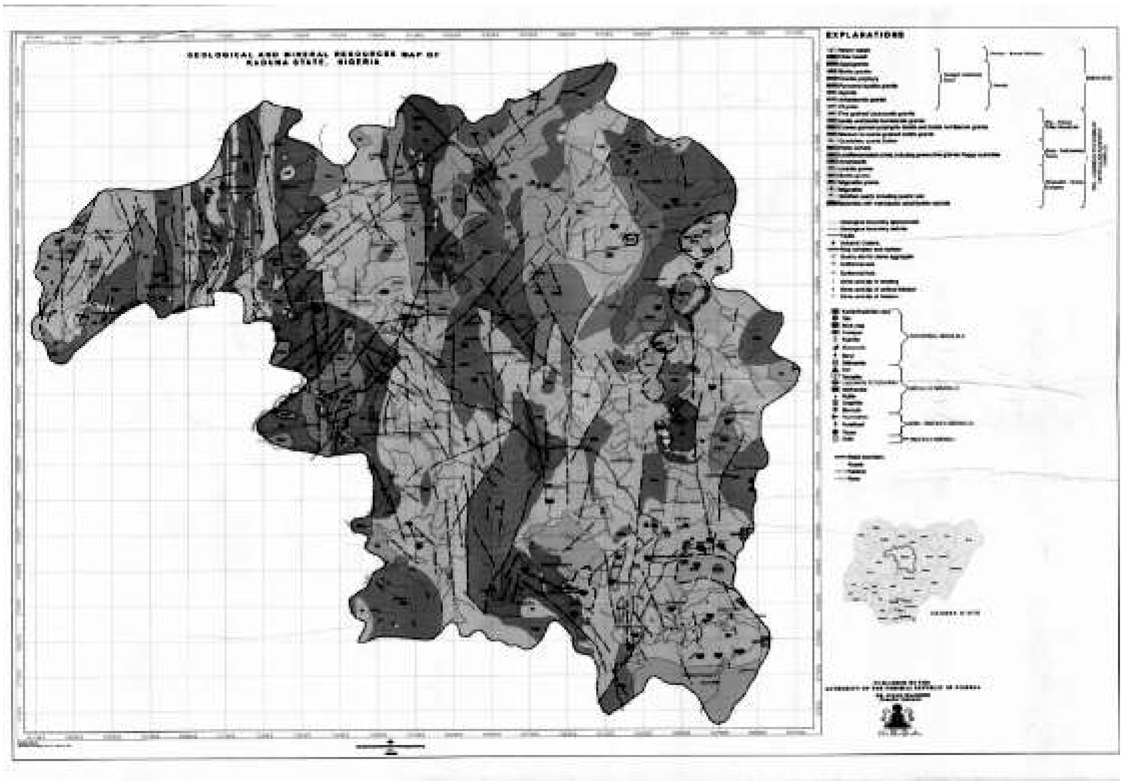
GEOLOGICAL AND MINERAL RESOURCES MAP OF KADUNA STATE, NIGERIA
EXPLANATIONS

Fig. 3: Kaduna State showing the Geology of the study area (NGSA 2007).

Geology of the Area

The study area lies within the Basement Complex of Northern Nigeria (Figure 3). The Basement Complex includes all rocks older than the late Proterozoic (McCurry., 1976) and is composed mainly of gneisses, migmatite, granites, and some extensive areas of schist, phyllites and Quartzites (Baimba.,1978), (Perez and Barber.,1965) according to (McMCurry.,1976).The whole Basement has been through at least two tectonic-metamorphic cycles and consequent metamorphism, magnetization and granitisation have extensively modified the original rocks so that they generally occur as relict rafts and xenoliths in migmatite and granites. Two groups of granites are present and these are the Older Granites and the Younger Granites. The Older Granites are Widespread and often give rise to smoothly domed hills which typically rise to about 170 m above the surrounding plains.(Russ.,1957).The Younger granites which include granites, syenites and rhyolites cover extensive areas in the plateau.

The area lies entirely within the Basement Complex of Northern Nigeria (Figure 3). The rocks consist of series of granites, gneisses, migmatite, low-grade schist, quartzite and amphibolites that have been grouped by the British authors as “Basement Complex of the Precambrian age” (Olugboye., 1975). The topsoil varies in composition, colour and texture at most places. They are predominantly laterite and quartz grains (deep browns or reddish brown soil). Geophysical investigation reports of (Eduvie., 2005) and (Dan –Hassan., 1999) showed that Kaduna is underlain by 3 to 5 geologic layers; the top lateritic soil, clayey sand/sandy clay, weathered transition zone, the fractured bed rock and the fresh bedrock. Geophysical investigation and borehole drilling reports have clearly established two major aquifers. These are the overburden weathered aquifer and the fractured crystalline aquifer (Dan-Hassan and Olarufemi.,1999) at some locations these aquifers are interconnected and form a hydrogeological unit of water table surface.

Pre-drilling Geophysical Investigation

A total spread of 100 m was covered with maximum current electrode separation (AB/2) of 50 m. An *ABEM SAS 1000 Terrameter*was used for the electrical resistivity survey. Schlumberger electrode configuration was used for the pre-drilling geophysical survey. The array consists of 2 current (C_1 and C_2) and 2 potential (P_1 and P_2) electrodes (Fig 4). It works under the principles of the wider the current electrodes, the deeper the current penetration (Olasehinde and Awojobi, 2004). The interpretation of the field data using WinResist Computer softwares were used to obtain of the apparent resistivity values (Annor et al., 1990; Edet and Okereke, 1997).

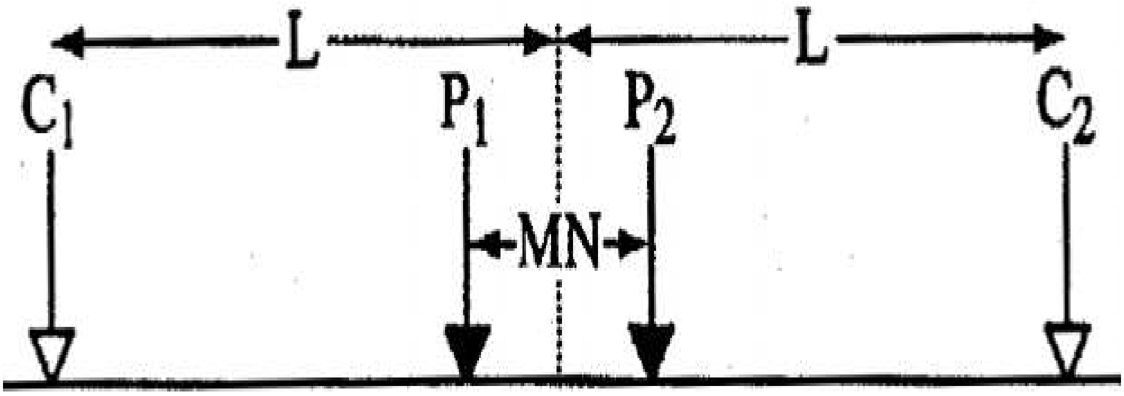

Fig. 4: Schematic Diagram of Schlumberger Array

Results and Discussion

Two different categories of model curve types were identified in the study area. The first category is those with four layers which represent about 60% of VES curves (Fig. 5) while the second category consists of three layers, which representing about 40% of the sounded points within the study area (Fig. 6). The geo-electric sections with the 4 layer show topsoil or laterite, wheathered/ fractured basement and fresh basement (Fig. 5) while the the 3 layer curves shows laterite, fractured basement and fresh basement rocks (Fig. 6). The subsurface lithology varies from place to place within the study area and the finding conforms to the work done other researchers (Olorunfemi and Olayinka, 2002; ***Osazuwa, I. B., &Abdullahi, N. K. (2008). Dan-Hassan, M. A., &Olarinfemi, M. O. (1991).***

More so, the geo-electric sections of the study area (Fig. 7 and Fig. 8) show that the subsurface lithology of the area is not uniformly distributed. Area with thick regolith materials shows great potential for groundwater exploitation (Ako, 1996). The regolith are a product of weathering which induces the geological materials to be porous and permeable, which qualifies them as aquifers, since they can store and transmit groundwater in economic quantity (Amadi et al., 2012; Momoh et al., 2012).

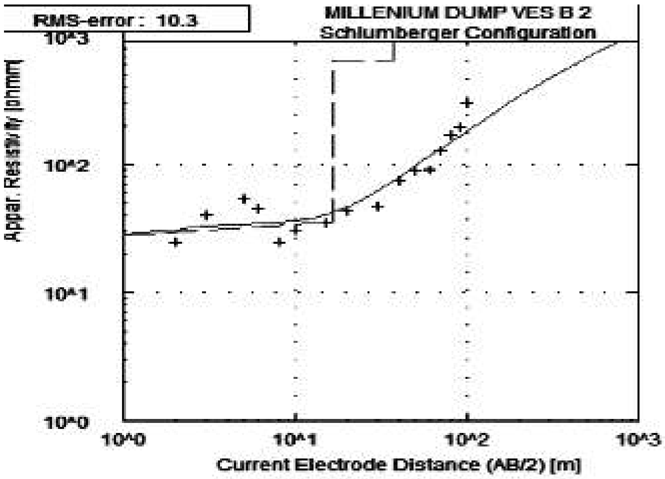

No	Res	Thick	Depth
1	27.3	0.7	0.7
2	35.3	15.7	16.4
3	654.7	21.1	37.5
4	1877.9	-.-	-.-

Fig.7: A typical VES curve for 4 layer system in the area

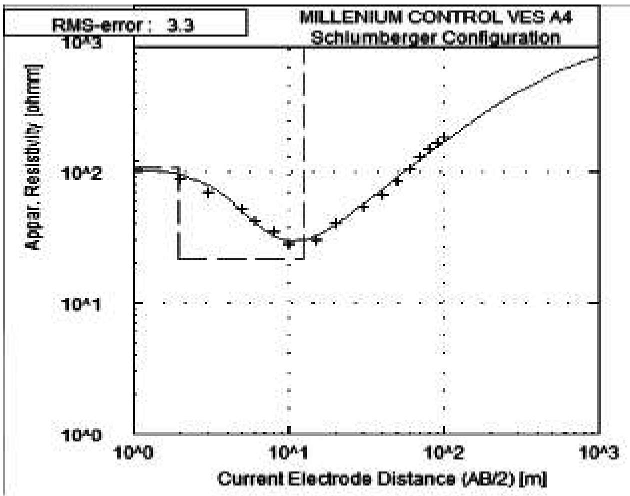

No	Res	Thick	Depth
1	106.8	2.0	2.0
2	21.5	10.5	12.5
3	1095.9	-.-	-.-

Fig. 8: A typical VES curve for 3 layer system in the area

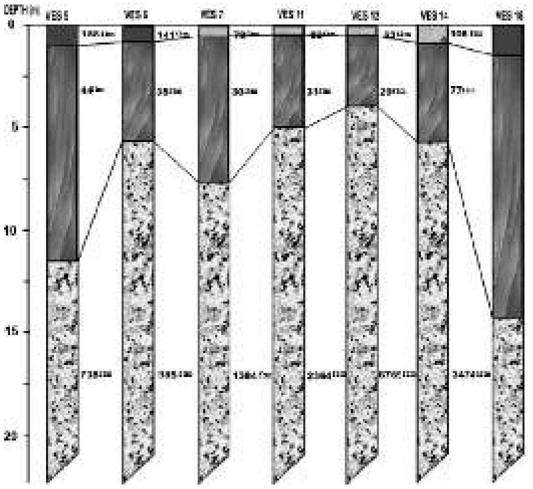

Fig 7: Geoelectric Sections for 3 Layer System

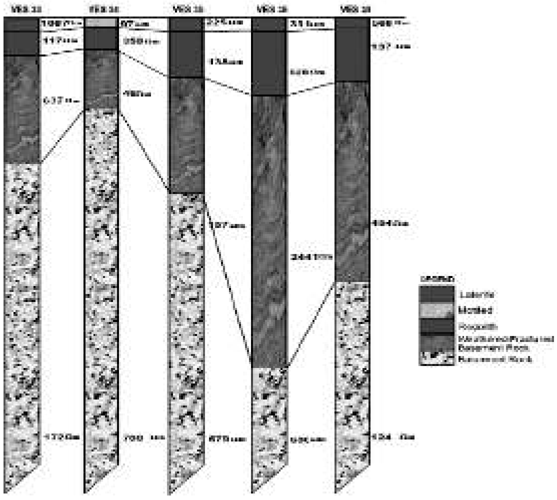

Fig. 8: Geoelectric System for 4 Layer System

Isoresistivity and Isopach maps of a three layer model curves

From the isopach map of regolith thickness for three layered curves (Fig. 9), it can be established that the northern portion of the area shows deep/thick overburden/regolith thickness, while south-western portion shows shallow overburden. This corresponds to the isoresistivity map, as the shallow overburden materials are seen around the ridge which shows lower resistivity values. The thicker the overburden materials the better chance for groundwater storage and this implies that the northern sector correspond to groundwater recharge zone while the southern portion are areas of groundwater discharge. The average thickness of regolith/overburden materials for the three layered curve is about 11m.

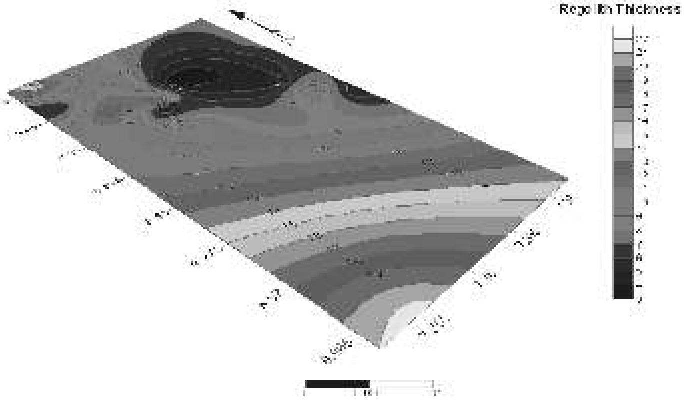

Fig. 9: Isopach map of regolith thickness for three layered model curves

The isoresistivity map of the three layer model curves indicates that the resistivity value is lower at the northern portion of the area compared to the southern portion of the area (Fig. 10). From the countour map the area with higher resistivity values indicate presence of no water or conducting materials while lower resistivity values are indicative of a thick overburden. For the 3 layer system, the weathered/fractured zone is the second layer which is regarded as the regolith aquifer zone (Amadi et al., 2015b; Olasehinde et al., 2016). It is characterized by low resistivity values (high conductivity) compared to the first and third layers as illustrated in Fig.10.

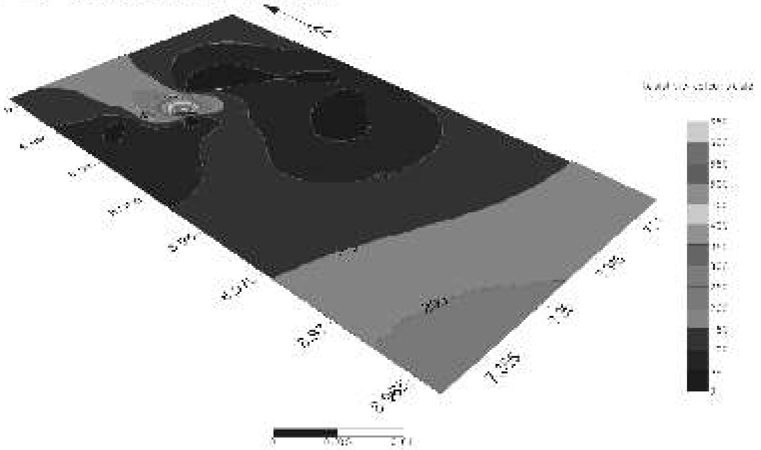

Fig. 10: Isoresistivity map of three layered model curves

Conclusions and Recommendations

The study aimed at investigating the groundwater potential of the Millennium City Housing Estate, Kaduna State, Nigeria using Vertical Electrical Sounding of the Electrical Resistivity method. The study became necessary due to the increase in population of the area. A total number of 40 VES points were conducted and the data obtained were analysed through curve matching and computer software. The area comprises of both 3 layer and 4 layer system. The 3 layers were predominantly H-type curve while the 4 layer system was mainly HA-curve type and are typical of the basement complex terrain. The field data, geoelectric section, isopach and isoresistivity maps of both the 3 and 4 layer model curves show that the northern parts of the study area correspond to recharge zone due thickoverburden materials which pave way for groundwater while the southern portion are areas of groundwater discharge as a result of low thickness of the overburden materials. The average thickness of regolith/overburden materials for the three layered curve is about 11m. A total drill depth of 40 to 55 m was recommended for optimum groundwater yields in the area.

References

Aiyegbusi, M.N. and Akujieze, C.N. (2010).Aspect of Geophysical Exploration for Groundwater using VES in Delta North District. Journal of African Sciences, 7(2), 61-68.

Annor, A. E., Olasehinde, P. I. and Pal, P. C. (1990). Basement Fracture Patterns in the Control of Water Channels – An example from Central Nigeria. Journal of Mining Geology 26(1), 5 -11.

Ako, B. D. (1996). An Integration of Geophysical and Geological Data in Damsite Investigation-The Case of Opa Dam. Journal of Mining and Geology, 13 (1), 1-6.

Amadi, A. N., Olasehinde, P. I., Okoye, N. O., Momoh, O. L. and Dan-Hassan, M. A. (2012). Hydrogeophysical exploration for groundwater potential in Kataeregi, North-Central Nigeria. International Journal of Scientific Research, 2(1), 9 – 17.

Amadi, A. N., Ameh, M. I., Idris-Nda, A., Okoye, N. O. and Ejiofor, C. I. (2013). Geological and Geophysical Investigation of Groundwater in parts of Paiko, Sheet 185, North-Central Nigeria. International Journal of Engineering Research and Development, 6(1), 1 – 8.

Amadi, A. N., Olasehinde, P. I., Ameh, I. M., Okunlola, I. A. and Dan-Hassan, M. A. (2015b). Investigating the groundwater potential at the Boys Hostel, Bosso Campus, Federal University of Technology Minna, using electrical resistivity method. Water Resources, Journal of the Nigerian Association of Hydrogeologists, 25(1&2), 92– 107.

Baimba, J.I. (1978). Electrical resistivity tomography applied to geologic, environmental and engineering investigation at a former waste-disposal site. Geophysics. 71.6. B231:B339

Breusse., G. (1963).Detection of Groundwater contamination near waste disposal sites with Electromagnetic methods Geotech.Envviron.Geophys.73-79 *11.S.E.G.*

Dan-Hassan,M.A. & Olarinfemi, M.O. (1991).Hydro-geohysical investigation of a Basement Terrain in the North-Central part of Kaduna State, Nigeria. Journal of Mining & Geology.Vol 35 (2). 18206

Edet, A.E. and Okereke, C.S. (1997).Assessment of Hydrogeological Conditions in Basement Aquifers of the Precambrian Oban Massif, Southeastern Nigeria. Journal of Applied Geophysics, 36, 95-204.

Eduvie, M.O.(1998). Groundwater Assessment and Borehole characterization: Case study from parts of Kaduna Metropolis (Kaduna State). Paper presented at workshop organized by Kaduna StateWater Board.

National Teachers Institute.

Eduvie, M.O.(2005).Exploration, Evaluation and Development of groundwater in Southern Kaduna State, Nigeria: unpublished PhD thesis, Department of Geology, A.BU, Zaria.

Frohlich, M.O., (1974). Assessment of Groundwater Potentials of Abuja Environs. 29th WEDC International Conference Abuja, Nigeria, 2003 towards the millennium development goals, 185-187.

Ikpokonte, A.E. (2010). Assessment of Groundwater Potential of Crystalline Aquifer for Gidanwaya and its Environs, Southern Part of Kaduna State, Northwest Nigeria. Journal of African Earth Science, 7(8), 66-71.

Mbonu, P.D.C., Ebeniro, J.O., Ofoegbu, C.O. and Ekine, A.S. (1991).Geoelectrical Sounding for the Determination of Aquifer Characteristics in Part of Umuahia Area of Nigeria. Journal of Geophysics, 56, 284-291.

McCurry, P. (1976). The Geology of Precambrian to lower Paleozoic rocks of Northern, Nigeria–A review in: Kogbe, C.A (Ed) Geology of Nigeria-Elizabeth and Published co. Lagos. 436pp.

Momoh, O. L., Amadi, A. N., Abdulfatai, I. A., Omananyi, Y. A., Onoduku, U. S. and Onah, M. (2012). Exploration of groundwater within the Mariam Babangida Girls Science Secondary School, Minna, Northcentral Nigeria using Schlumberger vertical electrical sounding techniques. Journal of Science, Technology, Mathematics and Education, 8(3), 21-32.

Ministry of Environmental and Natural Resources Kaduna. (2016). The Nigerian Climate Records. Unpublished Report, 26-28

Nigeria Geological Survey Agency (NGSA, 2006.): Generalized geological map of Nigeria.

Geological Survey of Nigeria Bulletin.39:46

Olugboye, N.O. (1975). Hydrogeology of Kaduna Town. G.N.S Report No 1539.

Olasehinde, P.I. and Awojobi, M.O. (2004). Geological and Geophysical Evidences of a North South Fracture System, East and West of the Upper Gwiara River in Central Nigeria. Water Resources, 15, 33-38.

Olasehinde, P. I., Amadi, A. N., Enwedo, E. O., Dan-Hassan, M. A. and Okunlola, I. A. (2016). Assessing the Groundwater Potential in Wuye District, Federal Capital Territory, Abuja, Nigeria. Development Journal of Science and Technology Research, 5(1), 67 – 78.

Olorunfemi, M.O. & Olayinka, A.I. (2002). An integrated used of geoelectrical imaging and hydrogeochemical methods in delineating limits of polluted surface and groundwater at a landfill site in Ibadan area, Southwestern Nigeria. Journal of Mining and Geology. 37.1:53-68.

Osazuwa, I.B. & Abdullahi, N.K.(2008). 2-D Electrical Resistivity and Induced Polarisation Investigation at an open solid Waste Dump site: Case Study from Kaduna North Central Nigeria, Journal of Environmental Hydrology. 16(29)1-11

Olorunfemi, M.O. and Okakune, E.T. (1992). Hydrogeological and Geological Significant of Geoelectrical Survey of Ile-Ife. Nigerian Journal of Mining and Geology, 28(1), 221 – 222.

Omeji, M., Husin, W., Noorddin, I., Oha, I.A., Onwuka, O.S., Ugwuoke, P.E. and Meludu, O. (2013).Geoelectrical Investigation of **Aquifer** Problems in Gosa Area of Abuja, Northcentral, Nigeria.
International Journal of Physical Sciences, 8(13), 549-559.

Perez, J. W. & Barber, M. (1965). Distribution and chemical quality of groundwater in northern Nigeria; Geological Survey of Nigeria Bulletin, 36

Russ, D. M. (1957). *The generalised reciprocal method of seismic refraction interpretation.* Society of Exploration Geophysicists, Tulsa. 53, 345-352

DELINEATION OF POTENTIAL GROUNDWATER AQUIFER ZONES AROUND OFFA, SOUTHWESTERN NIGERIA USING SURFACE GEOPHYSICS

Ologe Oluwatoyin[1] **and Abdulsalam N. Nasir**[2]
[1]Department of Applied Geophysics, Federal University Birnin Kebbi, Nigeria
[2]Department of Physics, University of Abuja, Nigeria
Email: toyin.ologe@gmail.com

ABSTRACT

Geoelectric survey using vertical electrical sounding technique was carried out in the Central part of Offa, south-western Nigeria in order to explore for ground water potential zones. Thirteen (13) VES was carried out using Schlumberger array configuration with half spacing of AB/2 from 1to 70m.Qualitative and quantitative interpretations involving partial curve matching and computer iteration techniques were used to interpret the resistivity data acquired from the study area. Results showed that there are four major layers (top soil, sandy/clay, fracture/weathered and bedrock) which described the lithological units of the study area. The resistivity values and their thickness ranges from; topsoil with resistivity and thickness values (7.68-2629Ωm and 0.4m-1.15m); sandy/clay (14.2-1279Ωm and 1.14-6.75m); fractured/weathered (5.41-415Ωm and 16.3m-33m) and bedrock (1724-∞and 34m-∞) for the first, second, third and fourth layers respectively. The most prolific layer among these is the third layer which consist of the fractured/weathered materials at the depth of 16.3 m to 33m. The groundwater potential map shows that the central and northern part has high groundwater potential, while the south-eastern and south-western part has low groundwater potential.Therefore, the groundwater potential of the central and northern part of the study area could be classified as zones where water can be maximally exploited while south-eastern and south-western parts of the study area can be classified as low groundwater potential zones. The electrical resistivity data therefore gives reasonably accurate results among other methods that can be used to understand the subsurface layers and basement configuration in groundwater prospecting.

Key words: *Electrical resistivity, fractured/weathered basement, groundwater potential, aquifers and vertical electrical soundings.*

Introduction

The global importance of groundwater as a major source of freshwater for agricultural and domestic uses cannot be over-emphasized (Oladeji *et al.,* 2012). Ground water refers to the water found in the pore spaces, crevices and rocks below the surface of the earth. Groundwater is usually extracted from the subsurface through a well or borehole drilled to the aquifer. An aquifer can be defined as a saturated water bearing stratum that is capable of holding, transmitting and yield sufficient water in underground to well (Sharma and Sharma; 2007). Geophysical investigations of the interior of the Earth involve taking measurements at or near the Earth's surface that are influenced by the internal distribution of physical properties and analysis of these measurements can reveal how the physical properties of the Earth's interior vary vertically and laterally (Keary*et al.,*2002).

Many dug wells that were sunk in the study area without an initial proper investigation failed and so were abandoned. There are several reasons for the failure of boreholes and these include inadequate or lack of pre drilling investigation, lack of expertise on the part of personnel handling the drilling and sometimes lack of proper development of a successfully dug hole. There is no doubt that going by the observation of many areas in Offa, there is evidence of limited availability of groundwater to the people. However, the presence of government institutions and establishments had led to the influx of people into the city thereby making the city to be densely populated. The resulting increase in population has greatly stressed the groundwater resources, hence the need for this study.The search for ground water is faced with lots of uncertainties; to minimize or avoid failures altogether, it is pertinent that the right exploration techniques are utilized in the delineation of subsurface water-bearing formations (Coker *et al.*, 2009). The objective of this study is to use the Vertical Electrical Sounding method to delineate the groundwater potential aquifers in the study area.

Physiography, Geology and Hydrogeology

The study area is located along the Ajase Ipo-Erinle roadway which falls within transitional zone of semi-arid north and humid coastal belt of Nigeria (Okeola, 2009). It lies between 100% bordered by Oyun Local Government. It is between latitude 4.62° - 4.74° N and longitude 8.11°-8.22° E covering a total area of about 1.97km^2 and bordered by Oyun (Figure 1).

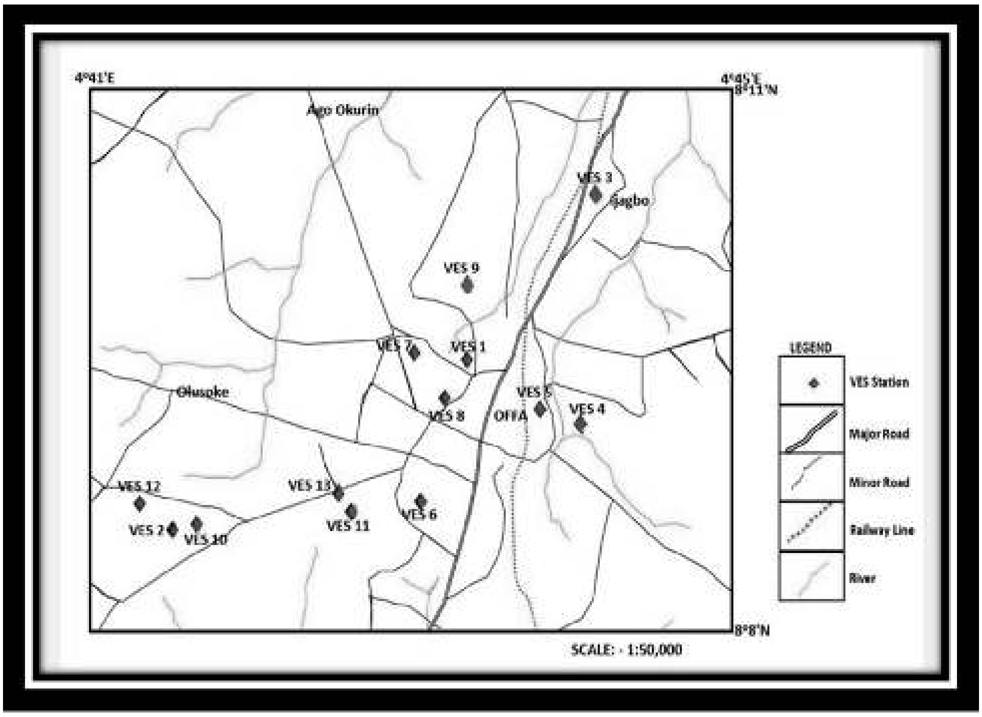

Figure 1: Location Map of the Study area Showing VES Stations

The terrain in the study area is mainly plain lands, with topographic elevation ranging from 393m to 410m above sea level. The area is traversed by the river Osin. The area is situated within the Savannah area, with a climate characterized by dry and wet seasons. Annual rainfall ranges between 1000 and 1500 mm with average temperature varying between 14.3^{0}c and 33^{0}c (**Iloeje, 1980)**. The vegetation is wooded savannah which includes; scattered trees,shrubs and tall grasses typical of savannah areas.Rock types in the area are poorly exposed and mostly covered by soil zone. The bed rock lies beneath an overburden of in-situ weathered basement (Adelana*et al.,* 2004) which are now sands and clays interspersed with lateralized superficial quaternary deposits. The area is generally underlain by the laterite formation, which is separated from the basement rocks by a lithomarge zone (clay zone above the bedrock).the soils are the red laterite type containing a high amount of gravels. The soils in most parts of the area are well drained and are reddish brown in colour. Generally, the water table is shallow, with poor drainage and the soils dry out less frequently.

Materials and Methods

Thirteen Vertical Electrical Sounding data were acquired and evenly distributed(Figure 2)within study area and the data were displayed (Tables 2.1). Interpretation of data were done quantitatively and qualitatively and bringing in to bare the knowledge of the local geology of the area. The apparent resistivity values were plotted against half the current electrode spacing on a log-log graph. The curves of best fit were then traced and the data obtained from the smooth curve (Smoothed values) were noted. Qualitative and quantitative interpretations of the field curves were carried out by inspection to obtain the type of curves and by partial curve matching respectively. The resistivity and thickness obtained from the partial curve matching were improved upon by employing an iterative computer program following the main ideas of (Zohdy *et al.*, 1974) to obtain the layers parameter (resistivity, thickness and depth) (Table 2.1)Here, the number of geoelectric layers and their corresponding specific resistivities were first taken to be equal to the number of measurable points and difference of adjacent current electrode spacing respectively. Layer parameters were consequently modified in iterative manner until subsequent iteration yields no improvement on the root mean square (rms) error values in percentage. From the preliminary interpretation, initial estimates of the resistivity and thickness of the various geoelectric layers at each VES location were obtained. These geoelectric parameters from the manual curve matching were later used as a starting model for a fast computer-assisted interpretation (Velpen, 1988). The algorithm takes the manually derived parameters as the starting geoelectric model, successively improved on it until the error is minimized to an acceptable level and the resulting layer parameters were then given geologic interpretation.

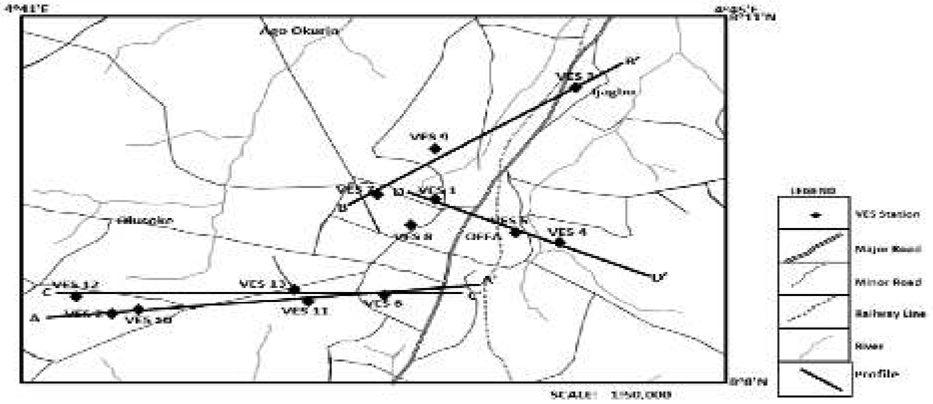

Figure 2:Data Acquisition map showing the profiles and VES points

Discussion of Results

The VES data (Table 2.1) were processed using IP2Win. Some of the field and modeled curves obtained revealed 4-layered case (figure 3)

The geoelectric sections (Figure 3.2a & 3.2b) were generated from the geoelectric parameters as obtained from the resistivity sounding curves. The depicted 4-layered earth modeled include: topsoil with resistivity and thicknesses ranging from 7.68-2629Ωm and 0.4 m to 2.04 m.

The second layer is sandy clay which may probably contains lateritic soil of varying saturation which is obvious from its resistive behavior. This layer has a minimum resistivity values from 14.2Ωm to 1279 Ωm with thickness from 1.14m to 6.75 m.

The third layer delineated is the weathered/fractured layer. The apparent resistivity and thickness of this layer varies from 5.41Ωm to 415Ωm and from 16.3 m to 33.3 m respectively. Fractured crystalline bedrock aquifers are good sources of potable water in many parts of the world (Olayinka and Barker,1990; Olayinka *et al.,* 1997; Ariyo and Adeyemi, 2009; and Ologe *et al.,* 2014).

The fourth layer is the fresh basement which has an apparent resistivity value varying from 1724- ∞). Depth to the bedrock ranges from 34m- ∞ across the study area. The geoelectric section were plotted along four profiles (AA', BB', CC' and DD') (Figure 2) with variation in lithology from one point to another (Figure 4a and 4b).The topsoil and lateritic layer have thicknesses generally less than 2m. The two layer almost thin out in some places. On the contrary, the thickness of the weathered layer is fairly constant and generally greater than 15 m in the study area. Also, along profile AA', the surface the weathered basement is undulating probably due to the topography of the basement.

Isoresistivity Maps

The isoresistivity maps are presented in Figures 5a and 5b.The isoresistivity maps of the top soil shows that the resistivity of this layer decreases from the western to eastern part of the study area. This might be due to the presence of lateritic materials. The resistivity of the weathered/fractured basement which forms the aquifer is generally above 200 Ωm in the southeastern and southwestern parts and generally below 150 Ωm in the central and other parts of the study area. Groundwater yields vary with aquifer resistivity (Emmanuel *et al.,* 2011).

Isopach Maps

The Isopach of the aquifer in the study area indicate that the aquifer thickness is generally above 22m in the study area (Figure 6a).An exception to this occurs at the eastern and southwestern part of the study area where the aquifer thickness is less than 22 m. The Isopach map of the overburden is the total thickness of all materials (aquifer and other layers) overlying the fresh basement rock. The overburden thickness increases progressively from the western part toward the eastern part of the study area. Hence, the overburden is thicker at the eastern portion of the study area (Figure 6b).

Basement Relief and Groundwater Potential Maps

The basement relief map shows the topography of the basement as estimated from the calculated depth to basement at various VES points (Figure 7a). The bedrock relief map of the study area was produced by removing the overburden thickness contour values from the elevation iso-contour values (Figure 7b). The map reflects the topography the bedrock underlying the area. The map shows that the basement structures in the area include both basement ridges and depressions

Table 2.1: Showing the apparent resistivity data obtained from the vertical electrical sounding (VES) carried out in the study area

AB/2 (m)	MN/2 (m)	GEOMETERIC FACTOR (K)	VES1 ρ(Ωm)	VES2 ρ(Ωm)	VES3 ρ(Ωm)	VES4 ρ(Ωm)	VES5 ρ(Ωm)	VES6 ρ(Ωm)	VES7 ρ(Ωm)	VES8 ρ(Ωm)	VES9 ρ(Ωm)	VES10 ρ(Ωm)	VES11 ρ(Ωm)	VES12 ρ(Ωm)	VES13 ρ(Ωm)
1	0.5	2.36	531	104	372	80.34	160	286.7	36.3	511	180	96	271.4	51.45	80
2	0.5	11.8	235.3	104	185	67.61	40	506.2	69.51	523	200	147	451.94	53.81	75
3	0.5	27.8	150.7	127	159	61.63	50	614.4	58.08	525	230	154	556	66.72	60
4	0.5	49.48	90.99	142	138	54.99	58	657.1	28.36	600	250	136	543.79	79.66	50
6	0.5	112	71.12	106	112	38.6	57	604.8	21.62	654	196	133	483.84	98.67	35
6	1	55	46.04	116	165	92.67	47	634.7	22.34	666	180	124	442.3	91.36	34
8	1	99	32.27	137	148	66.17	52	503.9	19.11	711	140	130	375.21	111.47	28
10	1	156	34.63	121	103	54.56	53	377.5	17.98	554	100	131	313.56	117.63	27
10	2.5	58.9	39.58	166	157	70.36	42	384.6	4.34	565	95	136	305.1	98.3	26
15	2.5	137	35.76	198	171	105.6	52	166	4.95	525	85	125	200.84	118.78	27
20	2.5	245	43.12	129	174	150.14	74	79.63	18.37	480	90	90	119.56	122.02	25
25	2.5	388.82	58.32	350	243	178.7	112	68.56	16.14	444	100	99.7	66.32	138.42	35
30	2.5	562	57.32	401	281	183.55	150	91.01	33.79	523	110	110	53.05	152.86	40
35	2.5	765	60.44	533	254	118.75	132	88.83	20.24	567	128	96	52.3	170.6	42
40	7.5	1001	64.06		307		200	112.1		589	129	156.41	75.26	196.2	58
40	7.5	323	62.34		484			136.5		623	134	110	93.49		66
45	7.5	412.4	70.52		412			162.2		654	127	121	145		100
50	7.5	512	80.38		248			186.1		712	126	140	136.89		120
60	7.5	742	96.46					192.2					133.93		
70	7.5	1014	114.6					194.7					150.15		
								212					168.96		

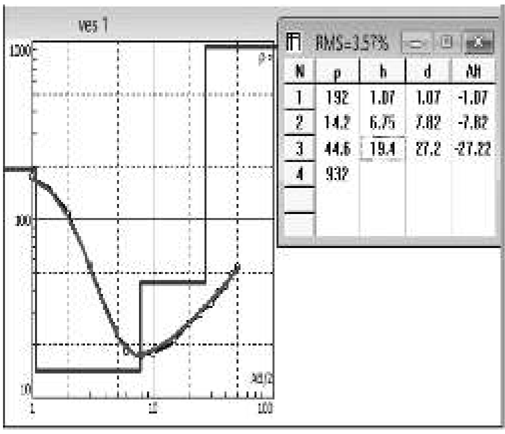

RMS=3.57%

N	ρ	h	d	Alt
1	192	1.07	1.07	-1.07
2	14.2	6.75	7.82	-7.82
3	44.6	19.4	27.2	-27.22
4	932			

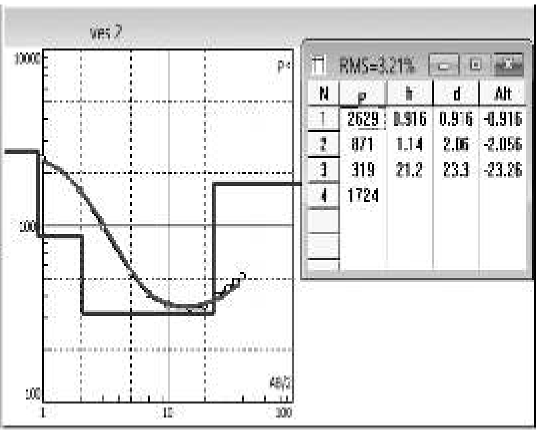

RMS=3.21%

N	ρ	h	d	Alt
1	2629	0.916	0.916	-0.916
2	871	1.14	2.06	-2.056
3	319	21.2	23.3	-23.26
4	1724			

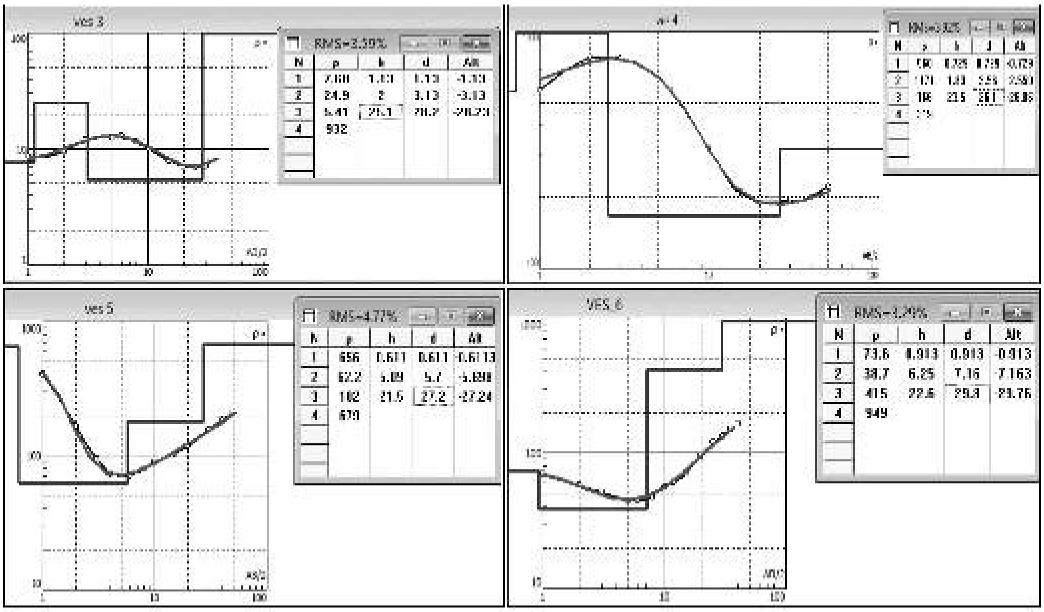

RMS=3.59%

N	ρ	h	d	Alt
1	7.60	1.13	1.13	-1.13
2	24.9	2	3.13	-3.13
3	5.41	21.1	24.2	-24.23
4	932			

RMS=3.32%

N	ρ	h	d	Alt
1	190	0.729	0.729	-0.729
2	121	1.83	2.56	-2.561
3	118	23.5	26.1	-26.06
4	[illegible]			

RMS=4.77%

N	ρ	h	d	Alt
1	656	0.611	0.611	-0.6113
2	62.2	5.09	5.7	-5.698
3	102	21.5	27.2	-27.24
4	679			

RMS=3.29%

N	ρ	h	d	Alt
1	73.6	0.913	0.913	-0.913
2	38.7	6.25	7.16	-7.163
3	415	22.6	29.8	-29.76
4	949			

Figure 3: Typical vertical sounding curves obtained in the study area

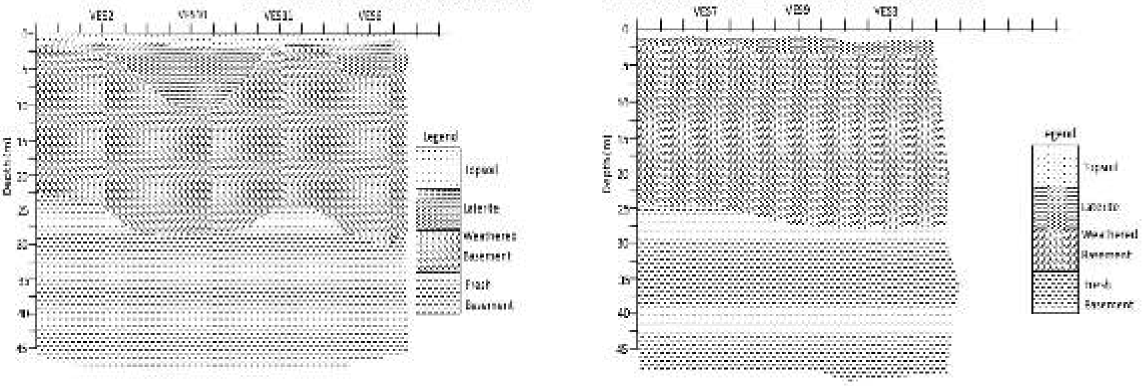

Figure 4a:W-E and N-E Geoelectric Section Embracing VES 2, 10, 11, 6 and 7, 9 and 3 along Profile AA and BB

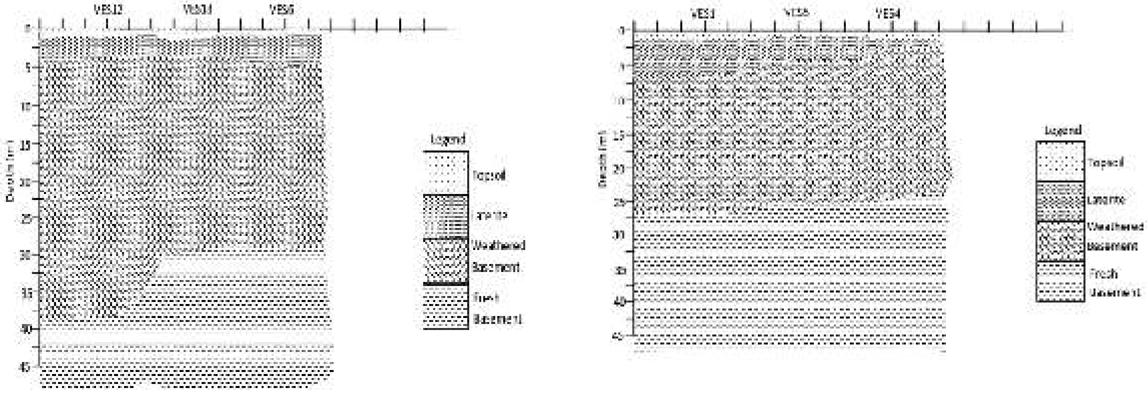

Figure4b: NW-SE and N-S Geoelectric Section Embracing VES 12, 13, 6 and,1, 5 and along Profile CC and DD

The groundwater potential map based on the recommended weighing of aquifer with respect to resistivity in Table 2. From the groundwater potential map (figure 3.5b), the northern part of the study area has maximum groundwater potential with weighing between 9.5-10.1 while the southeastern and southwestern part has minimum groundwater potential with weighing below 4.5.

Aquifer Potential as a Function of Saprolite Resistivity (Olayinka *et al.*, 1997)

Saprolite Resistivity (Ω-m)	Aquifer characteristics	Weighting	VES location
<20	Clayey; limited aquifer potential	7.0	VES3
20-100	Optimum weathering and groundwater potential	10.5	VES1, VES7, VES9, VES10,VES12, VES13
100-150	Medium aquifer conditions and potential	7.5	VES11
150-300	Limited weathering and poor potential	5.0	VES4, VES5, VES8
>300	Negligible	2.5	VES2, VES6

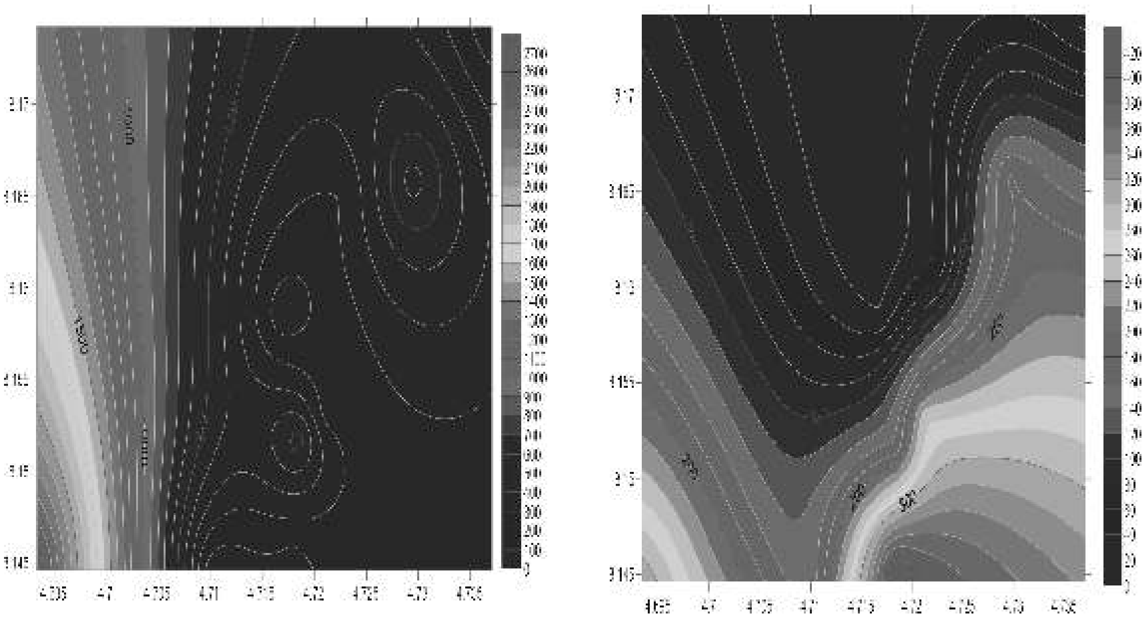

a b

Figure 5a and 5b:Isoresistivity maps of the top soil and weathered basement

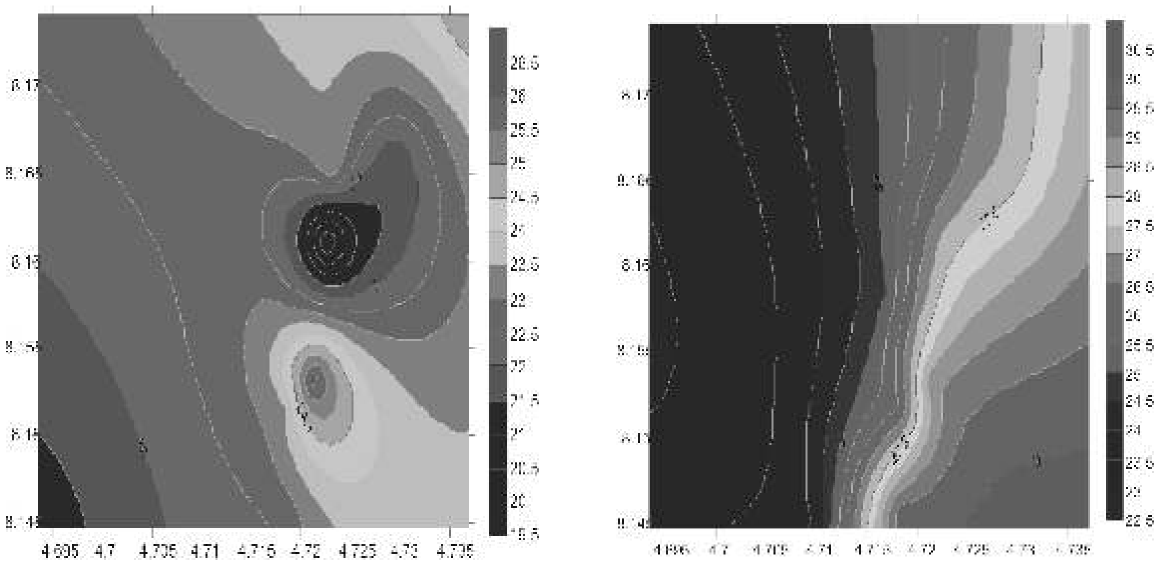

a b

Figure 6a and 6b: Isopac maps of aquifer and overburden

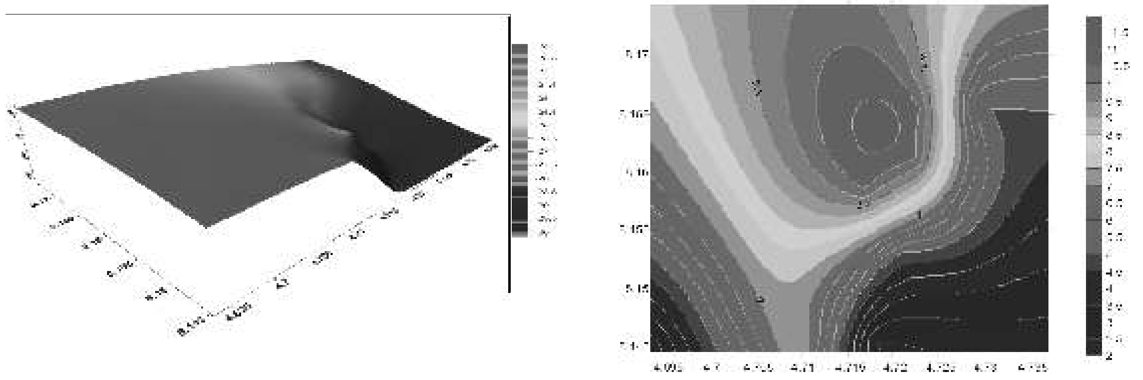

a b

Figure 7a and 7b: 2-D Basement Relief and Groundwater potential Maps of the Study Area

Conclusion and Recommendation

Groundwater potential aquifers producing zones have been delineated through investigation conducted by the electrical resistivity survey. Weathered and fractured horizons have been identified in the study area underlying VES stations, and all of these constitute the aquifer zones. Good prospects therefore exist for groundwater development in the study area where the depth to basement is relatively thick and has favourable low resistivity, while those with thin depth to bedrock and high resistivity value have a lower potential for an aquifer.

The productive groundwater potential zones are identified at the central and northern part, and as subordinately at the southeastern and southwestern part of the study area. The electrical resistivity as a surface geophysical method therefore gives reasonably accurate results among other methods that can be used to understand the subsurface layers and basement configuration in groundwater prospecting.

References

Adelana, S.M.A., Olasehinde,P.I. and Vrbka, P. 2004. Identification of groundwater recharge conditions in crystalline basement rock aquifers of the southwestern Nigeria. In: Special Volume UNESCO – ISMAR Publication, UNESCO, Paris.

Alabi, A.A., Bello, R., Ogungbe, A.S. and Oyerinde, H.O. 2010. Determination of groundwater potential in Lagos State University, Ojo; using geoelectric methods (vertical electrical sounding and horizontal profiling), Report and Opinion, 2(5), 68-75.

Ariyo, S. O. and Adeyemi, G. O. 2009. Role of electrical resistivity method for groundwater exploration in hard rock areas. A case study from Fidiwo/Ajebo areas of South-western, Nigeria. *Pacific Journal of Science and Technology*.10 (1), 483 –486.

Coker, J.O., Makinde, V. and Olowofela, J.A., 2009. Geophysical Investigation of Groundwater Potentials of Oke-Badan Estate, Ibadan, Southwestern, Nigeria. Proceedings of 3rd International Conference on Science and National Development University of Agriculture Abeokuta, 2nd-6th Oct., Pp 119.

Emmanuel, O. J., Olayinka, A.I. and Oladotun, O. F., 2011. Geoelectric investigation of the groundwater potential of Moniya Area, Ibadan. *Journal of Geology and Mining Research*, 3(3), 54-62.

Keary, P., Brooks, M. and Hill, I., 2002. An Introduction to Geophysical Exploration (3rd Edition). Blackwell Science Ltd. Pp. 281.

Iloeje, N.P 1980. A new geography of Nigeria (New Revised Edition) published by Longman Group, pp 32-45.

Olayinka, A. I. and Barker R. D. 1990. Borehole sitting in crystalline basement areas of Nigeria with a microprocessor controlled resistivity traversing system. Groundwater 28(6), 178 –183.

Olayinka, A. I., Akpan, E.J. and Magbagbeola, O.A., 1997: Geoelectric Sounding for Estimating Aquifer Potential in the Crystalline Basement Area around Shaki, South-Western Nigeria. *Water Resources- Journal of Nigerian Association of Hydrogeologits*. 8(2), 71-81.

Ologe, O., Bankole, S. A. and Adeoye, T. O., 2014. Geoelectric Study for Groundwater Development in Ikunri Estate, Kogi West, Southwestern Nigeria. *Ilorin Journal of Science*, 1(1); 154 – 166.

Oladeji, O.S, Adewoye, A.O and Adegbola, A., 2012. Suitability assessment of groundwater resources for irrigation around Otte Village, Kwara State, Nigeria. *International Journal of Applied Sciences and Engineering Research*, 1(3): 437-445.

Okeola, O. G. 2009. Development and application of multicriteria decision support models for sustainable operation of an urban water supply system. Ph.D. Thesis, Department of Civil Engineering, University of Ilorin. Nigeria.

Ralph, C. H., 1987. Basic Groundwater Hydrology, U.S. Geological Survey Water Supply paper 2220: Pp 4-5.

Sharma, R. K. and Sharma, T.K., 2007. Irrigation engineering including hydrology. S. Chand and Company Ltd, New Delhi.3rd Edition, Pp. 7 – 45.

Vander Velpen, B. P. A., 1988, Resist Version 1.0M.Sc Research Project, ITC, Delf Netherland.

Zohdy, A.A.R., Eaton, G.P., and Mabey, D.R. 1974. “Application of Surface Geophysics to Groundwater Investigations”. Techniques of Water Resources Investigations of U.S. Geol. Survey: Book 2, Chapter DI. U.S. Government Printing Office: Washington, D.C. 66.

MEASUREMENT OF SOUND ATTENUATION OF A PETROL GENERATOR IN AN ENCLOSURE

Musa, N. , Aliu, S.O. and Usman, M.
Department of Applied Science,
College of Science and Technology,
Kaduna Polytechnic, Kaduna, Nigeria.
Email: 4u.nasir@gmail.com

ABSTRACT

Beside wrappings, acoustic enclosures represent an efficient way to reduce the radiated noise from portable generator set. Using the passive noise control measure, a double wall acoustical enclosure has been constructed using plywood. A gap or partition was provided for the insertion of sound suppressants. A composite material was also molded from the mixture of sand, sawdust, white cement, glue and water. The work compared the percentage loss of fine sand, sawdust and fine sand composite, foam and sawdust. The generator was run on idle state and with a load of 2kW for three hours uninterrupted. The temperature rise of the engine block was noted for the two cases at an interval of thirty minutes using an infra-red thermometer with a range of –50 ^{0}C – 380 ^{0}C. It was observed that the respective percentage loss for fine sand, composite, foam and sawdust are 48.45%, 41.42%, 45.16% and 44.89% respectively. This means that the fine sand is more effective in attenuating the sound or noise emitted by the portable generator set compared to the rest because of its porosity. The maximum temperature recorded within the enclosure was 176^{O}C which is within tolerable limits for the generator brand used.

Keywords: *Sound, Transmission, Generator, Temperature, Reflection, attenuation, Passive noise, Active noise*

Introduction

There is a considerable body of medical evidence that directly implicate ambient sound levels exceeding 60 – 70dB as 'pollution' that leads to significant health problems. Noise is defined as an unpleasant sound which disturbs the human being physically, psychologically and cause environmental pollution by destroying environmental properties (Henry 2004). Luigi (2004) in his article, The Joys of Noise claims that noise has become so prominent that pure sound no longer exists. Henry (2004) also observes that noise can be perceived either physiologically or psychologically. We perceive noise physiologically when we “hear" it. On the other hand, when we listen to a noise we are doing this psychologically. When we perceive a physiological noise we subconsciously feel the vibrations of the noise (sound) waves with our particles in our physical body whereas psychological noise refers to noise that is perceived when our conscious awareness shifts its attention to that noise rather than letting it filter through our subconscious where it goes unnoticed. It is important to recognize that the term "noise" is also used to refer to other, non-audible forms, especially in electronics and in the radio/radar spectrum. But this work is limited to acoustic or environmental noise. Environmental noise is the comprehensive body of acoustic phenomena in the human environment which involve unwanted sound (Luigi 2004).

SOURCES OF NOISE

The principal sources of environmental noise are surface motor vehicles, aircraft, trains and industrial sources (e.g. power generators, turbine, etc.).These noise sources expose millions of people to noise pollution that creates not only annoyance, but also significant health consequences such as elevated incidence of hearing loss and cardiovascular disease. There are a variety of mitigation strategies and controls available to reduce sound levels including source intensity reduction, land use planning strategies, noise barriers and sound baffles, time of day use of regimens, vehicle operational controls and architectural acoustic design measures (McNamara and Buland 2004).

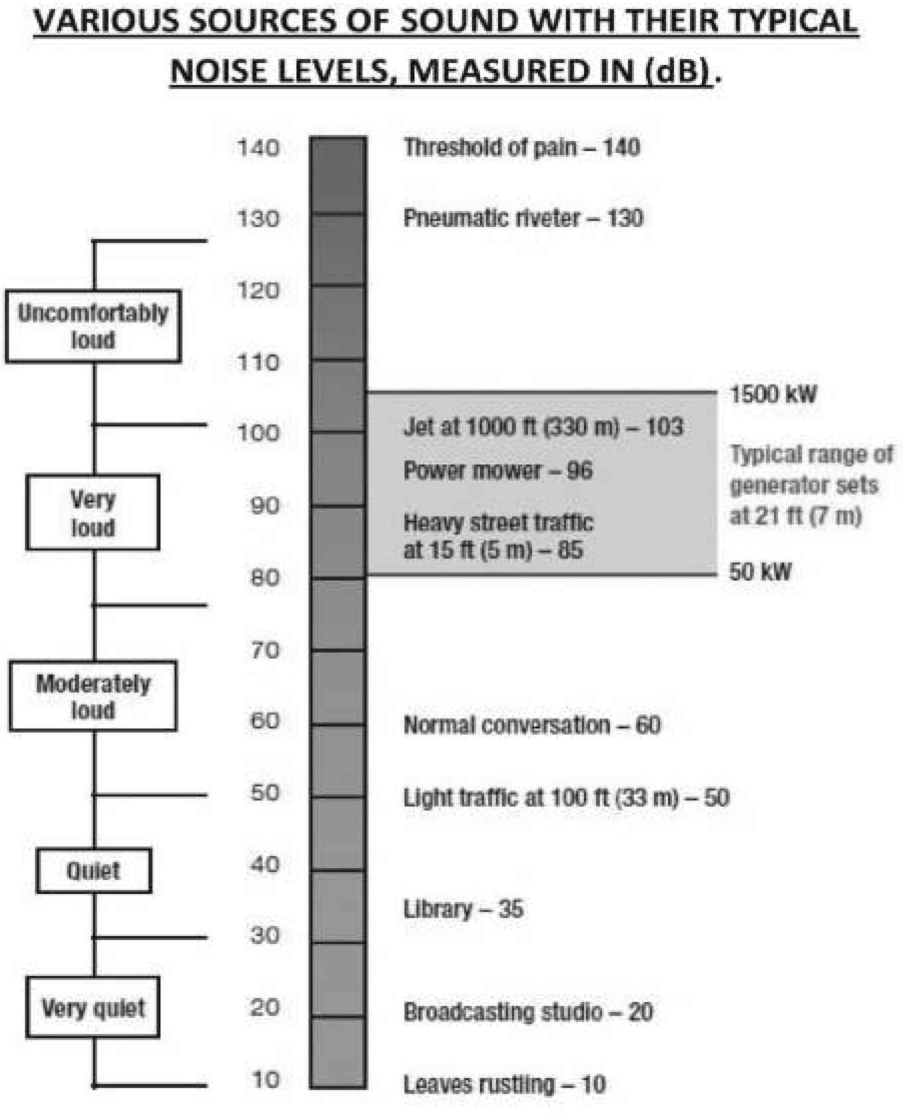

Figure 1: Noise Levels Measured in dB (McNamara and Buland 2004).

NOISE CONTROL MEASURES

There are two general methods which can be used to achieve the required noise levels these are;

Active control: It is a sound field modification, by electro- acoustic means. In its simplest form, a control system drives a speaker to produce a sound field that is an exact image of the offending sound (disturbance). The speaker cancels the disturbance and the net result is no sound at all (Rettinger 1973).

Passive noise control: This noise control treatment includes use of insulation, silencers, vibration mounts, damping treatments, absorptive treatments such as ceiling tiles, and conventional mufflers like the ones used on today's automobiles. Passive techniques work best at medium and high frequencies (Rindel 2005).

ACOUSTIC BARRIERS

Barriers are large panels that interrupt the direct "line of sight" from the noise source to the receiver. Technically, the barrier acts as a reflective surface. The noise is reflected off of the surface and back at the source. An example of these is the barriers seen along highways that "separate" the road from residential areas. Barriers are effective when the noise source or the receiver is too big to enclose in a structure (Beranek 1992).

ENCLOSURE

When the noise source is small enough to permit the construction of barriers on all sides of the source, the barrier effectively becomes an enclosure. Enclosures are used either to contain the noise emitted from a source or to protect a receiver (usually a person) from the noise source. Enclosures are specifically designed structures that reduce the amount of transmitted sound power impinging on the space of interest (Buckingham 1924).

In either barriers or enclosures, passive control is achieved by the use of an acoustic absorbing material or sound reflection. An absorbing material is used in this context to describe the material's ability to attenuate or "absorb" the sound's incident pressure wave, thus reducing the amplitudes of the transmitted and reflected pressure waves. The resulting sound pressure level on the opposite side of the absorbing material will therefore be reduced. The absorbing material is something as simple as a metal or plastic panel, or as elaborate as a multilayered partition which consists of specially engineered acoustic foam, different thicknesses of panel layers, as well as different panel materials. Sound reflection occurs when the acoustic wave is reflected back toward the source by the material. (http://www.dieselservicesupply.com/sound_Attenuated_enclosure. Retrieved 13th Feb.2016)

AIM

To measure the sound generated by a generator in open air and in a sound proof box and hence its insertion loss, the temperature generated by the engine block within a time interval of 3 hrs of uninterrupted running

SOUND TRANSMISSION THEORIES

Much of the interest in the study of transmission loss through panels began in the early 1900's. An elementary theory in transmission loss was published by Buckingham (1924). Where he defined transmission loss as the $\log_{10}$ of the ratio of transmitted to incident pressure waves on a surface. Figure 2, is a representation of incident, reflected and transmitted pressure wave on a surface (wall). This representation is only for normal incidence even though a noise source can produce random incidence on a

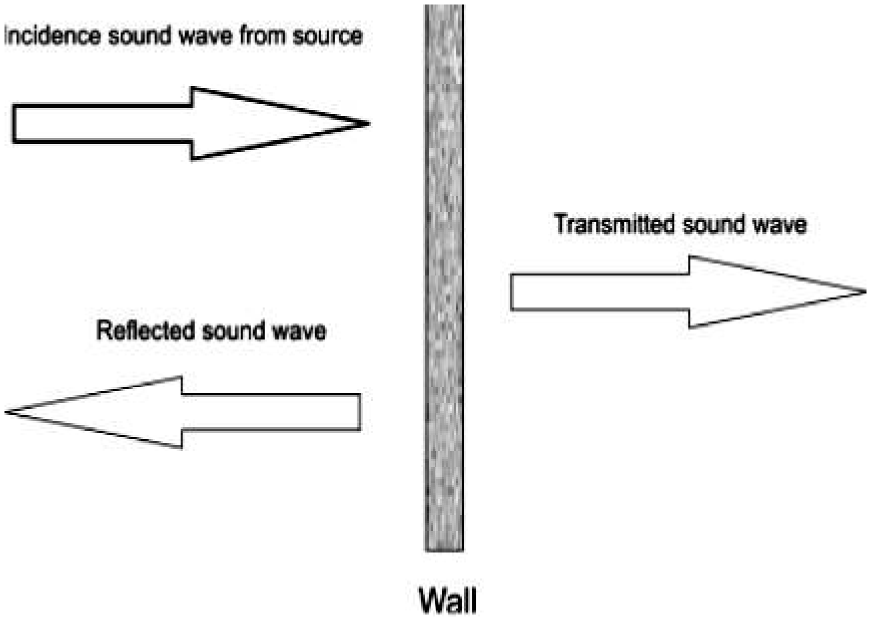

Figure 2: Incident reflected and transmitted pressure wave on a surface. (*Chonan and Kugo 1989).*

BASICS OF MASS LAW

The mass law states that within a limited frequency range, the magnitude of the loss is controlled entirely by the mass per unit area of the wall. The mass law's basic principle states that transmission loss increases 6 decibels for each doubling of frequency, or each doubling of the wall mass per area, up to a plateau for a given frequency. (Chonan and Kugo 1989).

DOUBLE WALLED SYSTEM

To increase transmission loss, a double walled system can be implemented. This type of configuration has two panels separated by a gap. The gap is usually filled with a sound absorbing material to further enhance the transmission loss (Figure 3).

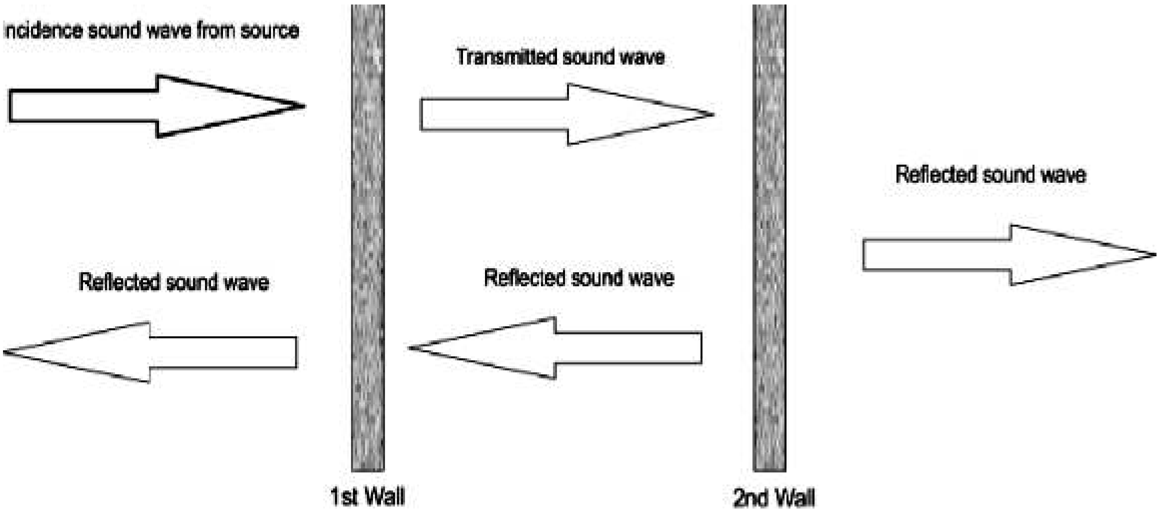

Figure 3: Pressure Waves Normally Incident on a Double Panel system (*Chonan and Kugo 1989)*

Beranak (1992) also assert that the transmission loss can be determined by adding the transmission losses of each of the single panels together with the transmission loss of the material in the gap between the panels. Hence,

$$T_L = T_1 + T_2 + T_g \qquad (1)$$

Where

T_L = total transmission loss

T_1 = the transmission loss of first panel,

T_2 = the transmission loss of the second panel, and

T_g = the transmission loss of the material in the gap between the panels (Beranek, 1992)

Closely coupled partitions are double walls that are separated by a few inches, while loosely coupled partitions are separated by several feet (*Buckingham 1924*).

Insertion Loss

Insertion loss is the reduction, in dB, of the sound pressure level or sound power level of a noise source. As long as the measurements are taken in the same locations and the background noise is taken into account, insertion loss measurements are rather simple (Joseph 1997).

Insertion Loss and the Performance Rating of Acoustical Enclosures

The insertion loss measured in decibels is a function of the characteristics and geometry of the material of the enclosure panel and the existing openings and it is defined as the logarithmic ratio of the effective sound power radiated by the noise source in free space (*W*) to the sound power radiated by the source inside the enclosed (*We*) (2).

$$I_L = 10\log(=-10\log t_e \qquad (2)$$

Where $t_e = (\frac{We}{W})$ is the insertion power ratio (George, 2007).

W represents the sound power radiated by the noise source (generator set) in free space; *We* is the sound power radiated by the enclosed source (generator set).

For convenience, expressing the sound power as sound power level yields to an insertion loss of the form:

$$I_L = L_W - L_{we} \qquad (3)$$

Where $L_W = 10\log\frac{W}{Wref}$ and $L_{we} = \frac{We}{Wref}$

Above, L_W and L_{We} are the corresponding sound power levels of *W* and *We* respectively, the reference sound power being $W_{ref} = 1$ pW (George, 2007).

The use of an enclosure is frequently limited by the space surrounding the equipment. The enclosure is considered "close fitting" when the noise source to panel dimension is usually less than 1 meter. It has been found that predicting insertion loss using the typical text book, or architectural methods as they are sometimes referred to, is impossible. There is considerable coupling between the noise source and the enclosure (Oldham and Hilarby 1991).

MATERIAL SELECTION

In general, noise control at its transmission path design is accomplished through installation of acoustic barriers and use of insulation material. Factors to be considered for selection of material for canopy fabrication include transmission loss, thickness, weight, cost, material properties and ease of fabrication. Most fabrications focused on noise suppression, so transmission loss and thickness parameters are preferred factors to consider. Values for thickness and transmission loss parameters of different materials are tabulated in Table 2.0 (See appendix).

Table1. Materials Thickness and Sound Transmission
(European Scientific Journal, December 2013)

MATERIALS	THICKNESS (mm)	SURFACE DENSITY (Kg/m^2)	TRANSMISSION LOSS (dB)
Dense Concrete	100	244	40
Light Concrete	100	161	36
Brick	150	288	40
Steel	0.6 – 1.97	4.9 – 15.20	18 – 30
Aluminum	1.59 – 6.35	4.4 – 17.1	23 – 27
Wood	25	18	21

Most Common Sound Attenuated Enclosures

The most common devices used to muffle noise from generators is an acoustical enclosure. Typical sound attenuators consist of panels that are multilayered composite treatments comprising of an impervious exterior layer as well as a layer of porous sound absorption material facing towards the inside of the equipment. The main absorption layer is impervious which blocks the passage of sound energy radiated from the generator. The porous sound absorbing lining will dissipate the retained sound energy, and also provide heat insulating properties.

In a typical skin-tight sound attenuated enclosure, maintenance is performed from outside hinged doors and the air intake louvers.

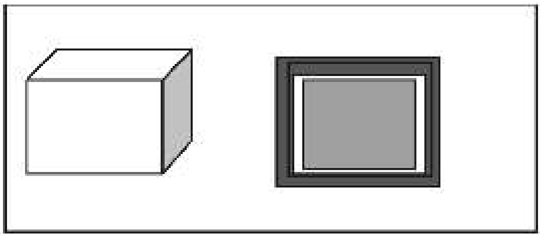

Figure 4. (a) Sound attenuated enclosure in form of a box
(b) Cross section of a double walled panel (Oldham and Hilarby 1991).

MATERIALS AND METHOD

The Sawdust/Sand Composite The composite was molded from sand, sawdust and white cement in the ratio 4:1:1. The bonding materials are white glue and water in a proportion 1:4. The composite was molded on a framework, which gave the panel its size and shape of length, breadth and thickness respectively. Four solid panels were constructed whose dimensions are

1) Two panels of length; 0.55m, breadth; 0.55m and thickness; 0.035m.

2) Two panels of length; 0.70m, breadth; 0.55m and thickness; 0.035m.

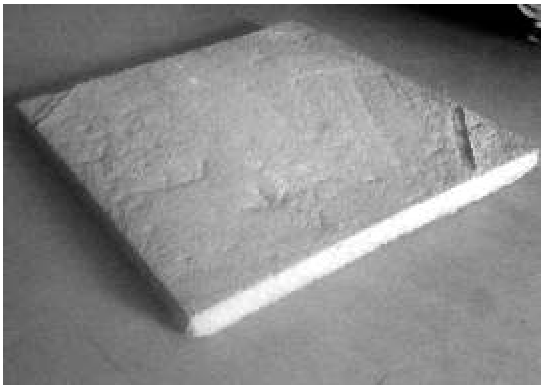

Plate 1. The Molded panel (solid sawdust/sand composite)

The Fine Sand

This is sand of 0.2mm particle size collected from a nearby building site. The fine sand is used here as sound suppression material which is poured (placed) between the walls of the constructed enclosure.

The Sawdust and Foam

The sawdust was collected from timber shed where the cutting of hard wood is being carried out. The foam is D 18 foam of 1.5inch (3.7cm) thick. The foam was cut in to shape of; Two 55cm x71cm x 3.5cm and Two 55cm x55cm x 3.5cm.

The Sound Measuring Device

The device is a sound level (decibel) meter used for measuring sound level .It is designed according to the IEC651, ANS S1.4 Standard for sound level meters.

It has the following specifications:

Model; TES-13050A.

It has 1/2 inch electric condenser microphone.

Measuring range: Lo- 35 to100dB. Hi- 65 to 135dB.

Accuracy: 1.5dB, Resolution; 0.1dB

Power supply: one DC 9V battery

Operating temperature: 0°C to 40°C.

The Infra-Red Thermometer:

Name: Nubee Infrared Thermometer Model No.: NUB8380
Range: - 50^{0}C – 380^{0}C
Accuracy: ± 2^{0}C
Resolution: 0.1^{0}C **Power supply**; DC 9V battery

The Test Generator

The model of the test generator set is TG 2700. it has the following average dimension: 20.5inch x 21inch x 17inch with a power rating of 2.5 kVA

The Enclosure

The enclosure (box) was constructed as a wooden structure with partition or space on all four sides to accommodate the test materials. The partition is 1.5 inch (3.7cm) wide which is approximately the thickness of the test material.

The dimensions of the enclosure are;

Outer: Length; 0.72m, breadth; 0.56m and height; 0.56m.

Inner; Length; 0.585m, breadth; 0.72m and height; 0.58m.

Air vent was created and fans installed to remove the hot air from the enclosure.

Plate 2.The constructed acoustical enclosure.

Measurement was carried out in a10m × 10m open field. The generator set was placed in the center of the field and the four sides were labeled A, B, C and D respectively.10 measurement points were marked at 1.0m intervals away from each side of the generator set. The generator was kick started in the open space and sound levels were measured at each marked measurement point.

The generator set (noise source) was placed under the enclosure with empty space between the wall (panel).Sound measurements were also taken at each measurement point while the generator is in operation.

The generator is placed in the enclosure with fine sand as sound suppression material in between the walls. The measurement procedure was repeated and the results were tabulated.

The solid sawdust/sand composite was also placed round the space between the enclosure walls and the measurement procedure was also repeated while the generator is operating in the enclosure. The results were also tabulated appropriately. Figure 5 shows the Layout of the measurement field with the generator set inside the enclosure.

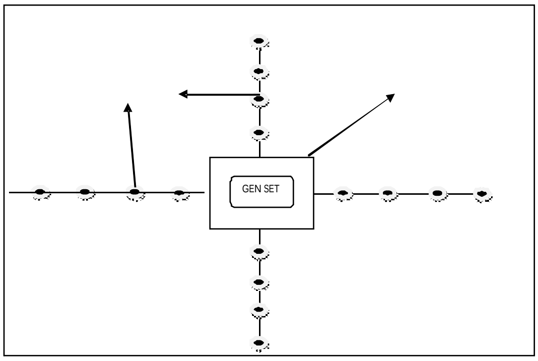

Figure 5: Layout of measurement field

RESULTS AND DISCUSSION

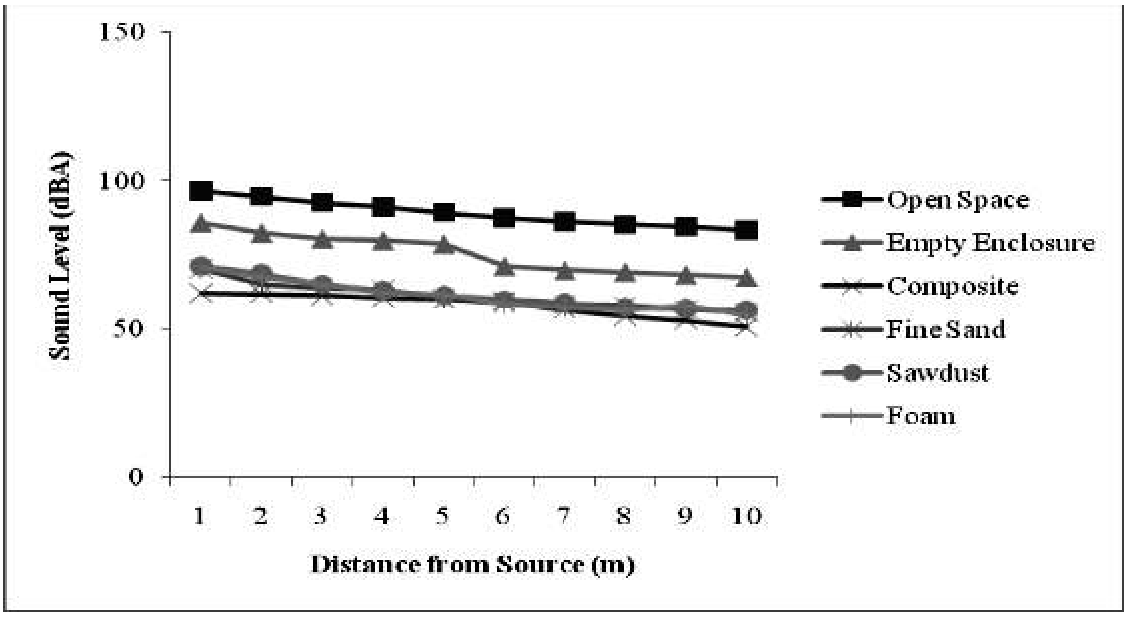

Figure 6: Graph of sound level against distance from source

Figure 6 shows that the average sound level emitted by the generator set has been reduced by the enclosure even when the partition (space between walls) is empty. The box with the composite performed best while the fine sand, sawdust and foam had a close average. The local materials have greatly suppressed the sound to a bearable level resulting in lower sound levels than when operated in open space or in the enclosure without suppressants.

PERCENTAGE REDUCTION

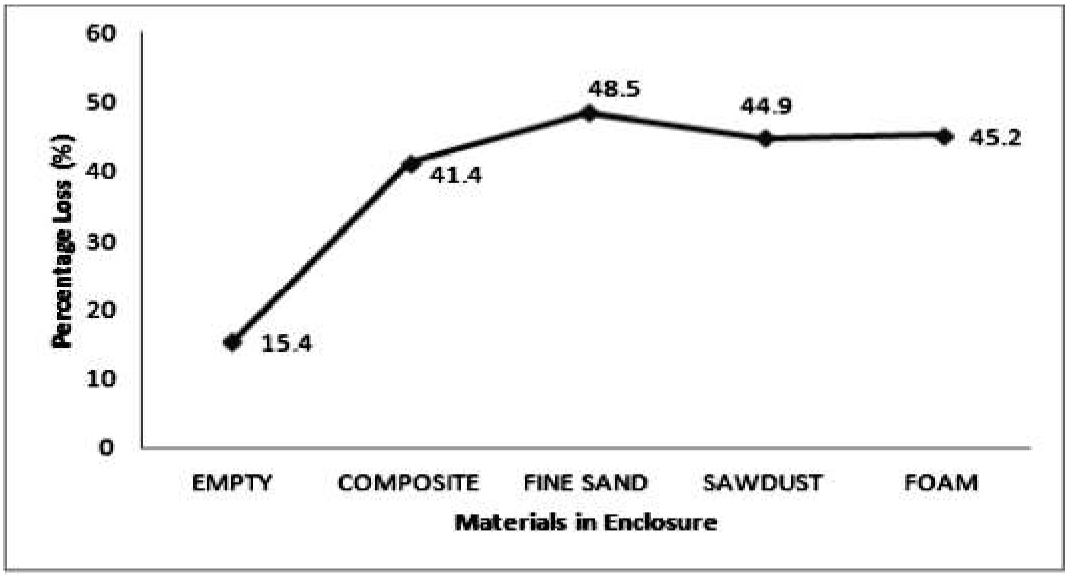

Figure 7: Graph of percentage loss for each material in enclosure

Figure 7 shows that fine dust has the greatest percentage loss compared to the other materials. This could be attributed to the very small space between the sand grains which helps to absorb the sound generated.

TEMPERATURE MEASUREMENT

Since the generator will be placed in a container, the behavior of the system in a heated enclosure is of paramount importance. Temperature measurements of the engine block were taken using the infrared thermometer. The temperature of the generator outside and inside the enclosure when idle and when under the influence of 2kW load was determined and the result is as shown in Fig. 8.

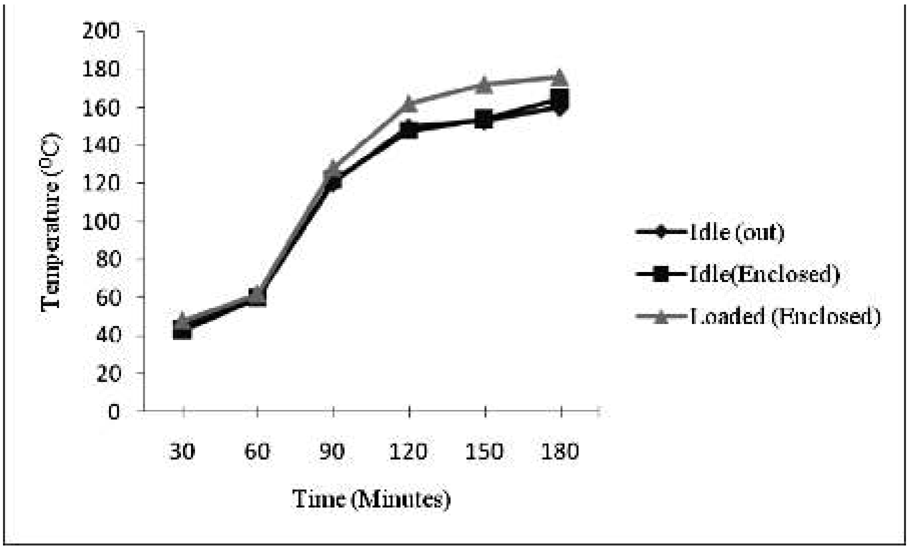

Figure 9: Temperature measurement of the generator outside and inside the enclosure

From Fig. 9, it can be seen that the highest temperature of 176 ^{0}Cwas recorded when the generator was operating under a loaded condition and running for three hours uninterrupted. This is still within tolerable limits of the maximum threshold of 230 ^{0}C for the Tiger brand generator.

CONCLUSION

An acoustical enclosure has been constructed using ply wood which serves as the double walls. The fine sand offered the highest average insertion loss of 28.155 dB equivalent 48.54% reduction, while the empty space offered the least average insertion loss of 13.73 dB, which is equivalent to 15.36% reduction. This is an indication that the fine sand is more effective in reducing the noise level than all the other materials. This high insertion loss by the fine sand can be attributed to higher compaction of sand particles. This in turn can be related to the basics of mass law which states that transmission loss increases for each doubling of the wall mass per area. The temperature recorded after running the generator for 3hrs is still within tolerable limits.

ACKNOWLEDGMENT

We will like to acknowledge the immense contribution of Innocent Johnson, Grace Igbul for their assistance in data collection and interpretation, Department of Applied Science for the enabling environment to carry out the research, Dr. S.S. Mohammed for technical advice.

REFERENCE

Beranek, I. L. (1992). *Noise and Vibration Control Engineering, New York, John Wiley and Sons.*

Buckingham, E. (1924). *Theory and Interpretation of Experiments on the Transmission of Sound through Partition Walls.Sci. Papers Natn. Bur. Standards vol. 20, p.193*

Chonan, S. and Kugo, Y.(1989).*Acoustic characteristics and the design of two-layered sound proof plates.J.Sound Vib.,129(3): 501-511.*

Crocker, M.J.(1994). "*A Systems Approach to the Transmission of Sound and Vibration Through Structures*", Noise Con 94, pp. 525 – 533

European Scientific Journal December 2013 */SPECIAL/ edition vol.4 ISSN: 1857 – 7881 (Print) e – ISSN1857- 7431*

George, S.B. (2007). *Sound Insulation of a Box. Acoustic Technology Ørsted. Technical University of Denmark*

Henry, C. (2004). *Acoustic Materials for Absorption Conference on Noise and Vibration Control for Industries, pp. 7.1- 7.4.*

Joseph, E.B. (1997). *Optimal Design of an Enclosure for a Portable generator. Virginia Polytechnic Institute and State University. Blacksburg, Virginia*

Luigi, R. (2004). *The Joys of Noise.* Department of Geography, University of Madras and Faculty of Environmental Studies, York University.

McNamara, B, and Buland, K. *(2004). Ambient noise levels in the continental United States. Bulletin of the Seismological Society of America: p. 15171527.*

Oldham, D. J, and Hilarby S. N. (1991).*The Acoustical Performance of Small Close Fitting Enclosures, Part 2;Experimental Investigation .Journal of Sound and Vibration vol. 150*

Rettinger, M. (1973).*Acoustic Design and Noise Control,* New York: Chemical Publishing Company.

Rindel, J. H. (2005). *"Sound Insulation in Buildings",* Note 4214, Ørsted- DTU

Sound attenuation basics, Generator noise reduction. *http://www.dieselservicesupply.com/Attenuated_enclosure. (13th feb.2016).*

wikipedia.org/wiki//active_noise_control, (9th feb.2016).

CHARACTERIZATION OF LANDSAT IMAGERY DATA FOR EXPLORATION OF GROUNDWATER SYSTEM IN KEBBI STATE, NORTHWESTERN NIGERIA.

[1]Ologe Oluwatoyin, [2]Abu Mallam and [3]Abdulsalam N Nasir
[1]*Department of Applied Geophysics, Federal University, Birnin Kebbi, Nigeria.*
[2, 3]Department of Physics, University of Abuja, Nigeria.
Email: toyin.ologe@gmail.com

ABSTRACT

Most of the researches carried out on Kebbi State hardly take into cognisance the structural implication as it affects the groundwater potential and its distribution in the state. Landsat Imagery technique was used to decipher groundwater potential and its distribution pattern across Kebbi State. Landsat Imagery Data was acquired for the study, processed using ENVI 4.8 software, ILWIS 3.3 Academic software and ArcGIS 10.0 software for enhanced and dependable results. The Landsat Imagery Data show thatdensity values are relatively high (0.3156-0.7030) at Zuru and Mahuta in the basement areas; medium density values (0.1188-0.3156)at Birnin Kebbi and environ in sedimentary area, while low density values (0-0.1188) were derivedfrom Giro and Dakingari situated in basement and sedimentary areas respectively. Landsat Imagery Data was found useful in delineating areas of high groundwater potential and its distribution pattern in the state. The application would help to reduce cost of exploration for water by individuals and government agencies, thereby,improve groundwater production.

Keywords: *Basement, Distribution pattern, Groundwater potential, Landsat imagery and Sedimentary.*

Introduction

Interpretation of hydrogeological data often requires that their spatial location be incorporated into the analysis (.Shamsuddin and Sankar, 2012) Geographic information system can be used for storinghydrogeological data as well as their spatial locations in a relational database. It also provides the facility to analyze the spatial data objectively using various logical conditions. Landsat imagery is widely used for spatial modeling of groundwater prospect of large areawith more reliability than land methods such as vertical electrical sounding in inaccessible areas.Surface water sources such as lakes, streams, and springs are easily affected by extreme weather conditions, vulnerable to pollution and can contain harmful pathogens. Therefore,these sources of water are no longer considered reliable, sustainable and suitable in many parts of the world (Adiat *et al.*, 2012). Consequently, there has been an increase in awareness to utilization and explorationfor groundwater as alternative source of reliable and sustainable water supply. In addition to this, rapid pace of urban development and increase in demand for domestic, public and commercial water supply, resulting from growing population, have also triggered the utilization of groundwater as an alternative source to surface water in supplementing water supply (Abdul*et al.*, 2001).Satellite imagery is a large scale surface geological mapping tool which offers uniqueopportunity to investigate the geological characteristics of remote areas of the earth surface without the need to access the area on the ground. The resolution of the technique is limitedby the resolution of the imagery. Remote sensing with its advantages of spatial, spectral and temporal availability of data covering large and inaccessible areas within short time has become a very handy tool in assessing, monitoring and conserving groundwater resources. In addition, satellite data provides quick and useful baseline information on the parameters controlling the occurrence and movement of groundwater, such as geology, lithology geomorphology, soils, land use / cover, lineaments (Mogaji *et al,*. 2011).Surface geological mapping, remote sensing data analysis and structural features in the rock body playimportant role in identifying probable zones for locating groundwater resource.The aim of this study is produce a regional surface structural map of Kebbi State from remotely sensed data.The interpretation is based on density values subject to the amount of structural features present in the rock body. Therefore, density values obtained were used to characterise the study area into different groundwater zones.

Description of the Study Area and Geology

Kebbi State, in Northwestern Nigeria lies between 10º 15' 00" and 13º 15' 00" North and 3º 40' 00" and 6º 00' 00" East with an area of about 36,800km^2(Figure 1). The geology of the study area is dominated basement and sedimentary rocks (Sheu *et al.,* 2004).The basement complex region is composed of volcanic and metamorphic rocks such as granites, schist, gneisses, quartzites and migmatites. In addition, there are metasediments such as phyllites and metaconglomerates. The sedimentary region consists of Gwandu Formation, Illo Formation and Rima Group whose ages range from the cretaceous to Eocene (Sheu *et al.*, 2004). The Gwandu Formation consists of differentiated massive clay grits inter bedded with sandstone; the Illo Formation consists of pebbly grits, sandstones while Rima Group consists of clays, mudstones and siltstones (John and Christopher, 2014).

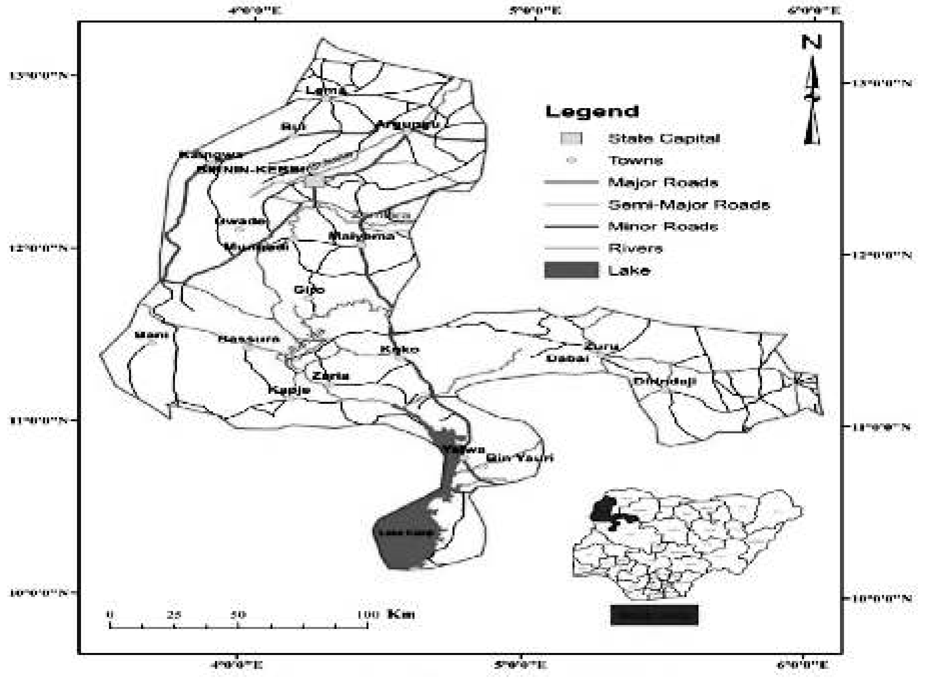

Figure 1: Location Map of Kebbi State Showing Major Towns and Inset: Map of Nigeria

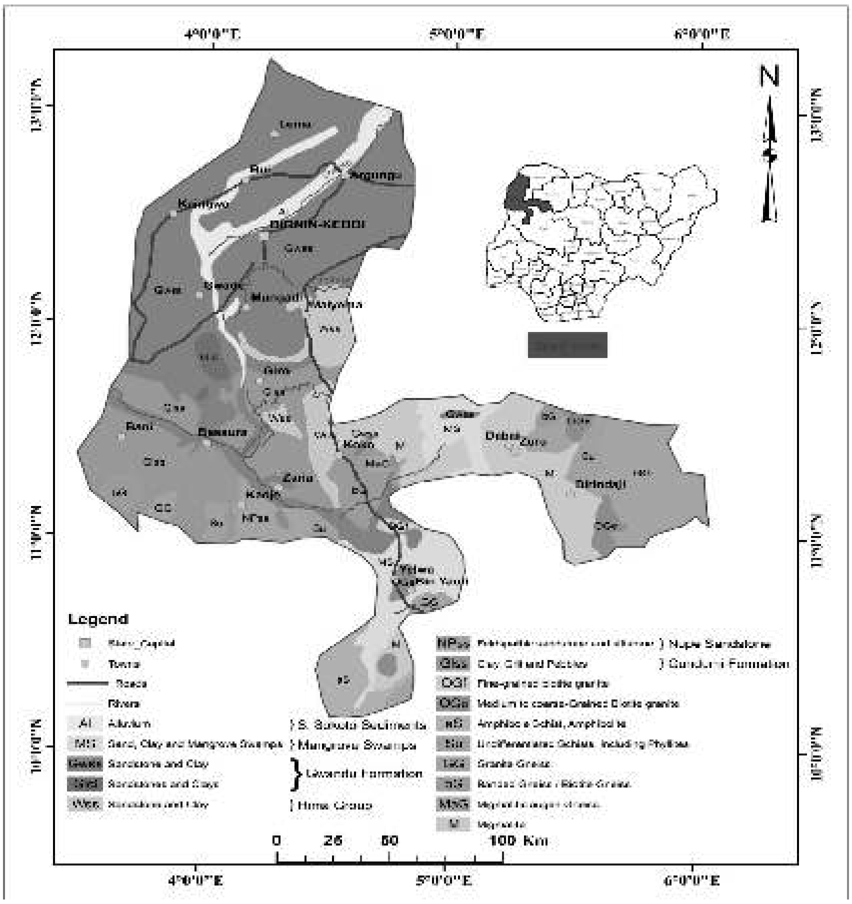

Figure 2: Geological Map of Kebbi State and Inset: Map of Nigeria (Modified after NGSA, 2006).

Hydrogeology of the Study Area

Kebbi State whichis part of Sokoto basin in the northwestern part of Nigeria serves as source of groundwater for domestic and industrial purposes. About 2000 m of clastic sequences rest upon the basement containing various lithofacies and basement rocks. Sequences of semi-consolidated gravels, sands, clay, some limestone and ironstone are found (Bassey *et al.,* 1999). Aquifers of the Sokoto Basin are exploited at various locations within the basin for domestic, irrigation, horticulture and animal husbandry. The aquifers are usually confined and composed ofsandstone, siltstone and sometimes limestone (Adelana *et al*.,2008). An artesian condition has been reported in Sokoto town and in nearby villages in Kebbi State. The depth to the water table is not usually static depending on the season of the year and the groundwater system regime of the area.In addition, the concealed basement rocks may contain highly faulted and folded areas, incipient joints and fracture systems derived from multiple tectonic events that they have experienced. These structures may house abundant groundwater in a typical basement setting. The detection and delineation of such structures that are diagnosed by lineaments may facilitate the identification of prospective groundwater zones

Materials and Method

Image data

Image data referred to as LANDSAT 8 was acquired from Nigerian Geological survey

Agency (NGSA), Abuja. The imagery data from NGSAwas obtained from the acquired subsets from four (4) scenes of path 189 and row 055 and path 190 and row 55 of 2001 and 2002 respectively. Other ancillary data include ASTER DEM and geological map (sourced from Nigeria Geological Surveys Agency (NGSA), 2006) of the study area. The software used in processing the acquired materials for Landsat imagery data include ENVI 4.8software, ILWIS 3.3 Academic software and ArcGIS 10.0 software.

Landsat Image Processing and Enhancement

Remote sensing is the art and science of making measurements of the earth using sensors on airplanes or satellites. These sensors collect data in the form of images and provide specialized capabilities for manipulating, analyzing, and visualizing those images. It can also be seen as obtaining information and observations about physical objects and environment without actually being in direct contact. The main goal in using remote sensing techniques for groundwater exploration is to identify and isolate regional and sub-regional factors of significance to groundwater occurrence in a cost effective and rapid manner (Greenbaum, 1992a, Gustafsson, 1993).Landsat 8 is obtained from a sensor that orbits the earth at a height of 705km on a sun-synchronous orbit (Jensen, 2005). This aid in identifying structural features because a specific location on an image will have the same sun illumination angle on multiple images over time. Different digital image processing methods were applied in this work to enhance the appearance of linear features by emphasizing tonal, topographic and textural changes. However, two distinct processes are involved in the interpretation of Landsat 8 imagery; (1) the pre-processing of the data (2) the image enhancement technique section which is the processing of the image to enhance information extraction.The first step is the pre-processing which is to carry out the necessary corrections in order to make the data conform to referenced and remove any probable error. The image enhancement technique includes the radiometric correction and the geometric corrections. Radiometric correction involves corrections to errors that could be caused by detector failure and/or power failure from detectors operating simultaneously. A geometrical correction, also called geo-referencing, is the procedure where the content of a map will conform to a known geographical space or spatial coordinate system.

RESULTS AND DISCUSSION

The main data used for the mapping of surface structures in the study area is LANDSAT 8Imagery downloaded from global land cover facility as shown in Figure 3.The resultsof the analysis derived from LANDSAT 8 are presented as surface structuralmap and density map (Figures 4 and 5).Surface structural map (Figure 4) was delineated by visual interpretation of false colour composite. The map shows the distribution of surface structures across the entire study area with their concentration more pronounced in the eastern part (basement area) and other areas are sparsely populated with these geological surface structures. This high concentration of surface structures may be largely due to tectonic activities in the basement area. However, the essence of using Landsat for surface structure study is to identify areas of high density associated with groundwater.

The availability and distribution of the structures in either sedimentary or basement rocks are of interest in identifying high groundwater potential areas within the state.

This was done by generating density maps (Figure 5).Examples of areas characterized by high density values (0.3156-0.7030) are Zuru and Mahuta in the basement area; medium density values (0.1188-0.3156)is at Birnin Kebbi and environ, while low density values (0-0.1188) are at Giro and Dakingari situated in basement and sedimentary areas respectively (Figure 5). According to Amigun

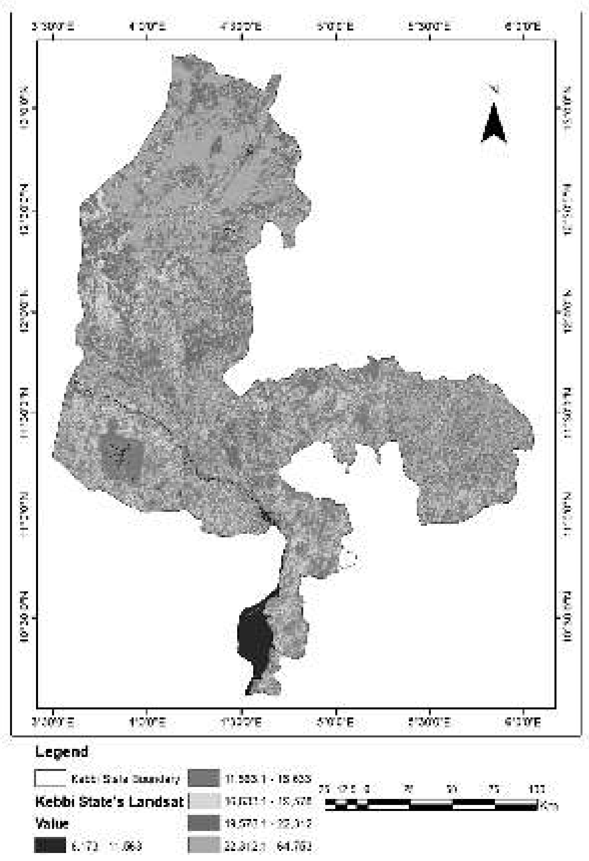

Figure 3: Landsat imagery over Kebbi State

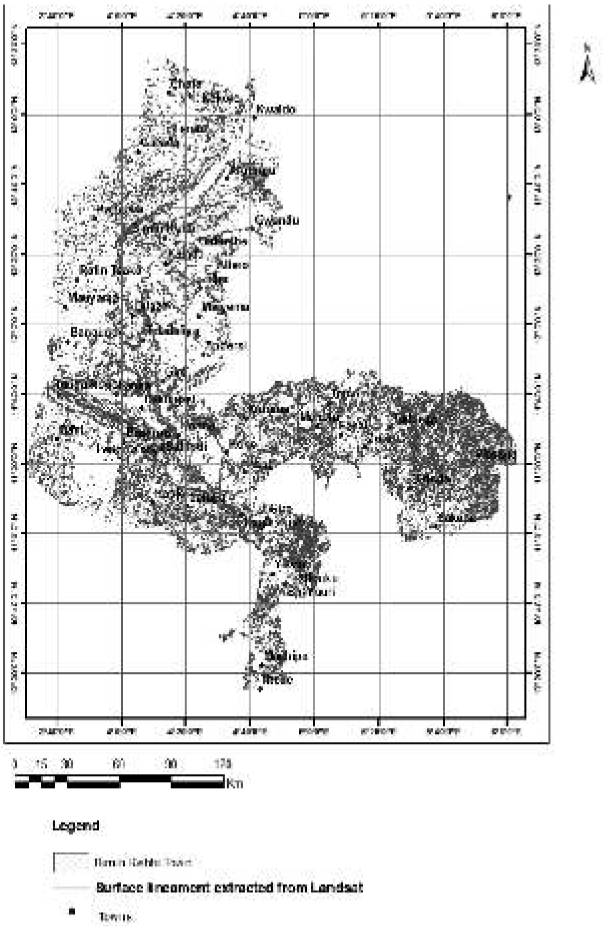

Figure 4: Surface lineament map of the study area

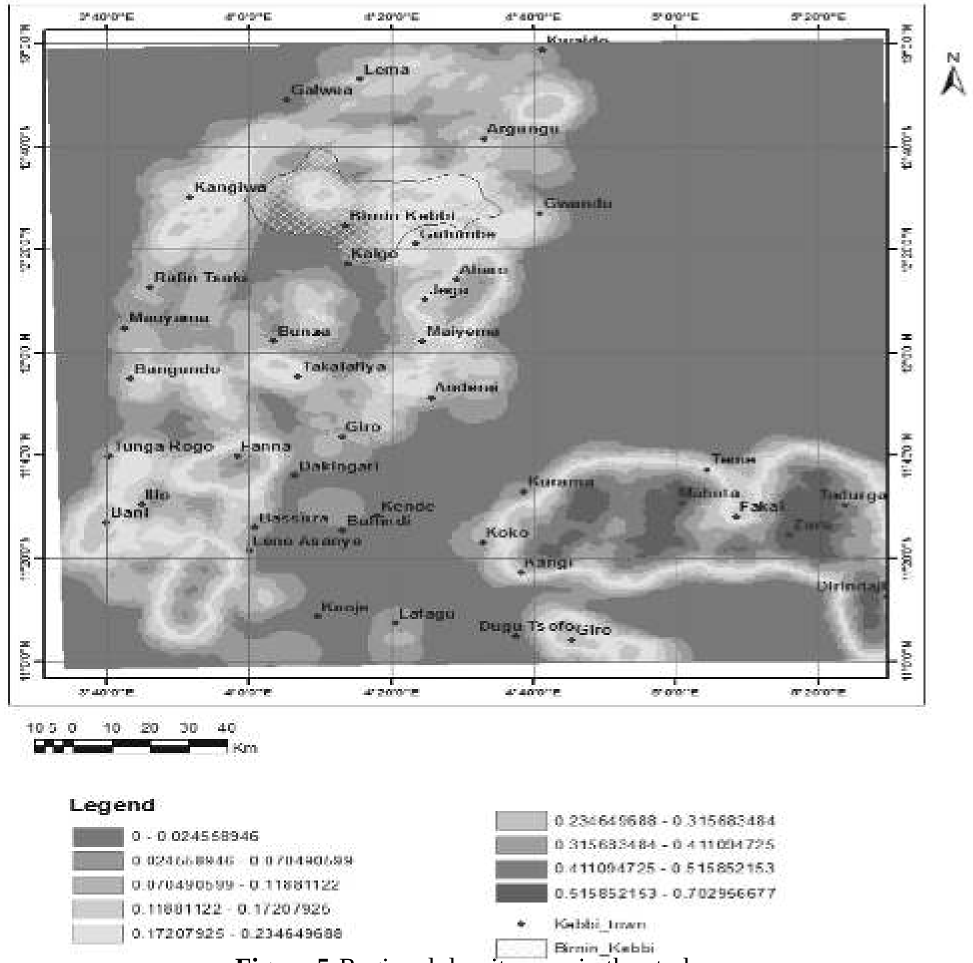

Figure 5: Regional density map in the study area

CONCLUSION

Landsat TM density data analysis are carried out on Kebbi State in Northwestern, Nigeria shows that they are identified areas in basement and sedimentary regions that characterized by high, medium and low density values which are used to identify susceptible areas to groundwater system. The designatedby high density values are suggested to be associated high structural features while areas with low density values are suggested to possess low structural features. In effect, areas associated with high density values contain high groundwater potential as indicated in Zuru and Mahuta (0.3156-0.7030); medium density values (0.1188-0.3156) at Birnin Kebbi and environ in sedimentary areas, while low density values (0-0.1188)at Giro and Dakingari situated in basement and sedimentary areas respectively.

Reference

Abdul, R.S., Umar, H., and Zuraidah, R. 2001. Geophysical investigation of the OlakLempit Quaternary Basin, Selangor, Malaysia. In: Proceedings of 10th GEOSEA regional congress on geology, mineral and energy resources, Jogjakarta, Indonesia, pp 280– 282.

Adelana, S.M.A., Olasehinde, P.I., Bale, R.B., Vrbka, P., Edet, A.E. and Goni, I.B. (2008).

An Overview of the Geology and Hydrogeology of Nigeria, Applied Groundwater Studies in Africa, 11:171-197.

Adiat, K.A.N. Nawawi, M. N. M. and Abdullah, K. (2012). Assessing the accuracy of GIS-based elementary multi criteria decision analysis as a spatial prediction tool – A case of predicting potential zones of sustainable groundwater resources. Journal of Hydrology 440–441, 75–89.

Amigun, J. O., Richard, A. F, and Akinola, A. K. (2015).Integrated Landsat Imagery and Geophysical Exploration for Groundwater Potential Evaluation of Okene and Its Environs, Southwestern Nigeria. International Journal of Geosciences, 209-229 Published in SciRes. http://www.scirp.org/journal.

Bassey, J. O., Maduabuchi, C., Onugba, A., Verhagen, B.T. and Vrbka, P. (1999).Preliminary results of Hydrogeological and Isotopic Research the Rima River Basin, NW Nigeria. Journal of Water Resources, 10:13-37.

Edet, A. E., Teme, S. C., Okereke, C. S. and Esu, E. O. (1994).Lineament Analysis for Groundwater Exploration in Precambrian Oban massif and Obudu plateau. Southeastern Nigeria. *Journal of Mining and Geology.*30(1): 87 -95.

Greenbaum D (1992a). Remote sensing techniques for hydrogeological mapping in semiarid basement terrains. British Geological Survey, Report WC/92/28.

Gustafsson, P. (1993): High resolution satellite imagery and GIS as a dynamic tool in exploration in a semi-arid area. Proceedings of the IAHS conference on Application of Geographic Information Systems in Hydrology and Water Resources Management held in Vienna, Austria, on April 19-22 1993, pp. 93-100. Vienna.

Mogaji, K. A., Aboyeji, O. S and Omosuyi, G. O. (2011a). Mapping of lineaments for groundwater targeting in the basement complex region of Ondo State, Nigeria, using

Remote sensing geographic information system (GIS) techniques. International Journal of Water Resources and Environmental Engineering Vol. 3(7), pp. 150-160

Jensen, J. R. (2005).*Introductory digital image processing: a remote sensing perspective,* New Jersey, USA, Prentice Hall Inc.

John, A. S and Christopher, M. M (2014). Integrated and Sustainable Management of the Shared Aquifer Systems and Basins of the Sahel Region: Paper presented at the First Coordination & Governance Meeting on Project RAF7011, Vienna, Austria, Pp 6-7.

Nigeria Geological Survey Agency (NGSA) (2006).Published by the Authority of the Federal Republic of Nigeria.

Shamsuddin, S., and Sankar, K.N. 2012. GIS Integration of Remote Sensing and Electrical Sounding Data for Hydrogeological Exploration. J. of Spatial Hydrology, Vol.2 No.1Pp 1-12.

Sheu, A. T., Udensi, E. E., Adeniyi, J. O and Jonah, S. A. (2004).Spectral analysis of the magnetic residual anomalies over the Upper Sokoto Basin, Nigeria. Zuma Journal of Pure and Applied Sciences, 6: 213-219.

COMPUTATION OF THE TOTAL SCATTERING CROSS SECTIONS FOR THE ALKALI METALS

ABDU, S. G.
Department of Physics, Kaduna State University, Kaduna-Nigeria
Email:sgabdul@kasu.edu.ng

ABSTRACT

Calculated Total Cross-Sections (TCS) of elastic electron-atom scattering for Li, Na, K, Rb, Cs and Fr are presented. The computed TCS were calculated using Bon, Eikonal and the Optical Theorem approximation methods with the Lenz-Jensen potential, at electron incident energies between 1to1000eV.Results obtained are in good agreement with experimental TCS data.

Keywords: *Total Cross-Section, elastic scattering, alkali metals, optical theorem, Born approximation, Eikonal approximation*

Introduction

In scattering theory, the Total Cross-Section (TCS) is a measure of the probability that an interaction occurs; the larger the cross section, the greater the probability that an interaction will take place when a particle is incident on a target (Anchaver, 2003).

Elastic electron-atom scattering takes place if the final state of an atom after the interaction coincides with the initial one (Winitzki, 2004). Total and differential cross-sections for such a process can be calculated in various approximations — Born (Merzbacher, 1970)), Eikonal (Innanen, 2010; Shajesh, 2010), optical theorem (Lokajicek & Kundrat, 2009; Ronniger, 2006), partial wave method (Cox & Bonham, 1967), etc. In this work, the total cross-sections of the alkali metals Li, Na, K, Rb, Cs and Fr (Halka & Nordstrom, 2010) were computed using the three approximation methods listed above.

MATERIALS AND METHODS

We used the FORTRAN code program developed by Koonin & Meredith (1989) which takes the relativistic differential cross-section as a sum of squared modules of the real and imaginary scattering amplitudes. The amplitudes can be calculated through the phase shifts of spherical waves, which are obtained by integration of equations for radial wave functions. In these computations the analytical approximation for the atomic electrostatic potential given by Lenz and Jensen, called the Lenz-Jensen potential (Blister & Hautala, 1978), based on the Thomas-Fermi model, is used.

Scattering Theory

For particles of mass m and energy

$$E=\frac{\hbar^2 k^2}{2m}>0 \qquad 1.0$$

scattering from a central potential, V(r) is described by a wave function, ψ(r) that satisfies the Schrodinger Wave Equation (SWE)

$$-\frac{\hbar}{2m}\,¿^2 y+Vy=Ey \qquad 2.0$$

with the boundary condition at large distance

$$Y_{r\rightarrow\infty}\rightarrow e^{ikz}+f(q)\ \frac{e^{ikz}}{r} \qquad 3.0$$

Equation (3.0) holds for a beam of electrons incident along z-axis, and the scattering angle, θ is the angle between r and $\hat{z}$ while f is the complex scattering amplitude, which is the basic function we seek to determine (Babaji, Abdu &Taura, 2012). The differential cross-section is given by:

$$\frac{d\sigma}{d\Omega} = |f(\theta)|^2 \qquad 4.0$$

The total cross-section is

$$\sigma = \int d\Omega \frac{d\sigma}{d\Omega} = 2\pi\int_0^\pi d\theta \sin\theta |f(\theta)|^2 \qquad 5.0$$

f is a function of both E and θ (Koonin & Meredith, 1989).

Approximation Methods

Approximations play a very important role in our understanding of processes that cannot be solved exactly. The calculation of scattering cross sections is one of the most important uses of Fermi's Golden Rule (Wacker, 2011). Fermi's rule involves only one matrix element of the interaction which makes it a first order approximation to the exact result. This approximation suggests an approximation to the complex scattering amplitude.

The Born approximation involves an approximation to the complex scattering amplitude (Merzbacher, 1970). It has been extensively used to study low energy as well as high energy scattering processes. The Eikonal approximation is a technique for estimating the high energy behaviour of a forward scattering amplitude (Innanen, 2010). It was originally developed for potential scattering in quantum mechanics, where one approximates the classical trajectory corresponding to forward scattering by a straight line and uses a WKB approximation for the wavefunction (Sakuri, 1985). The optical theorem relates the forward scattering amplitude to the cross section (Lokajicek & Kundrat, 2009).

Partial Wave Method

The method of partial wave expansion is a special trick to simplify the calculation of the scattering amplitude, f (Newton, 1982). The standard partial wave decomposition of the scattering wave function ψ is

$$\psi(r) = \Sigma_{l=0} (2l+1)\, i^l e^{i\sigma} \frac{R_l(r)}{kr} P_l(Cos\theta) \qquad 6.0$$

When equation (2.6) is substituted into the SWE (2.0) the radial wave functions, R_l are found to satisfy the radial differential equations:

$$\left[\frac{\hbar^2}{2m}\frac{d^2}{dr^2} + V(r) + \frac{l(l+1)\hbar^2}{2mr^2} - E\right] R_l(r) = 0 \qquad 7.0$$

This is the same equation as that satisfied by a bound state wave function but the boundary conditions are different. In particular, R vanishes at the origin, but it has the large-r asymptotic behaviour

$$R_l \to kr[cos\delta_l\, j_l(kr) - sin\delta_l\, n_l(kr)] \qquad 8.0$$

Where j_l and n_l are the regular and irregular spherical Bessel functions of order l. The scattering amplitude is related to the phase shifts δ_l by equation 9.0 below:

$$f(\theta) = \frac{1}{k}\Sigma_{l=0}^{\infty} (2l+1) e^{i\delta_l} sin\delta_l P_l(Cos\theta) \qquad 9.0$$

From equations *(5.0)* and (9.0) the total cross-section is given by

$$\sigma = \frac{4\pi}{k^2}\Sigma_{l=0}^{\infty} (2l+1)\, sin^2\delta_l \qquad 10.0$$

Although the sums in equations (9.0) and (10.0) extend over all l, they are in practice limited to only a finite number of partial waves. This is because for large l, the repulsive centrifugal potential in equation (7.0) is effective in keeping the particle outside the range of the potential and so the phase shift is very small.

$$\frac{l_{max}(l_{max}+1)\hbar^2}{2mr^2_{max}} = E \qquad 11.0$$

$$\Rightarrow \quad l_{max} \; ?kr_{max} \qquad 12.0$$

This estimate is usually slightly low since the penetration of the centrifugal barrier leads to non-vanishing phase shifts in partial waves somewhat higher than this (Koonin & Meredith, 1989).

The Phase shifts

To find the phase shift in a given partial wave, we must solve the radial equation (7.0). The equation is linear, so that the boundary condition at large r can be satisfied simply by appropriately normalizing the solution.

If we put R_l (r = 0) = 0 and take the value at the next lattice point, R_l (r = h), to be any convenient small number we then use

$$f'' \approx \frac{f_1 - 2f_0 + f_{-1}}{h^2} \qquad 13.0$$

for $R_l''(h)$, along with the known values $R_l(0)$, $R_l(h)$ and $k(h)$ to find $R_l(2h)$. Now we can integrate outward in r to a radius $r^{(1)} > r_{max}$. Here, V vanishes and R must be a linear combination of the free solutions, $krj_l(kr)$ and $krn_l(kr)$:

$$R_l^{(1)} = Akr^{(1)}\,[cos\delta_l\, j_l(kr^{(1)}) - sin\delta_l\, n_l(kr^{(1)})] \qquad 14.0$$

Although the constant, A above, depends on the value chosen for $R(r = h)$, it is largely irrelevant for our purposes; however, it must be kept small enough so that overflows are avoided. Now we continue integrating to a larger radius $r^{(2)} > r^{(1)}$:

$$R_l^{(2)} = Akr^{(2)}\,[cos\delta_l\, j_l(kr^{(2)}) - sin\delta_l\, n_l(kr^{(2)})] \qquad 15.0$$

Equations (14.0) and *(15.0)* can then be solved for δ_l to obtain

$$tan\mathrm{d}_l = \frac{Gj_l^{(1)} - j_l^{(2)}}{Gn_l^{(1)} - n_l^{(2)}} \; ; G = \frac{r^{(1)}\, R_l^{(2)}}{r^{(2)}\, R_l^{(1)}} \qquad 16.0$$

where $j_l^{(1)} = j_l(kr^{(1)}$ etc. Equation (16.0) determines d_l only within a multiple of p but this does not affect the physical observables [see equations (9.0) and (10.0)]. The correct multiple of p'sat a given energy can be determined by comparing the number of nodes in R and in the free solution, krj_l which occur for $r < r_{max}$. The phase shift in each partial wave vanishes at high energies and approaches N_l p at zero energy, where N_l is the number of bound states in the potential in the l 'the partial wave (Koonin & Meredith, 1989).

The Lenz-Jensen Potential

One practical application of the theory discussed above is the calculation of the scattering of electrons from neutral atoms. In general this is a complicated multi-channel scattering problem since there can be reactions leading to final states in which the atom is excited. However, as the reaction probabilities are small in comparison to elastic scattering, for many purposes the problem can be modeled by the scattering of an electron from a central potential (Koonin & Meredith, 1989). This potential represents the combined influence of the attraction of the central nuclear charge (Z) and the screening of this attraction by the Z atomic electrons. For a neutral target atom, the potential vanishes at large distances faster than r^{-1}. A very accurate approximation to this potential can be had by solving for the self-consistent Hartree-Fock potential of the neutral atom. However, a much simpler estimate can be obtained using an approximation to the Thomas-Fermi model of the atom given by Lenz and Jensen (Blister & Hautala, 1978)

$$V = -\frac{Ze^2}{r} e^{-x}(1 + x + b_2x^2 + b_3x^3 + b_4x^4); \qquad 17.0$$

with

$$e^2 = 14.409; b_2 = 0.3344; b_3 = 0.0485; b_4 = 2.647 \text{ x } 10^{-3}; \qquad 18.0$$

and

$$x = 4.539Z^{1/6\; r_{1/2}} \qquad 19.0$$

This potential is singular at the origin. If the potential is regularized by taking it to be a constant within some small radius r_{min} (say the radius of the atom's 1s shell), then the calculated cross-section will be unaffected except at momentum transfers large enough so that $qr_{min} >> 1$. The incident particle is assumed to have the mass of the electron, and, as is appropriate for atomic systems, all lengths are measured in angstrom (Ā) and all energies in electronvolt (eV). The potential is assumed to vanish beyond 2Å. Furthermore, the r^{-1} singularity in the potential is cutoff inside the radius of the 1s shell of the target atom.

Research Methodology

A FORTRAN program developed by Koonin & Meredith (1989) was the main program used for all the computations. The program is made up of four categories of files: common utility programs, physics source code, data files and include files. The physics source code is the main source code which contains the routine for the actual computations. The data files contain data to be read into the main program at run-time and have the extension .DAT. The first thing done was the successful installation of the FORTRAN codes in the computer. This requires familiarity with the computer's operating system, the FORTRAN compiler, linker, editor, and the graphics package to be used in plotting. The program runs interactively. It begins with a title page describing the physical problem to be investigated and the output that will be produced. Next, the menu is displayed, giving the choice of entering parameter values, examining parameter values, running the program, or terminating the program. When the calculation is finished, all values are zeroed (except default parameters), and the main menu is re-displayed, giving us the opportunity to redo the calculation with a new set of parameters or to end execution.

RESULTS AND DISCUSSION

Results were generated for several electron incident energies as presented in tables 1-3 below:

Table 1: Computed Total Cross-Sections for Elastic Electron- Atom Scattering for Li, Na, K, Rb, Cs and Fr Using the Born Approximation Method with the Lenz-Jensen Potential

E (eV)	TOTAL CROSS SECTION (ANGSTROMS**2)					
	Li	Na	K	Rb	Cs	Fr
1.0	50.110	186.800	3.030	521.200	708.300	998.800
5.0	27.470	120.000	2.078	385.700	547.200	808.000
10.0	16.720	81.780	1.488	292.800	429.800	658.900
20.0	9.405	50.850	6.629	202.000	307.400	491.300
30.0	6.568	37.270	7.264	156.200	242.200	396.400
40.0	5.027	29.440	5.824	127.600	200.600	333.800
50.0	4.068	24.350	4.868	108.200	171.700	289.100
60.0	3.417	20.790	4.188	94.030	150.300	255.400

70.0	2.944	18.140	3.677	83.220	133.800	229.000
80.0	2.585	16.090	3.278	74.670	120.600	207.700
90.0	2.302	14.450	2.957	67.740	109.800	190.200
100.0	2.075	13.120	2.694	62.000	100.900	175.400
200.0	1.042	6.834	1.431	33.730	55.870	99.950
300.0	0.695	4.618	9.752	23.210	38.750	69.830
400.0	0.521	3.485	7.398	17.710	29.690	53.850
500.0	0.417	2.798	5.960	14.310	24.070	43.840
600.0	0.348	2.337	4.990	12.010	20.240	36.980
700.0	0.298	2.006	4.291	10.350	17.470	31.990
800.0	0.261	1.757	3.764	9.091	15.360	28.180
900.0	0.232	1.563	3.352	8.105	13.710	25.190
1,000.0	0.209	1.407	3.022	7.312	12.380	22.770

From table 2, using the Eikonal method, the TCS for Li exhibited a number of minima and maxima between 1 to 10 eV, then decrease with increasing incident energy between 10 to 1000 eV. The TCS for Na, K, Rb, Cs and Fr exhibited a number of minima and maxima between 1 to 100 eV, then decrease with increasing incident energy between 100 to 1000 eV.

Table 3: Computed Total Cross-Sections for Elastic Electron- Atom Scattering for Li, Na, K, Rb, Cs and Fr Using the Optical Theorem with the Lenz-Jensen Potential.

E (eV)	TOTAL CROSS SECTION (ANGSTROMS**2)					
	Li	Na	K	Rb	Cs	Fr
1.0	15.700	17.720	1.415	1.508	15.020	14.700
5.0	8.720	10.900	1.121	1.009	9.717	7.346
10.0	6.409	8.134	9.540	8.288	9.874	8.462
20.0	4.487	6.819	9.687	7.814	6.561	5.366
30.0	3.687	5.658	6.551	6.041	6.775	6.247
40.0	3.155	5.243	5.674	5.374	5.888	6.006
50.0	2.757	4.717	4.979	5.178	4.801	5.623
60.0	2.447	4.240	4.578	5.165	4.851	5.123
70.0	2.197	3.939	4.457	5.279	4.571	4.334
80.0	1.993	3.748	4.408	4.897	4.548	3.793

90.0	1.823	3.592	4.245	4.440	4.602	3.964
100.0	1.679	3.441	4.021	4.092	4.566	4.020
200.0	0.935	2.398	2.866	3.382	3.164	3.685
300.0	0.647	1.932	2.440	2.805	2.959	2.060
400.0	0.494	1.632	2.067	2.392	2.840	2.608
500.0	0.400	1.423	1.834	2.196	2.470	2.542
600.0	0.336	1.270	1.677	2.090	2.135	2.480
700.0	0.290	1.152	1.555	2.003	1.995	2.409
800.0	0.254	1.057	1.451	1.893	1.918	2.249
900.0	0.227	0.978	1.360	1.775	1.855	2.090
1,000.0	0.205	0.912	1.281	1.664	1.803	1.921

From table 3, using the Optical theorem method, the calculated TCS for K, Rb, Cs and Fr exhibited a number of minima and maxima in the energy range 1 to 100 eV, then decrease with increasing incident energy between 100 to 1000 eV. No minima or maxima were observed for Li and Na, where all computed TCS decrease with increasing incident energy between 1 to 1000 eV.

The calculated TCS using Eikonal and Optical theorem approximation methods are in good agreement with the experimental TCS obtained by Sinha, Singh & Antony (2017). However TCS calculated using the Born approximation method are much higher than the experimental values for the energy range considered. This is because the Born approximation is only valid at high electron incident energies.

Conclusion

Computed Total Cross-Sections (TCS) of elastic electron-atom scattering for the alkali metals have been computed using the Born, Eikonal and the Optical theorem approximation methods with the Lenz-Jensen potential, at incident energies of 1to1000 eV. Results obtained using the Eikonal and Optical theorem methods are in good agreement with the experimental TCS values.

REFERENCES

Anchaver, R.S. (2003), *Introduction to Non-relativistic Quantum Mechanics*, Identity Books, Kano-Nigeria.

Babaji G., Abdu S.G. and Taura L.S. (2012), *The Effect Of Electron Incident Energy On Total Cross Section Calculations For The Noble Gases*, Journal of the Nigerian Association of Mathematical Physics, Vol. 21 (No. 1), pp. 143-150.

Blister, M. and Hautala, M. (1978), *Calculation of the Lenz-Jensen Potential Using the Third Order Approximation,* Physics Letters A, 68 (1), pp. 98-100.

Cox, H.L. and Bonham, R.A. (1967), *Elastic Electron Scattering Amplitudes for Neutral Atoms Calculated Using the Partial Wave*

Method at 10, 40, 70 and 100kV for Z=1 to Z=54, J. chem. Phys., 47, pp. 2599.

Halka, M. and Nordstrom, B. (2010), *Alkali and Alkaline Earth Metals,* Facts on File, New York.

Innanen, K.A. (2010), *A Scattering Diagram Derivation of the Eikonal Approximation.* Available at www.crewes.org/ForOurSponsors/ConferenceAbstracts/2010/CSEG/Innanen_GC_2010.pdf Accessed on 21/06/2017.

Koonin, S.E. and Meredith, D.C. (1989), *Computational Physics (FORTRAN Version),* Addison-Wesley, New York.

Lokajicek, M.V. &Kundrat, V. (2009), *Optical Theorem and Elastic Nucleon Scattering,* arXiv: 0906.396 1v1 [hep-ph].

Merzbacher, E. (1970), *Quantum Mechanic, 2nd ed.,* J. Wiley & Sons Inc., New York.

Newton, R.G. (1982), *Scattering Theory of Waves and Particles, 2nd ed.,* Springer-Verlag, Berlin.

Ramazanov, T.S., Dzhumagulova, K.N., Omarbakiyeva, Y.A. and Ropke, G. (2007), *Scattering of Low-Energy Electrons by Noble Gas Atoms in Partially Ionized Plasma,* 34th EPS Conference on Plasma Physics, Warsaw, ECA, vol. 31F, pp. 2.093.

Ronniger, M. (2006), *The Optical Theorem and Partial Wave Unitarity,* Seminars on Theoretical Particle Physics, University of Bonn, held 29/06/2006 (unpublished).

Sakuri, J.J. (1985), *Modern Quantum Mechanics,* Addison-Wesley, New York.

Shajesh, K.V. (2010), *Eikonal Approximation,* Available at http://www.nhn.ou.edu/~shajesh/eikonal/sp.pdf Accessed 12/10/ 2016.

Sinha N., S. Singh and B. Antony (2017), *Positron Total Scattering Cross-Sections for Alkali Atoms,* Journal of Physics B: Atomic, Molecular and Optical Physics, Vol. 51(1).

Wacker, A. (2011), *Fermi's Golden Rule.* Available at www.matfys.lth.se/Andreas.Wacker/Scripts/fermiGR.pdf Accessed on 22/06/2017.

Winitzki, S. (2004), *Scattering Theory Lecture Notes,* Uni-Muenchen. Available at www.theorie.physik.uni-muenchen.de/~sergie/scattering.pdf Accessed on 30/06/2006.

QUANTITATIVE ANALYSIS OF TWO STAGES AMPLIFIER BANDWIDTH FORMULA

S. S., Maidawa[1], M. H. Ali[2], F. S. Koki[2], A., Aliyu[1]
[1]Physics Unit, Ahmadu Bello University,
School of Basic and Remedial Studies, Funtua.
[2]Physics Department, Bayero University, Kano
Email**:** saidushuaibumaidawa@gmail.com

ABSTRACT

This paper presents a quantitative analysis of an empirical formula used to determine the degree of bandwidth shrinkage of a two stage amplifier system. To quantitatively verify the empirical formula a single stage and a two stage cascaded amplifiers were designed and simulated using multisim 8.0 version and numerical data obtained were used for the verification. The frequency responses of the amplifier stages were also developed and their individual bandwidth were determined and compared with the ones proposed by the empirical formula. The results obtained for simulated and calculated bandwidths of a single stage amplifier are 478MHz and 478MHz, and 207MHz and 307MHz for the two stage cascaded amplifier respectively. The trends of the results obtained are found to be similar with the theoretical one proposed by the empirical formula. Also, when the difference between the simulated and calculated bandwidth results were taken, an equal trend of shrinkage was obtained at 0MHz and 100MHz for the two individual stages respectively.

Keywords: *Quantitative analysis, Cascaded amplifiers, Frequency response, bandwidth shrinkage,*

Introduction

The ever-growing demand for higher information transfer rates has resulted in a rapid emergence of high speed data communication system. Silicon transistor circuits are the only candidates that can achieve the required level of speed (Mohan ,2000). Wide- band amplifiers are one of the most critical building blocks at both the transmitting and receiving ends in conventional circuit implementations. Furthermore, a wideband as well as high power design are needed at the transmitting ends (Norman and Helge, 2001). Silicon based transistor with large transition frequency are available only at lower power. The demand of large power at the transmitting end is achieved by cascading. When an amplifying stage is in cascade with another one in demand of large power, the overall bandwidth will be smaller than the smaller of the two. However, silicon based transistors circuits implementation faces serious challenges due to the inferior parasitic characteristics in silicon-based transistor technology complicating the procedure for a wide-band design. One of the major effects of these parasitic elements is shrinking bandwidth (Sedha, 2005). The degree of the bandwidth shrinkage is proposed by (Robert, 2009) in an empirical formula. This work intends to quantitatively verify the trends of the bandwidth shrinkage proposed by the empirical formula

CIRCUIT TOPOLOGY

This paper brings to fore a topology that will enhance the transmission of data at high rate by using the features of cascaded amplifiers at high frequency and at the same time verify the shrinking features suffered by the bandwidth as more stages are cascaded (Paul, 2000).

A small-signal, class A, common-emitter voltage amplifier was used with a radio-frequency (RF) response. The circuit of a single stage CE amplifier using an NPN transistor that was use is shown in the figure 1 below.

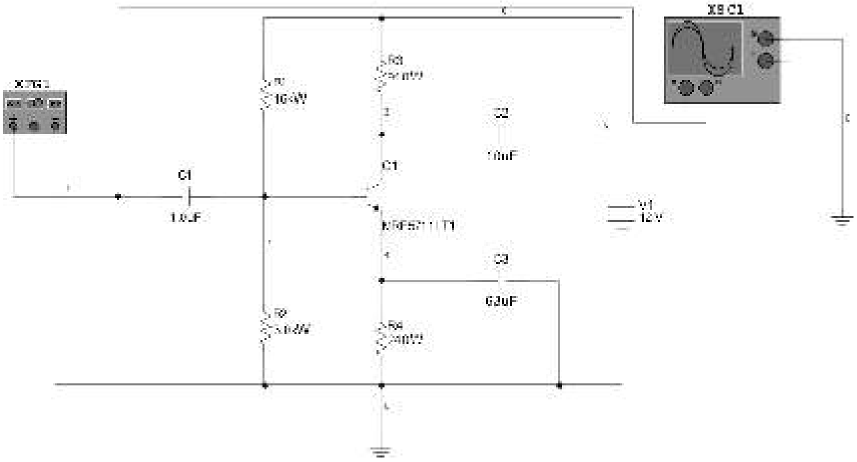

Fig. 1 A single state common emitter(CE) amplifier (Robert and Louis, 2009).

Here, base is the driven element. The input signal is injected into the base emitter circuit whereas output signal is taken out from the collector-emitter circuit. From previous works, the emitter-base junction E/B is forward bias by V_{BB} and the collector –base junction C/B is reverse-biased by V_{cc}. The Q-point or working condition is determined by Vcc together with R_E and Rc (Theraja, 2000).

In this paper, a two stage cascaded amplifier is used to show the trends of bandwidth shrinkage.

Suppose the individual gain of the stages is known, the overall gain can be calculated using equations 1 and 2.

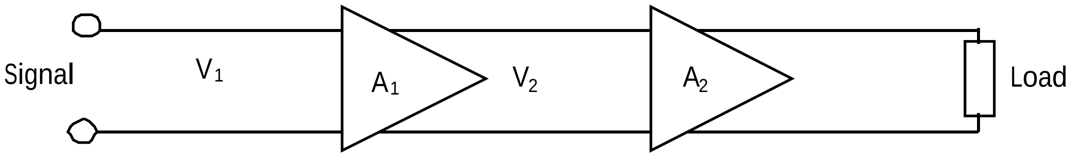

Fig. 2 Amplifier Stages in Cascade

$$Av = \frac{V_3}{V_1} = \frac{V_2 V_3}{V_1 V_2} = A_1 A_2 \qquad 1$$

The decibel voltage gain will be

$$Av = 20 \log_{10} \frac{V_0}{V_{in}} dB \qquad 2$$

$$\text{Cut-off frequency} \quad \frac{Av\ (mid\ gain)}{\sqrt{2}} \qquad 3$$

(Gupta, 2007)

Bandwidth of an Amplifier

Most amplifiers have relatively constant gain over a certain range (band) of frequencies; this is called the bandwidth (BW) of the amplifier.

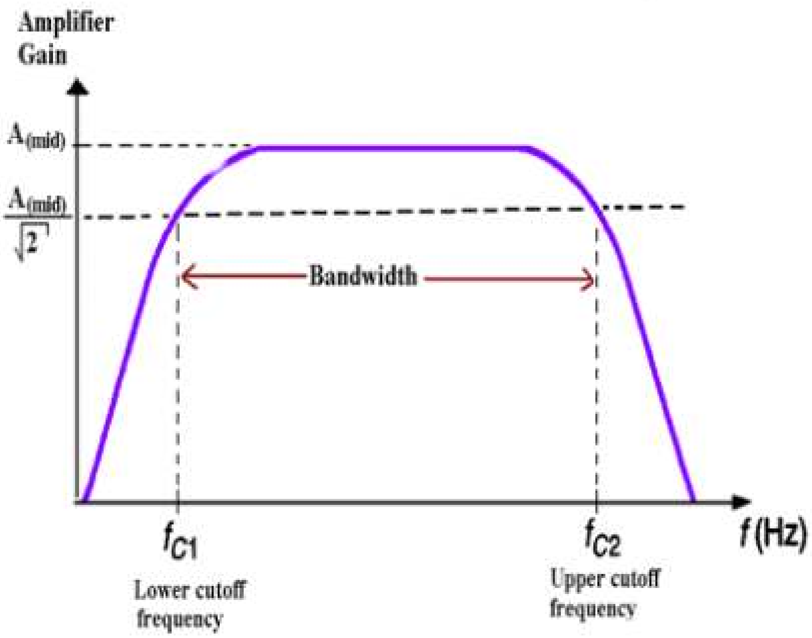

Fig. 3 Typical frequency response of an Amplifier

$$BW = f_{c2} - f_{c1} \qquad 4$$

The operating frequency of an amplifier is equal to the geometric center frequency f_0

$$f_0 = \sqrt{(f_{c1} f_{c2})} \qquad 5$$

The ratio of f_0 to f_{c1} equals the ratio of f_{c2} to f_0, that is:

$$f_0/f_{c1} = f_{c2}/f_0 \qquad 6$$

Therefore, we also have that:

$$f_{c1} = f_c^2 - f_{c1}, \quad f_{c2} = f_0^2 - f_{c1} \qquad 7$$

(Gupta *et al*, 2007).

BANDWIDTH SHRINKAGE

In multistage amplifier i.e. when two or more amplifiers are cascaded, there is always the problem of bandwidth shrinkage. The theoretical empirical formula used for determining this bandwidth shrinkage is given by

$$f_{3dB} = 1.1\frac{1}{\sqrt{f_1^{-2} + f_2^{-2} + f_3^{-2} + \ldots\ldots + f_N^{-2}}} \qquad 8$$

This implies that,

$$\frac{1}{f_{3dB}} = 1.1\sqrt{\frac{1}{(f_1^{-2})^2} + \frac{1}{(f_2^{-2})^2} + \frac{1}{(f_3^{-2})^2} + \ldots\ldots + \frac{1}{(f_N^{-2})^2}} \qquad 9$$

Equations (8) and (9) are the overall theoretical bandwidths for non-identical cascaded amplifiers. If the cascaded amplifiers are identical, then their overall theoretical bandwidth would be

$$\frac{1}{f_{3dB}} = 1.1\sqrt{\frac{1}{(f_N)^2}} \qquad 10$$

Thus, equation (10) is the theoretical empirical formula for determining the bandwidth of identical multistage amplifiers (John, 2003).

AMPLIFIER DESIGN

A single stage bipolar junction transistor amplifier would be designed and used as the unit stage of the other one to have a two stage cascaded amplifiers. The amplifier design was carried out using Multisim 8.0 with MRF5711LT1 Transistor and other adjoining components. The 'origin' was thereafter used to plot all the graphs using the data obtained from the simulation and from the graph other values were obtained. Firstly, the input and output data of the selected transistor were determined using the designed circuits in figures (6) and (7) respectively. The characteristics curves were drawn as shown in figures (8) and (9) respectively. From the characteristics curve of figure (8) V_{BE} was obtained and from the characteristics curve of figure (9) the biasing voltage Vcc, resistors and capacitors were obtained. The Vcc (dc supply) battery was chosen along the Vcc axis. The biasing voltage V_{CE} was approximated to be ½ Vcc. By selecting a particular value of I_B, the Q-point was located as the intersection of the selected values. The value of Ic at the Q-point was obtained from the curve (Edward,2006). When analyzing common- emitter (CE) amplifier one has to bear in mind that the collector resistor/impedance for one stage becomes the base resistor for the next stage (Navas, 2000). The design was intended to use high efficiency class A amplifier with a single MRF5711LT1 (NPN transistor) (Theraja, 2000). A single stage common- emitter was designed, then, cascaded to obtain a two-stage amplifier as shown in figures (6) and (7). It is common to encounter a lot of iterations at the course of the design (Alan & Davis, 2001). The simulated gains and bandwidths were calculated from the graphs obtained in Figures (10), (11) and (12) respectively for each stage using 'origin'. Theoretical empirical formula for bandwidth was used to calculate the bandwidth for each stage and compared with the one obtained from the simulated results. The difference between the simulated and calculated bandwidth results was also obtained.

Using ohms law, the emitter resistor is given by

$$R_E = \frac{V_E}{I_E} \qquad 11$$

Where $R_E = \frac{V_{CC}}{10 I_C}$ 12

And from the output loop

$$R_C = \frac{V_{CC} - V_{CC} - V_E}{I_C} \qquad 13$$

The collector emitter current amplification factor is given by (John, 2003)

$$b = \frac{I_C}{I_B} \qquad 14$$

For silicon $V_{BE} = 0.7V$

$$R_2 = \frac{1}{10}(bR_E) \qquad 15$$

From potential divider (Robert, 2009)

$$R_1 = \frac{V_{CC} R_2 - V_{BB} R_2}{V_{BB}} \qquad 16$$

The coupling capacitor C and the emitter by pass capacitor C_E were obtained using (Gupta, 2007)

$$C = \frac{10}{2pf\,(R_E - R_{in})} \qquad 17$$

And

$$C_E = \frac{10}{2pf R_E} \qquad 18$$

Where

$$R_E = R_2 // R_1 \qquad 19$$

$$R_{in} = R_2 // R_1 \beta r_e \qquad 20$$

$$r\pi = \beta r_e \qquad 21$$

and

$$r_e = \frac{26mV}{I_E} \qquad 22$$

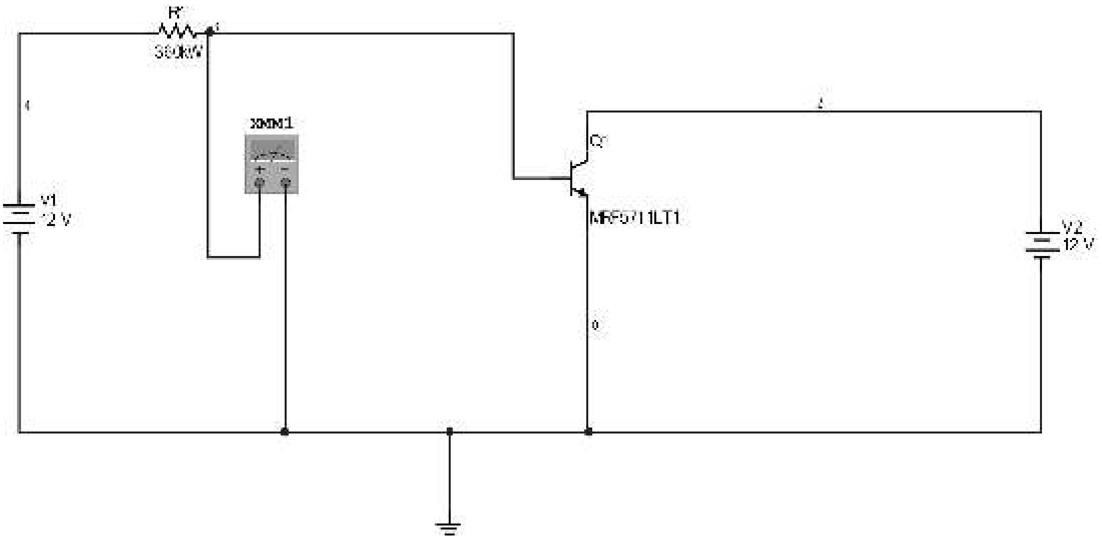

Fig. 4 Circuit for the input transistor

Table 1: Transistor input data

V_{BE}/V				
$I_B/\mu A$	$V_{CE=O}$	$V_{CE=O.2V}$	$V_{CE=O.4V}$	$V_{CE=O.6V}$
0	0	0	0	0
10	0.63473	0.70770	0.70794	0.70794
20	0.65357	0.72494	0.72519	0.72519
30	0.66508	0.73714	0.73740	0.73741
40	0.67216	0.74412	0.74438	0.74439
50	0.67819	0.75009	0.75037	0.75038
60	0.68312	0.75502	0.75531	0.75532
70	0.68596	0.75788	0.75819	0.75820
80	0.69090	0.76288	0.76320	0.76320
90	0.69477	0.76685	0.76718	0.76721
100	0.69694	0.76908	0.76943	0.76945

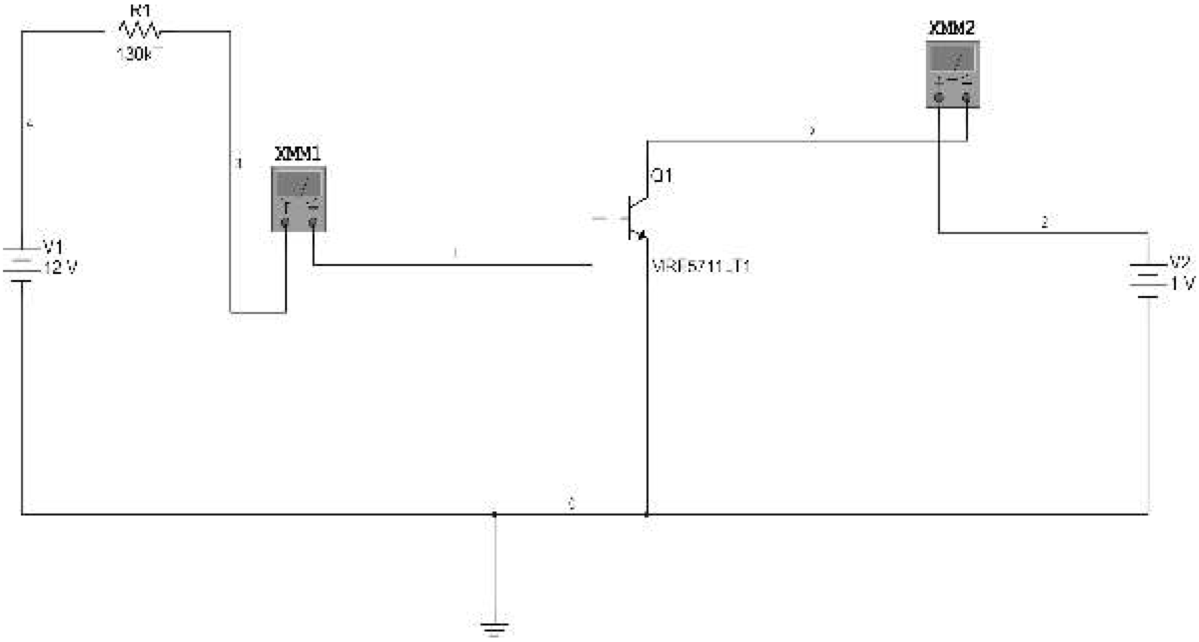

Fig. 5 Circuit for the output transistor

Table 2 Transistor output data

$I_C/\mu A$							
V_{CE}/V	$I_B=10\mu A$	$I_B=20\mu A$	$I_B=30\mu A$	$I_B=40\mu A$	$I_B=50\mu A$	$I_B=60\mu A$	$I_B=70\mu A$
0	0	0	0	0	0	0	0
1	1.052	2.041	3.136	4.142	5.067	6.154	6.907
2	1.101	2.136	3.282	4.336	5.306	6.445	7.234
3	1.149	2.231	3.429	4.531	5.545	6.736	7.561
4	1.198	2.326	3.576	4.725	5.784	7.027	7.881
5	1.246	1.420	3.722	5.921	6.023	7.318	8.215
6	1.295	1.515	3.869	5.114	6.262	7.608	8.542
7	1.343	2.610	4.015	5.309	6.500	8.899	8.868
8	1.392	2.705	4.162	5.503	6.739	8.190	9.195
9	1.441	2.801	4.309	5.699	6.978	8.482	9.523
10	1.489	2.895	4.457	5.892	7.217	9.772	9.850
11	1.537	2.990	4.603	6.088	7.455	9.063	10.177
12	1.586	3.084	4.750	6.281	7.693	9.353	10.504

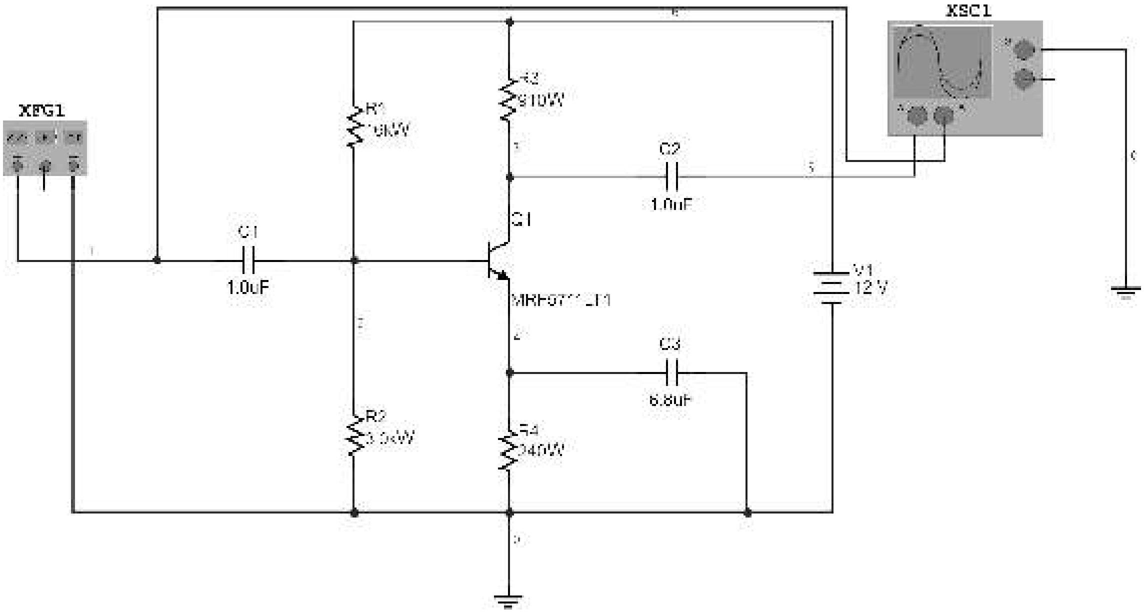

Fig. 6 A Single Stage Amplifier

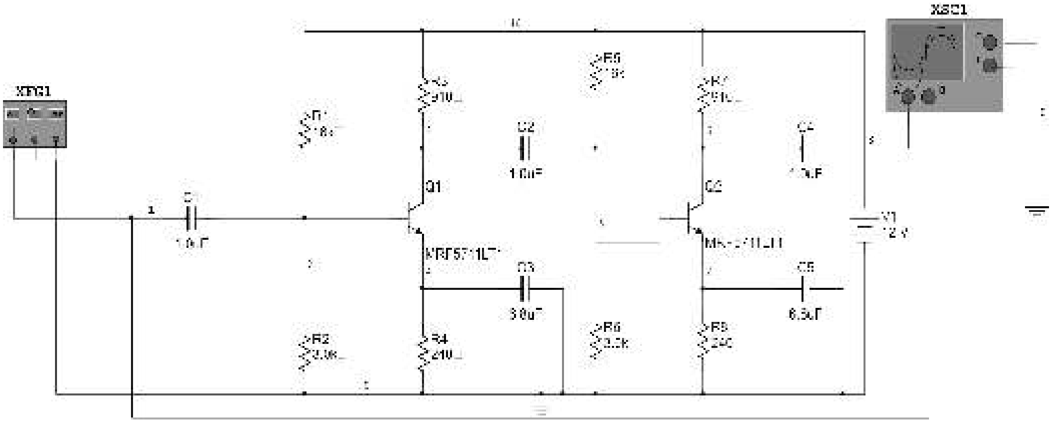

Fig. 7 A two stage cascaded amplifier

RESULTS AND DISCUSSION

The following are the data obtained from the input and output characteristics:

$V_{EE} = 0.7V$, for silicon transistor,

$V_{CC} = 12V, V_{CE} = \frac{1}{2} V_{CC} = 6V$

$I_C = 5.2mA, I_B = 40\mu A, I_E = I_C = 5.2mA$

In this section, the configurations designed for the two stages of amplifiers using multisim simulation software version 8.0 and frequency responses of each stage was plotted using data analysis and technical graphics, 'origin' software version 5.0 and also using the empirical formula for the multistage amplifier bandwidth in equation (10).

Using the above design equations the following data were obtained and used in the simulation:

Using the above design equations the following data were obtained and used in the simulation:

R_1 = 16*k*? , using equations (15) and (16) above;

R_2 = 3*k*? , using equations (11),(14) and (15) above;

Rc = 923? , used 910 ? (std) , using equations (11),(12) and (13) above;

R_E = 230.8? , used 240 ? (std) , using equation (12) above;

C = C_1=1.03μF, used 1.0 μF (std) , using equations (17),(19),(20),(21), and(22) above; and

C_E = 6.8μ*F*, using equations (11) and (18) above.

The simulation results obtained are as follows:

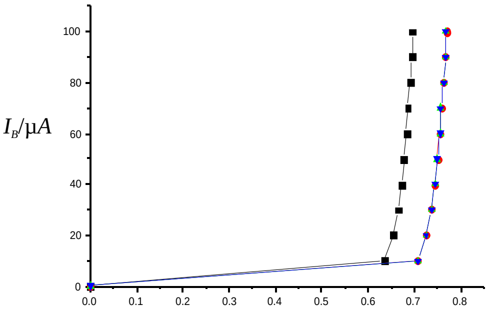

Fig. 8 Transistor input characteristics

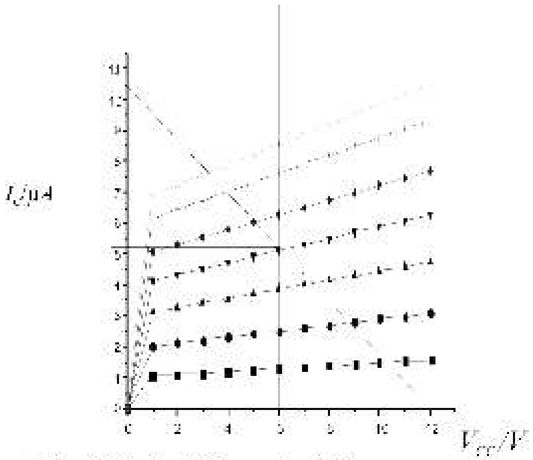

Fig. 9 Output Characteristics

*T*able 3 Table 1 Values of the Voltage Gain, Av of the Single-Stage Amplifier.

f/Hz	V_{in}/mV	V_{out}/mV	$A_V = \frac{V_{out}}{V_{in}}$	$A_V = 20log\frac{V_{out}}{V_{in}}$ dB
100	80	340	4.25	12.
1000	80	2700	33.75	30.57
10000	80	8600	107.5	40.63
100000	80	9600	120.00	41.58
1000000	80	10000	125.00	41.94
10000000	80	10000	125.00	41.94
100000000	80	10000	125.00	41.94
1000000000	80	1250	15.63	23.88

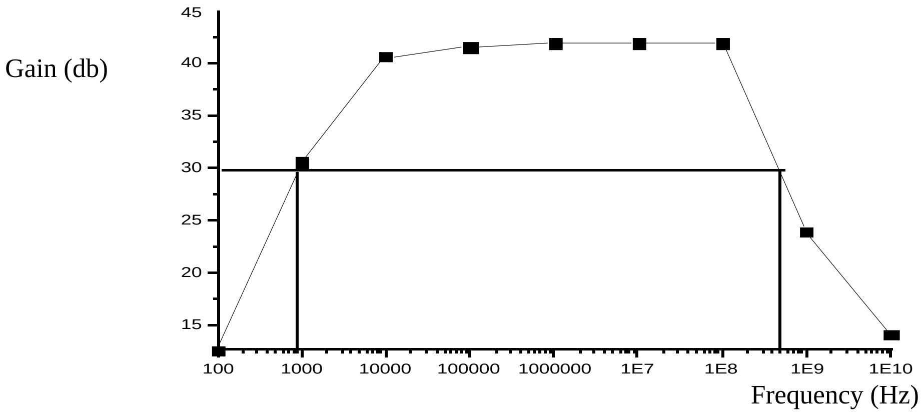

Fig. 10. Frequency response of the Single – stage Amplifier.

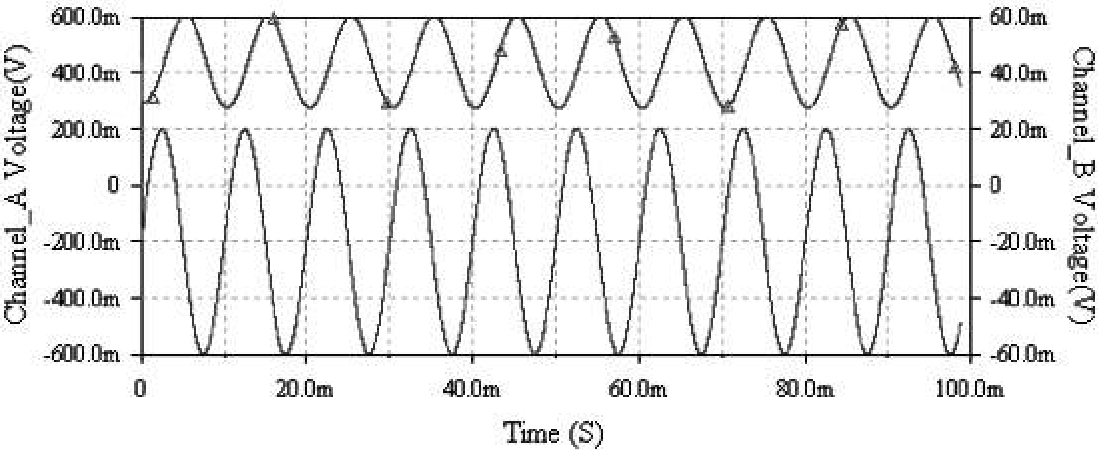

Fig. 11 Single stage oscilloscope at 100Hz

Table 4: Table 2 Values of the Voltage Gain, Av of two -stage Cascaded Amplifier

f/Hz	V_{in}/mV	V_{out}/mV	$A_V = \frac{V_{out}}{V_{in}}$	$A_V = 20log\frac{V_{out}}{V_{in}}$ dB
100	80	1100	13.75	22.77
1000	80	11000	137.50	42.77
10000	80	11000	137.50	42.77
100000	80	11000	137.50	42.77
1000000	80	11000	137.50	42.77
10000000	80	11000	137.50	42.77
100000000	80	7000	87.50	38.84
1000000000	80	300	3.75	11.48

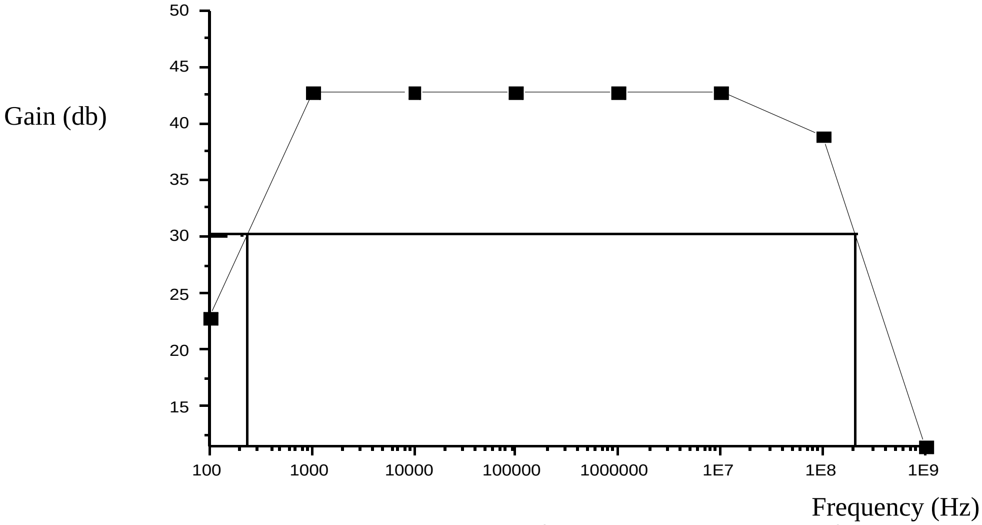

Fig. 12 Frequency response of two stage cascaded Amplifier

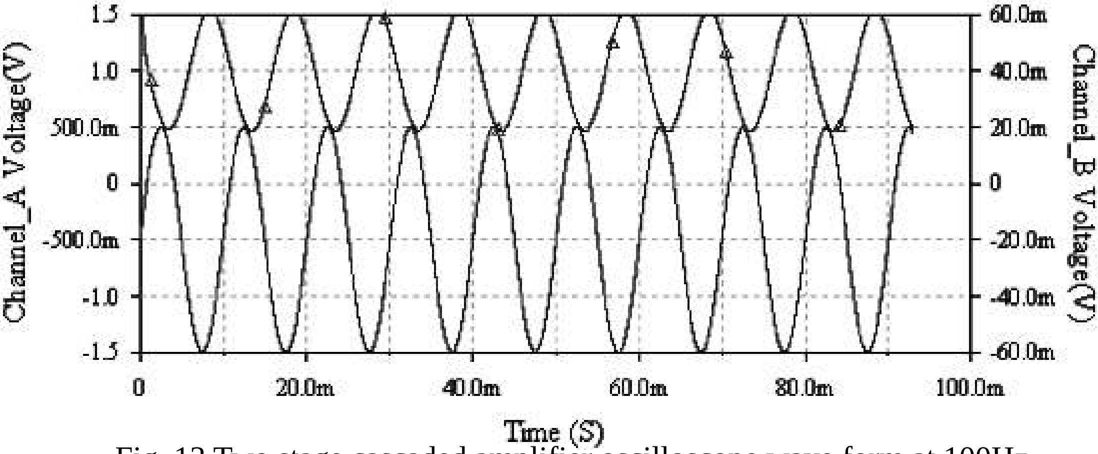

Fig. 13 Two stage cascaded amplifier oscilloscope wave form at 100Hz

Table 5: Summary of Results

AMPLIFIER CONFIGURATION	GAIN(dB)	SIMULATED BANDWIDTH(MHz)	CALCULATED BANDWIDTH(MHz)	DIFFERENCE BETWEEN THE SIMULATED AND CALCULATED BANDWIDTH (MHz)
Si ngle stage	41.94	478	478	0
Two stage cascaded	42.77	207	307	100

CONCLUSI0N

This paper presents a quantitative analysis of two stages amplifier bandwidth formula to determine its bandwidth shrinkage using Multisim 8.0. In both the simulated and theoretical results obtained, single-stage amplifier showed wider bandwidth of 478MHz with a gain of 41.94 dB and a theoretical bandwidth of 478MHz. The two-stage cascaded amplifier showed bandwidth shrinkage of 207MHz with a gain of 42.77dB and theoretical bandwidth shrinkage of 307MHz. Also, the difference between the simulated and calculated bandwidth results showed a shrinkage of 100MHz, that is, between single stage and two stage cascaded are 0MHz and 100MHz. This indicates that the trends of shrinkage of the bandwidth in the simulated results is comparable with the empirical formula.

REFERENCES

Alan, W. and Davis, K.A (2001),'Radio Frequency circuit Design, John Willey & sons Inc. publications pp33-45.

Benedict, R.R (1976), 'Electronics for Scientist and Engineers', prentice-Hall international, pp171-223.

Edward, H. (2006), 'Electrical and Electronics Technology', Dorling Kingsley (India) PVt.LTD, p362.

Gupta, S.C, Kulshreshtha, D.C and Bhargava, N.N (2007), 'Basic Electronics and Linear Circuits', Tata McGraw-Hill Publishing Company LTD, New Delhi (India) pp201-205,p301

John Bird, (2003), Electrical Circuit Theory and Technology', Newnes, An imprint of Elsevier science Linacre House , Jordan Hill, oxford ox28DP 200 Wheeler Rd, Burlindton, pp145-151.

Mohan, S. (2000),'Bandwidth extension in CMOS with optimized on-chip inductors ',IEEE,ISSC, vol35,pp346-355

Norman, D. and Helge, G. (2001). 'Radio Frequency Transistors, Principles and Practical Applications', 2nd edition, Published by Butterworth-Heinemann. Pp120.

Randy, G.S (2000), 'Tab Electronics Guide to understanding Electricity and Electronics', McGraw-Hill Companies, Inc. pp301-306.

Robert, L.B and Louis N. (2009), 'Electronic Devices and Circuit Theory' , Dorling Kindersley (India) PVt.LTD, pp573-578.

Sedha, R.S (2005), 'Applied Electronics' S. Chand and company LTD. New Delhi, pp462-463.

Theraja B.L (2000), 'Fundamentals of Electrical Engineering and Electronics', S. Chand & Company LTD, Ram Nagar, New Delhi (India), pp679-

INVESTIGATIONS OF BOREHOLES USING SEISMIC REFRACTION TOMOGRAPHY IN NIGERIAN DEFENCE ACADEMY KADUNA, KADUNA NIGERIA

[1*]Shaibu, I.,[2]Udensi, E. E., [1]Chinwuko, A. I., [2]Usman, D. A., and [2]Adetona, A. A. Omale. M. E
[1]Department of Geology, Federal University Gusau, Zamfara State
[2]Department of Physics, Federal University of Technology, Minna, Niger State
Email: isahshaibu1982@gmail.com

ABSTRACT

Seismic refraction tomography is unique in the sense that shot are taken at every receiver position along the spread. In that way, it becomes possible to conduct both forward and reverse shooting simultaneously along the profile lines. Therefore, every point within the subsurface along the profile lines is probed by both forward and reversed shots. This leads to what one might call the scanning of the subsurface. The data were processed with ReflexW software and a conventional forward and reversed travel time curve was plotted for each profile lines. Thereafter joint inversion of the travel time picks was carried out. This resulted in the generation of an iterative model, which was used to generate tomographic sections. The result of seismic refraction tomography showed lateral and vertical variation in velocity along most of the profile lines, thereby giving a true image of velocity distribution, both vertically and laterally within the subsurface. Refraction Tomography gave accurate depth and thickness of the overburden along the profile and to delineate aquifer potential in the basement topography. The aquifer is estimated to be around 55m to 65m along the entire profile line. In sub profiles lines, the velocity range of the first layer is 600 m/s to 1400 m/s , the thickness range of the first layer is 0.7 m to 2.3 m , the velocity indicate loose materials around the zones. The velocity range of the second layers is from 1500 m/s to 2000 m/s , with thickness range of 11.0 m to 15.7 m. The third layer is characterized by velocity of 2400 m/s which is the fresh/fractured basement with good aquifer potentials.

Keywords: *Seismic Refraction Tomography, Groundwater Investigations, Nigerian Defence Academy, Kaduna, Nigeria.*

Introduction

Seismic refraction tomography is an imaging technique (Tien-When and Phillips,2002), which applies the same basic principle as conventional refraction shooting , except for the fact that an offshot is fired before the first geophone, at each geophone point, and beyond the last geophone, thereby having far more number of shots than the conventional seismic method. (Kearey and Brooks, 2002).

The conventional seismic refraction method which involves only shooting of aforward and reversed shot has long been used to determine depths and velocities within the subsurface. Experiments have shown that this can only be used to determine the velocities at the shot points not along the entire profile. This has in time past led to erroneous assumption of the same velocity across the entire profile within the subsurface, thereby masking area of anomalous velocities and depth variations merely covered by a very thin overburden thickness (Dobrin, 1976). When the refractor is suspected to have a dip, the velocities of the beds and the dip of the interface can be obtained by shooting a second complementary profile in the opposite direction. (Lowrie, 1997). According to Osemeikhian and Asokhia (1994) the refraction method is mainly used for mapping of the weathered layer, for determining depth to water table and for engineering purposes, also for applying correction to reflection data.

Objectives Of This Work Include:

(i) To image the subsurface and determine the nature of the strata,

(ii) To determine the image of the aquifer,

(iii) To determine the depth to the refractor and the overburden thickness at the shot points and along the entire profile.

Instrumentation

The major instruments employed in this survey include the 24 channels digital seismograph (Terraloc Mark 6), sets of 25 vertical geophones, reels of cables and sledgehammer.

The multi-channel digital seismograph records 24 traces at the same time. It has a very high dynamic range that gives a very high resolution for both refraction and reflection survey. It can be used anywhere in the world and in all weather conditions(Sandmeier, 2003).The sets of 25 vertical geophones with one acting as the trigger geophone, has a frequency range of 4 -100Hz. It is used to pick the seismic signals generated by the energy source (the sledge hammer).

Methodology

Seismic refraction survey is a geophysical method to map geological structures by using head waves. Head waves involve energy which enters a high velocity medium near a critical angle and travels in the high-velocity medium nearly parallel to the refractor surface. The main quantity measured in the seismic refraction method is the time between the ignition of the seismic wave and the first arrival of energy along the path between the shot point and detectors. The first arrivals are evidences of the fastest traveling waves which are longitudinal waves. By observing first arrivals for a variety of shot detector distance, a time-distance curve can be constructed. The time-distance relations can be analyzed in term of the variation with distance of minimum time paths. Then the elastic discontinuities can be deduced from these variations, and can be interpreted in terms of the nature, depth and attitude of geologic units below the surface (Keary *et al.,* 2014).The objective is to determine the arrival times of the head waves to map the depth to the refractors in which they travel. It is a faster method that often finds application in locating the ground water table, determining depth to bedrock and configuration, mapping near-surface poorly consolidated/slow velocity layer, among other uses.

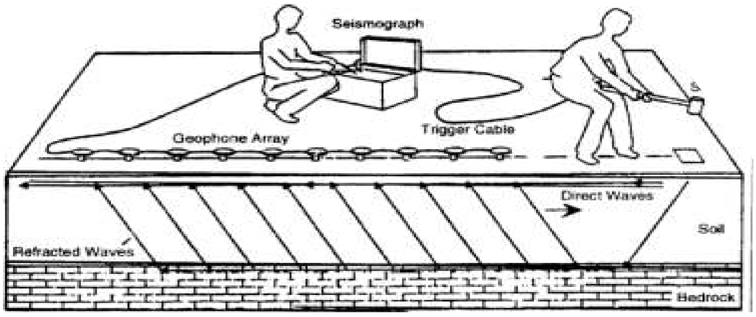

Fig.1a:Field lay out showing the path of directed and refracted seismic waves (EPA, 2002; Benson *et al.,* 1984)

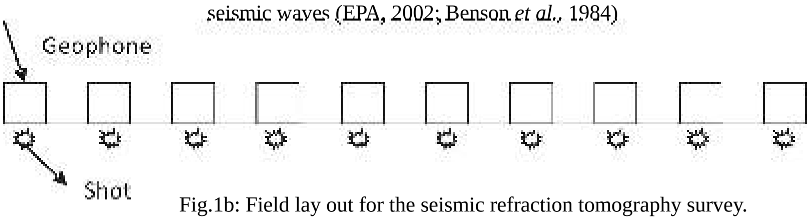

Fig.1b: Field lay out for the seismic refraction tomography survey.

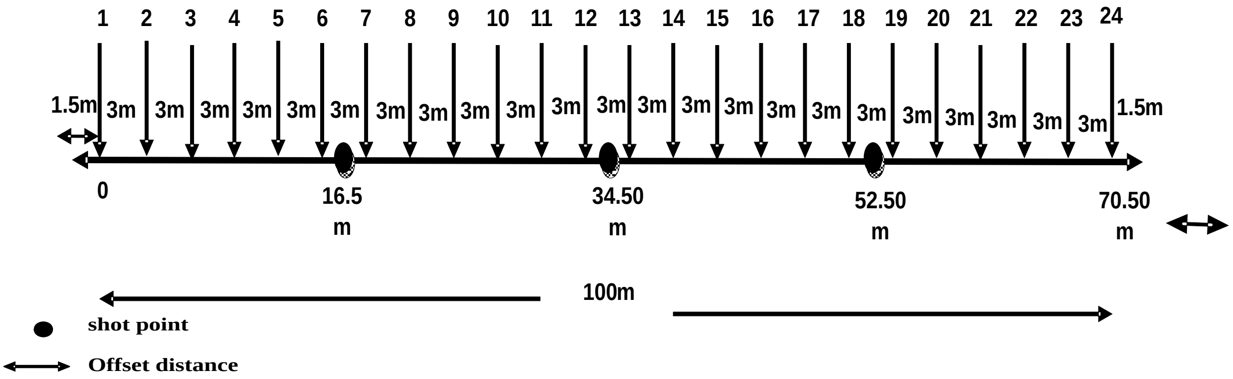

Fig. 1c: General Field set up of the geophones

Plate I: Seismic Refraction Tomography in Millennium City

Study Area Description

The Nigeria Defence Academy (NDA), located along airport road Kaduna, with coordinate of $10^{O}35^{?}$ N and 07 ^{O} 19 $^{?}$E, with elevation 648 m, was created in 1964, following the decision to expand the school in other to accommodate more staffs and students, the new site was form along airport road Kaduna Nigeria. (Fig.2) showss the study area and it is accessibility through major and minor roads, (Fig.3) shows geological maps of Nigeria showing the study area and (figure .4) shows geological map of Kaduna State (NGSA 2007).

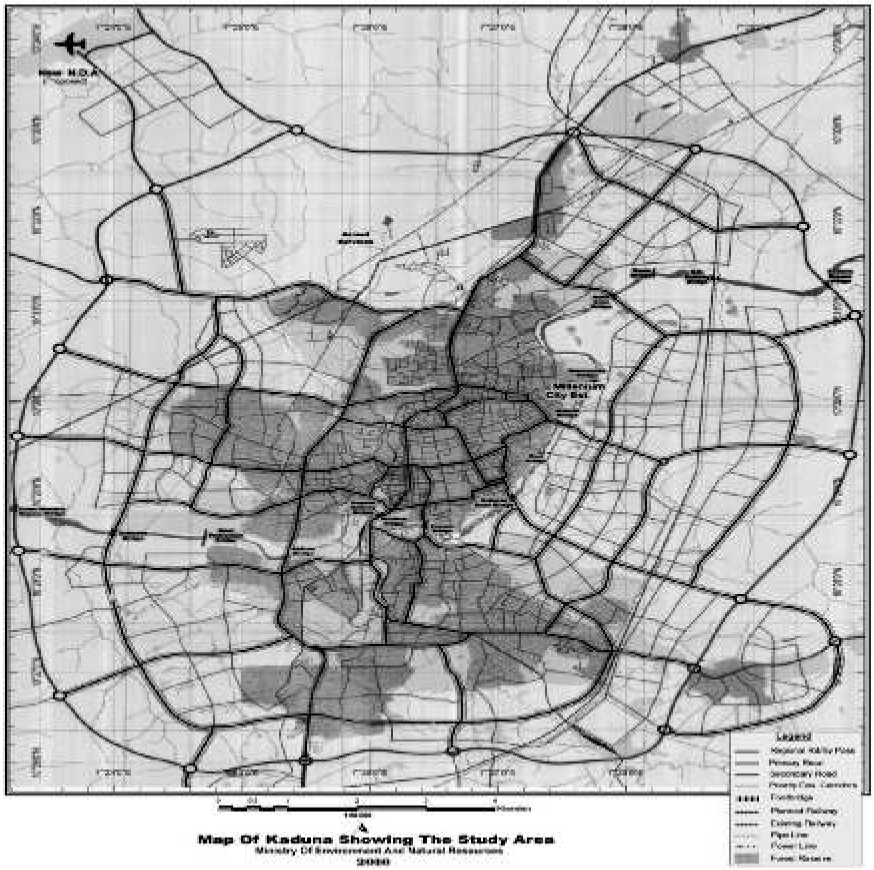
Map Of Kaduna Showing The Study Area
Ministry Of Environment And Natural Resources
2000
Legend

Fig. 2. Map of Kaduna showing the accessibility of the study areas

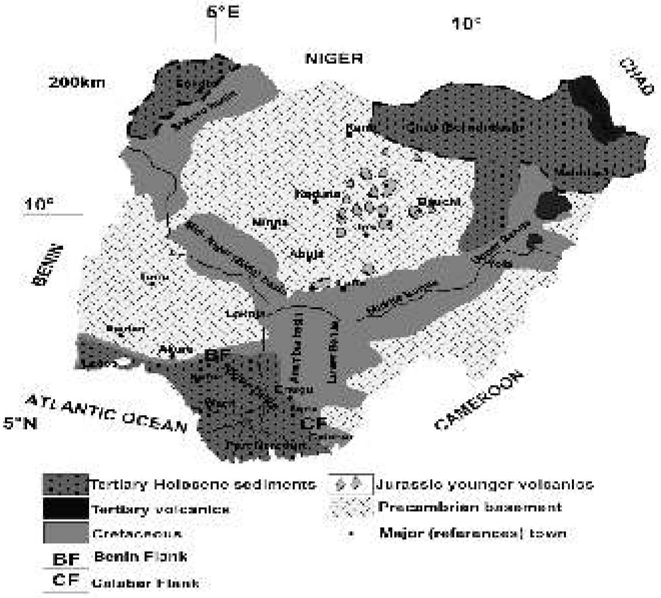

Fig. 3: Geologic map of Nigeria showing the Study Area (NGSA, 2000)

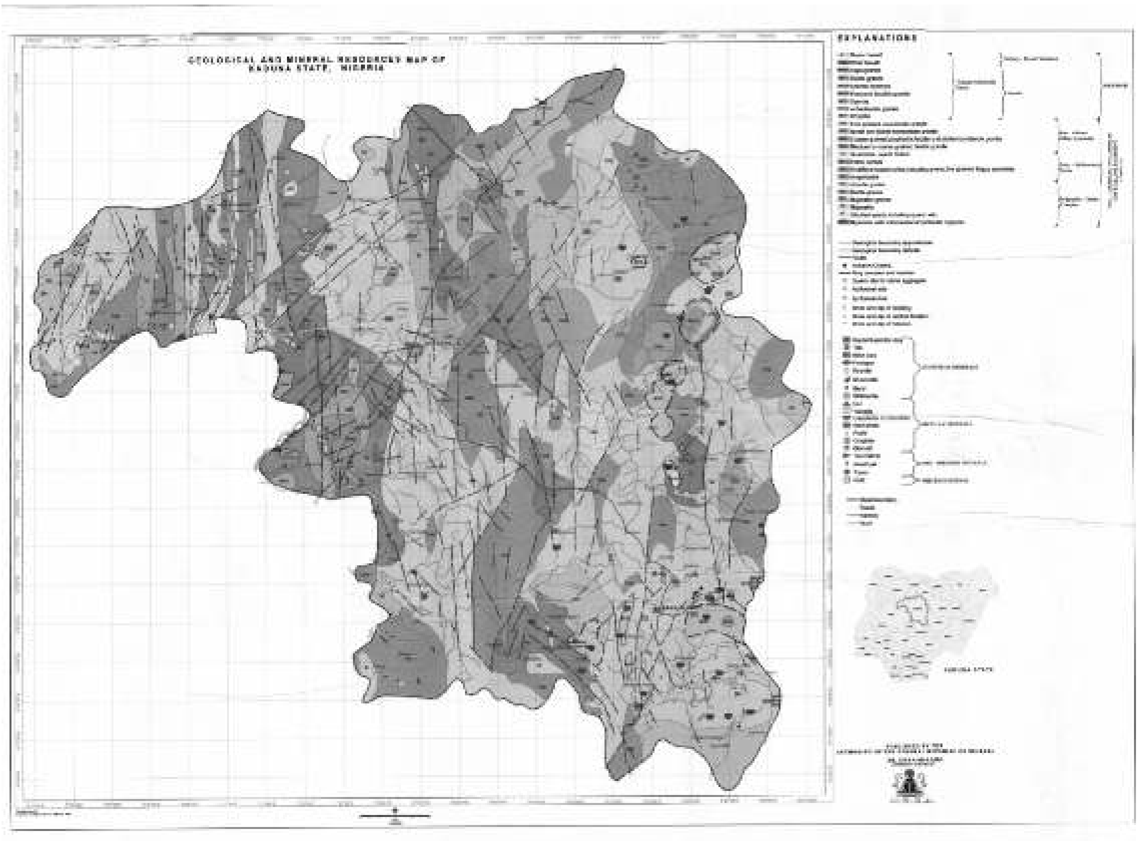
GEOLOGICAL AND MINERAL RESOURCES MAP OF KADUNA STATE, NIGERIA
EXPLANATIONS
KADUNA STATE

(Figure 4). Shows geological map of Kaduna State (NGSA 2007).

The study area lies within the Basement Complex of Northern Nigeria (Figure 3). The Basement Complex includes all rocks older than the late Proterozoic (McCurry., 1976) and is composed mainly of gneisses, migmatite, granites, and some extensive areas of schist, phyllites and Quartzites (Baimba.,1978),(Preez and Barber.,1965) according to (McMCurry.,1976).The whole Basement has been through at least two tectonic-metamorphic cycles and consequent metamorphism, magnetization and granitisation have extensively modified the original rocks so that they generally occur as relict rafts and xenoliths in migmatite and granites. Two groups of granites are present and these are the Older Granites and the Younger Granites. The Older Granites are Widespread and often give rise to smoothly domed hills which typically rise to about 170 m above the surrounding plains. (Russ.,1957). The Younger granites which include granites, syenites and rhyolites cover extensive areas in the plateau.

The area lies entirely within the Basement Complex of Northern Nigeria (Figure 3). The rocks consist of series of granites, gneisses, migmatite, low-grade schist, quartzite and amphibolites that have been grouped by the British authors as “Basement Complex of the Precambrian age” (Olugboye., 1975). The topsoil varies in composition, colour and texture at most places. They are predominantly laterite and quartz grains (deep browns or reddish brown soil). Geophysical investigation reports of (Eduvie., 2005) and (Dan –Hassan., 1999) showed that Kaduna is underlain by 3 to 5 geologic layers; the top lateritic soil, clayey sand/sandy clay, weathered transition zone, the fractured bed rock and the fresh bedrock.

Geophysical investigation and borehole drilling reports have clearly established two major aquifers. These are the overburden weathered aquifer and the fractured crystalline aquifer (Dan-Hassan and Olarufemi.,1999) at some locations these aquifers are interconnected and form a hydrogeological unit of water table surface.

Data Collection

In seismic refraction tomography, there are many shots along each profile. The seismic sources and receivers are arranged so that multiple seismic rays pass through each elements of that volume. The total travel-time for each ray are the basic data acquired for interpretation. The refraction tomography profiling adopted for this research work, seismic refraction shooting along the profile, A, B, C, D, E, D and F, of the field layout, with the 24 geophone equipment will be used in the survey. At first, measurement of geophone spacing kept at 3 m interval along each profile line will be carried out. Then the geophones will be planted firmly to the ground. They will be connected to the recording instrument (Seismograph) placed between the 12th and 13th (34.50 m) and (106.50 m) geophone respectively (mid-point of the layout) and amplifiers filters and gains will be accurately set. Source will be placed at 1.5 m offset away from the first geophone and the first shot is made. Then shots are made between the 6th and 7th geophone, 12th and 13th geophone, 18th and 19th geophone and 1.5 m offset away from 24th geophone. Then the resulting signals will be recorded in the Seismograph. The signals will be stored on the hard disk of the Seismograph. They will be 360 shot points for the dumpsite and 200 shot points for control site, the total shot points will be 560 shot points. Figure 3.9a, 3.9b and 3.9c is the field set up for the geophones and the field layout for the data collections.

Seismic Refraction Data Processing

Seismic refraction data analyses and interpretations such as delay time method, plus-minus method and the generalized reciprocal method suffer near surface attributes, such as lateral discontinuities and heterogeneity and gradients. Therefore, the analytical method used in this particular research work is refraction tomography, which is/are not subject to these constraints. The seismic refraction tomography is able to resolve velocity gradients and the lateral velocity differences or velocity changes which may be applied where conventional refraction methods fail, such as area of compaction, fault zone and karst, Zhang and Toksoz (2002), the seismic tomography method was successful in smothering lateral variations and velocity model provided by it. The software used for the seismic refraction tomography is called (Reflex W)Is a full refraction modeling and integrated software package that runs on geometric seismograph, it is an inversion routine software package. The raw data is normally stored in SEG formats were opened with Reflex W and the first particular breaks were recognized or identified and picked from wiggle mode with an automated picker, Figure 6 and adjusted manually with an interactive cursor. The first break pick files for each station were saved to plot. The tomogram through inversion was transformed into velocity models in this research works and figure 6: Representative of the seismic arrival signal in a wiggle form and picking of the first arrival were also used in this research work.

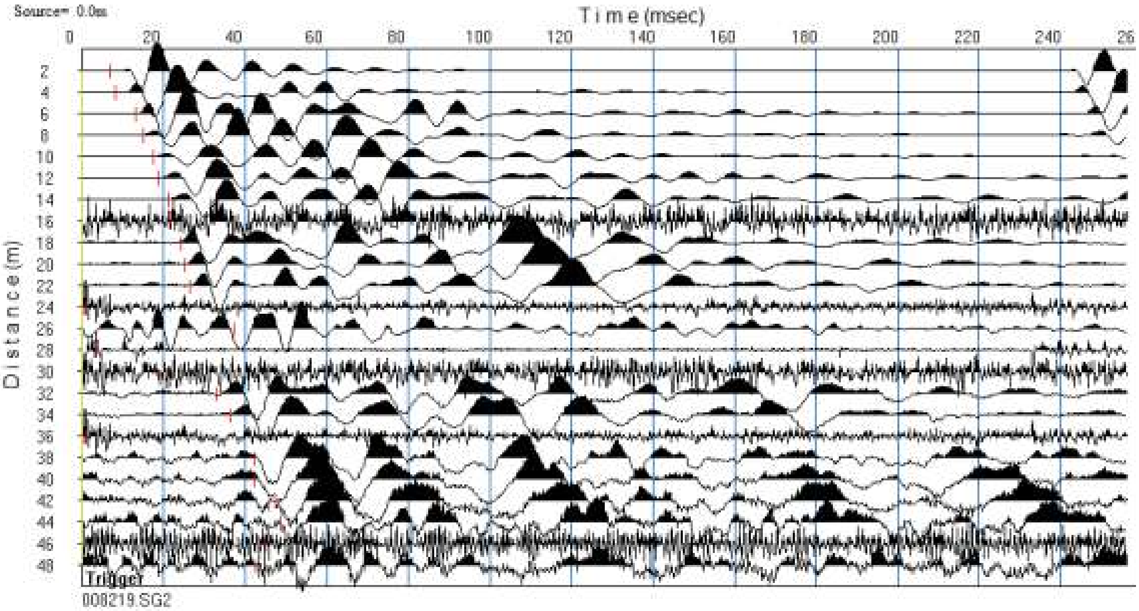

Figure 6: Representative of the seismic arrival signal in a wiggle form and picking of the first arrival

Results and Interpretation

Three seismic profiles (Figure 6, 7 and 8), were analyzed for the seismic refraction tomography techniques in other to determine the fracture zones called aquifer.

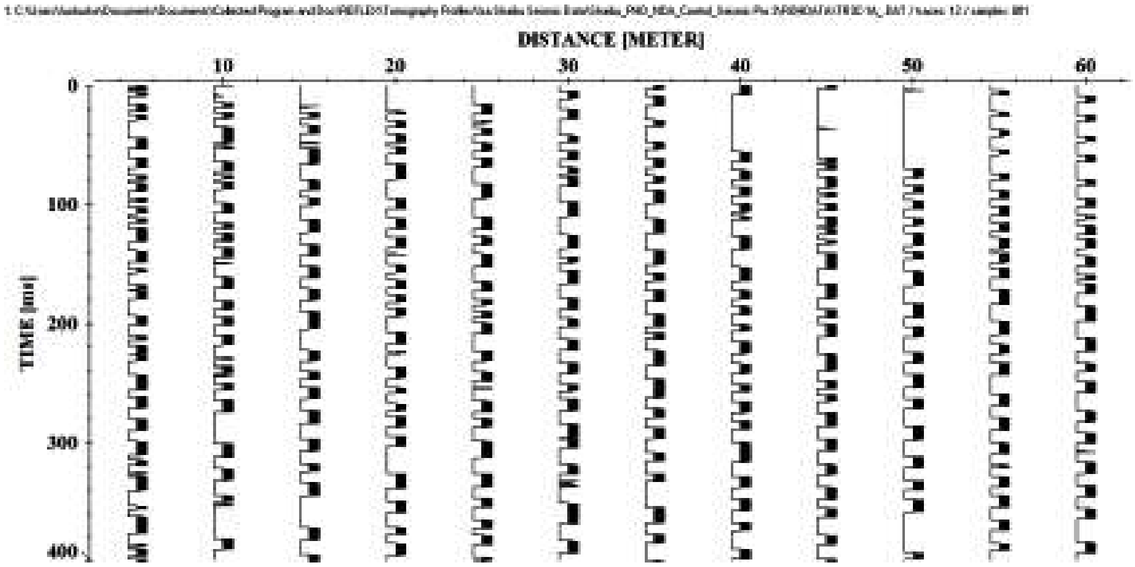

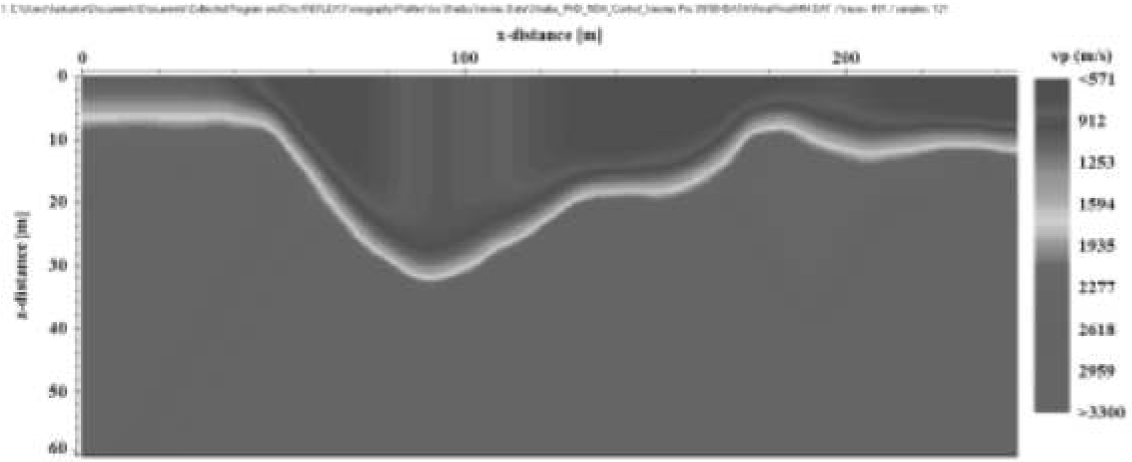

Fig. 6: Seismic Tomographic Model in Millennium city Kaduna profile 1

The tomography model (Figure 6) was able to delineate the overburden with velocity of 600 m/s to 1200 m/s and depth range of 1.0 m to 1.4m and average thickness of 1.0 m to 1.4 m, the weathered basement with velocity range of 1500m/s to 2000 m/s with average depth of 11.2 m to 16. 5 m, the average thickness of 9.7 m to 15.5 m, while fresh basement velocity is 3000m/s with of depth is 24.6m above with average thickness of 12.1 m. Comparison of the difference in depth to weathered basement and depth to the fresh basement, which represent the thickness of the weathered basement, showed that, profile as above have thicker weathered basement (11.0 m) and much more thicker at the center which is more

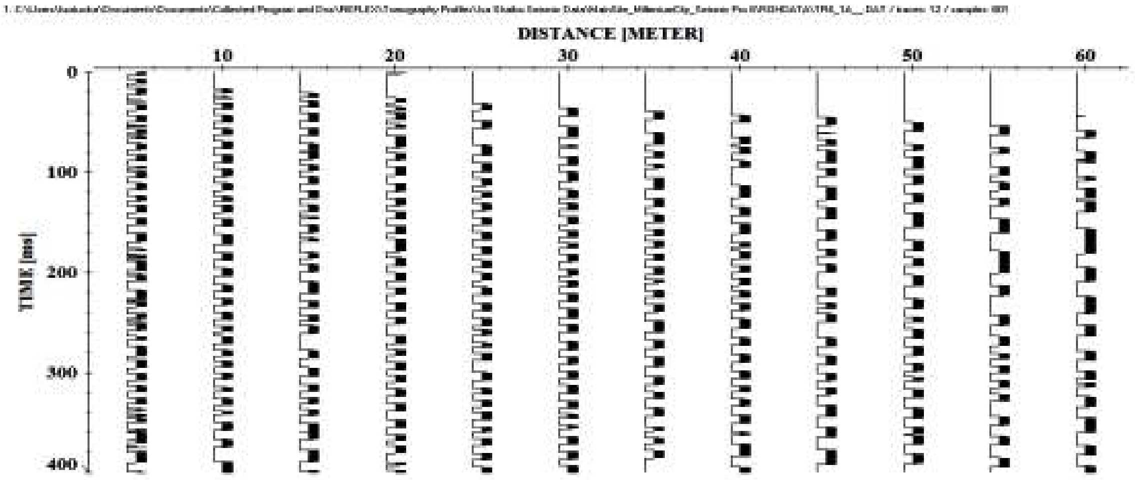

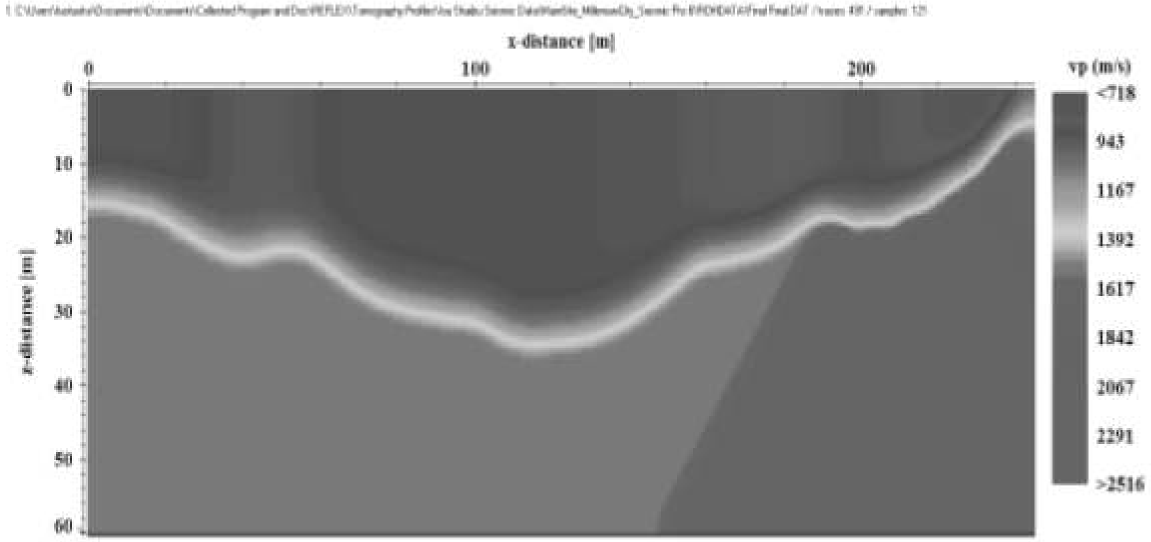

Figure 7: Seismic Tomographic Model in Millennium city Kaduna profile 2,

The tomography model (Figure 7) was able to delineate the overburden with velocity of 400 m/s to 1400 m/s and depth range of 0.9 m to 1.3m and average thickness of 0.8 m to 1.3 m, the weathered basement with velocity range of 1600m/s to 2500 m/s with average depth of 11.1 m to 13. 5 m, the average thickness of 10.1 m to 12.0 m, while fresh basement velocity 3300m/s with depth of 23.0 m above with average thickness of 12.0 m. Comparison of the difference in depth to weathered basement and depth to the fresh basement, which represent the thickness of the weathered basement, showed that, profile have thicker weathered basement (16.6 m) at the center which is about 10.8 m and much more thicker at the center, which are much more good aquifer zone.

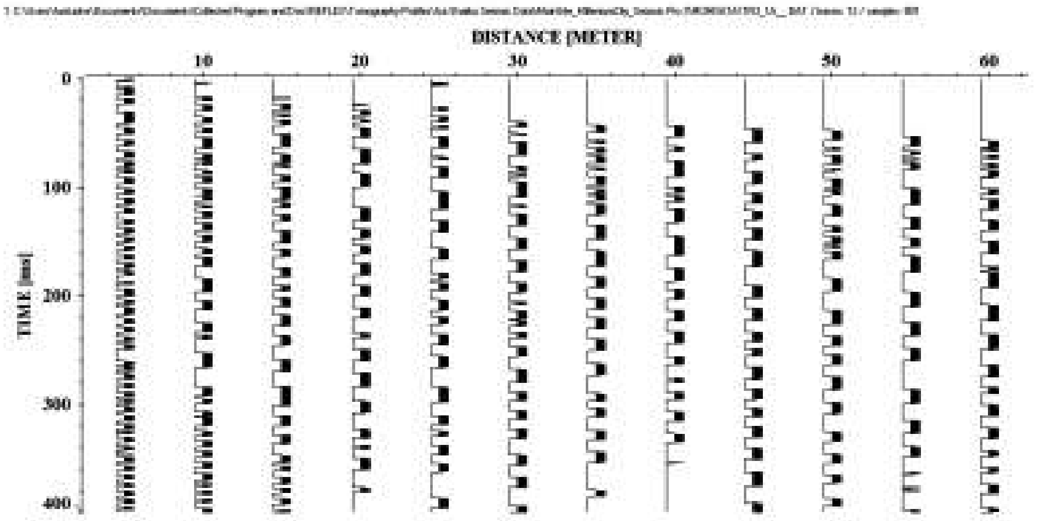

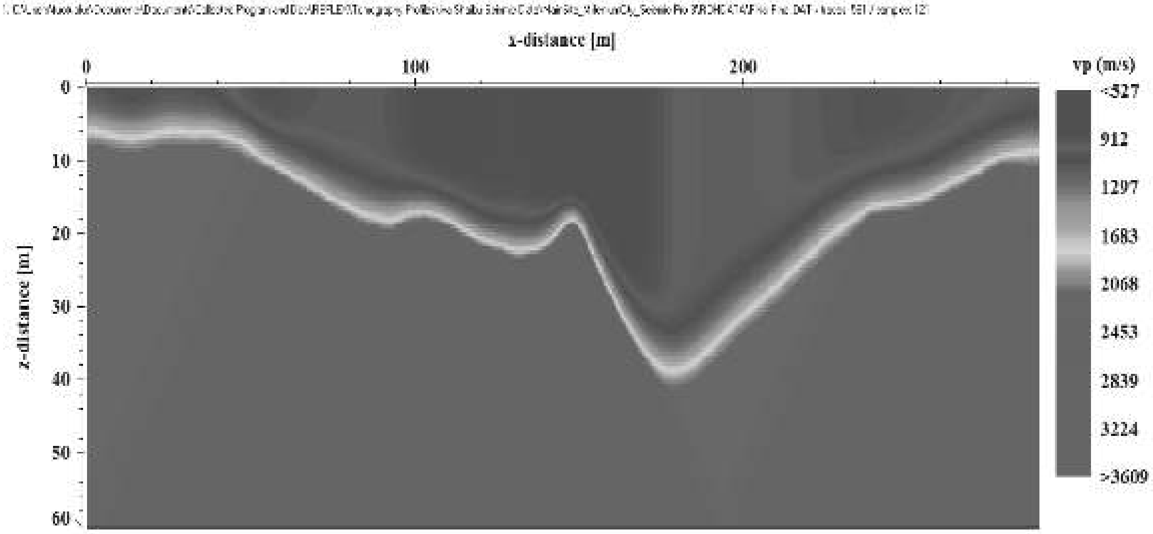

Figure 8: Seismic Tomographic Model in Millennium city Kaduna Profile 3

The tomography model (Figure 8.) was able to delineate the overburden with velocity range of 250 m/s to 1000 m/s and depth range of 0.9 m to 1.6 m and average thickness of 0.9 m to 1.6 m, the contact area between overburden and the basement showed very much undulation, the weathered basement with velocity range of 1200m/s to 1500 m/s with average depth of 8.0 m to 14. 5 m, the average thickness of 6.3 m to 13.6 m, while fresh basement velocity range is 3000 m/s, with depth of 23.1 m above with average thickness of 8.6 m. Comparison of the difference in depth to weathered basement and depth to the fresh basement, which represent the thickness of the weathered basement, showed that, profile 3 have thicker weathered basement (6.3 m) and much more thicker at the centre on this particular profile line with a very good aquifer at the center.

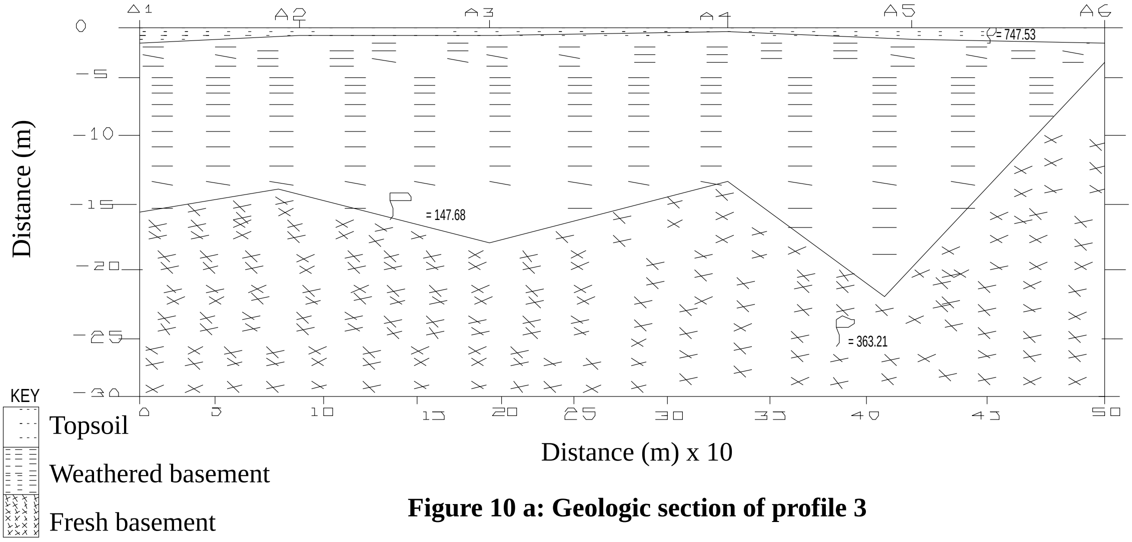

Figure 10 a: Geologic section of profile 3

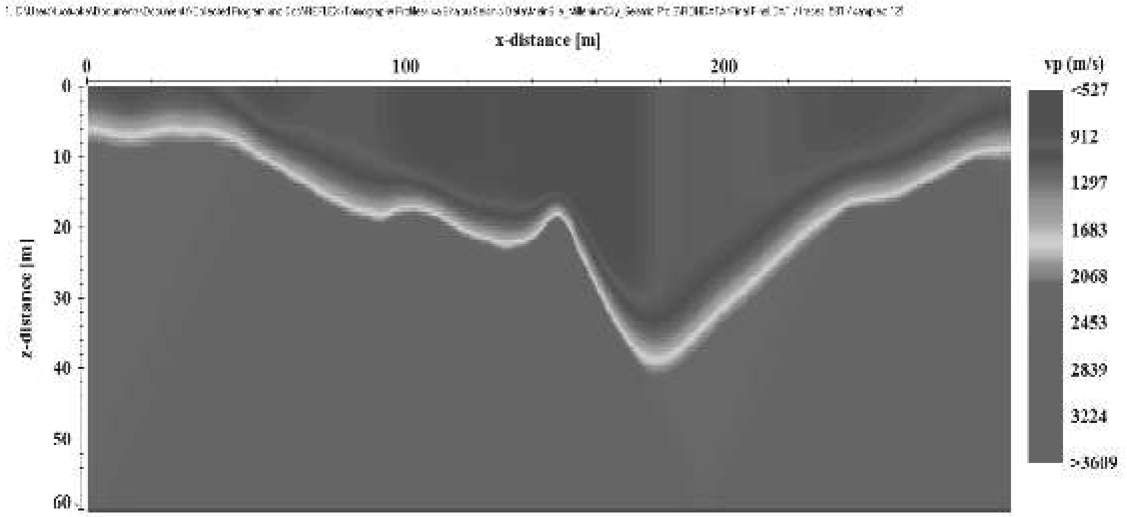

Figure 10 b: A Tomogram of Sub profile 3

Discussion

The tomographic section of figure 8, showed how velocity varied with depth along the entire profile. It would have been very erroneous to have assumed the velocities at a distance of 10 m and 50 m along the profile, at the same depth of 10m are the same, similarly for a depth of 15 m at the same distance along the profile. Figure 9 depict clearly how velocities vary along the entire profile at the same depth

Seismic refraction tomography method also delineated three to four velocity layers with different thickness and various compositions of lithology. The velocity then increases down the depth. The seismic refraction tomography indicates that even though the same number of layers is delineated, variations in thickness also exist due to different properties.

The geologic sections indicated areas or zone with very good aquifer potentials in the entire profile lines.

Conclusions

Data analysis and the interpretation of this survey have indicated the suitability and efficiency of the Seismic Refraction tomography methods in probing subsurface structures and delineating groundwater potential in basement terrain like Kaduna. These particular methods have delineated variations in velocity distributions. Fractures observed suggests geological feature that could facilitate a very good aquifer reservoir. The seismic refraction tomography has shown three to four velocity layers with different lithological compositions and thickness. The velocity increases down the depth, velocity models were used to image the subsurface geology of the entire study areas. Maximum of four layers were also delineated.

From Figure 7 above , sub profiles lines, the velocity range of the first layer is 600 m/s to 1400 m/s , the thickness range of the first layer is 0.7 m to 2.3 m , the velocity indicate loose materials around the zones. The velocity range of the second layers is from 1500 m/s to 2000 m/s , with thickness range of 11.0 m to 15.7 m. The third layer is characterized by velocity of 2400 m/s which is the fresh/fractured basement with a good aquifer potentials.

Recommendations

The present study, investigations of boreholes using seismic refraction tomography in

Nigerian Defence Academy Kaduna, Kaduna Nigeria. The study became necessary due to the increase in population of the area and the incessant water scarcity experienced by the occupants of the estate. A total drill depth of 55 m to 65 m was recommended for optimum groundwater yields in the area with a good industrial borehole if need be.

References

Baimba, J.I. (1978). Electrical resistivity tomography applied to geologic, environmental and engineering investigation at a former waste-disposal site. *Geophysics.* 71.6. B231:B339

Benson, R.C., Glaccum, R.A.,& Noel., M.R.(1984). Geophysical Technique for sensingburied wastes and waste migration. Environmental Protection Agency, pp 236.

Dan-Hassan,M.A. & Olarinfemi, M.O. (1999).Hydro-geohysical investigation of a Basement Terrain in the North-Central part of Kaduna State, Nigeria. Journal of Mining & Geology. Vol 35 (2). 18206.

Dobrin, M. B. (19976) Introduction to Geophysical Prospecting (3rd Edition), Mcgraw-Hill, New York.

Eduvie, M.O.(2005).Exploration, Evaluation and Development of groundwater in Southern Kaduna State, Nigeria: unpublished PhD thesis, Department of Geology, A.BU, Zaria

Environmental Protection Agency (EPA) United Nations.,(2002).Use of Airborne, Surface and Borehole Geophysical Techniques at contaminated sites. Reference Guide.EPA/625/R-92/007.

Kearey P. and Brooks M. (2002) An Introduction To Geophysical Exploration. Adlard and Sons Limited, The Garden City Press, Letchworth.

Lowrie W. (1997) Fundamental of Geophysics Cambridge University Press.12

McCurry, P. (1976). The Geology of Precambrian to lower Paleozoic rocks of Northern Nigeria–A review in: Kogbe, C.A. (Ed) Geology of Nigeria-Elizabeth and Published co. Lagos. *436pp.*

Ministry of Environmental and Natural Resources Kaduna. (2016). The Nigerian Climate Records. Unpublished Report, 26-28

Nigeria Geological Survey Agency (NGSA, 2006.): Generalized geological map of Nigeria. Geological Survey of Nigeria Bulletin.39:46

Osemeikhian J. E. A and Asokhia M. B. (1994) Applied Geophysics, Stamatas Services Ltd.

Olugboye, N.O. (1975). Hydrogeology of Kaduna Town. G.N.S Report No 1539.

Sandmeier, K. J., (2003) User's Guide Manual on Reflex Software, Zipser Strabe Karlsruhe, Germany.

Tien-When, Lo., and Philips, L. (2002) Fundamentals of Seismic Tomography. Geophysical Monograph Series; no. 6, Society of Exploration Geophysicists Tulsa.

Perez, J. W. & Barber, M. (1965). Distribution and chemical quality of groundwater in northern Nigeria; *Geological Survey of* Nigeria Bulletin, 36

Russ, D. M. (1957). *T*he generalised reciprocal method of seismic refraction interpretation. Society of Exploration Geophysicists,Tulsa.53, 345 – 352

Zhang, H.E. and Toksoz, A.S. (2002). Assessment of Hydrogeological Conditions in Basement Aquifers of the Precambrian Oban Massif, Southeastern Nigeria. *Journal of Applied Geophysics*, 36, 95-204.

COMPARISON OF PERFORMANCE CHARACTERISTICS OF MONOCRYSTALLINE AND POLYCRYSTALLINE PV MODULES

Jamila Tasi'u, M. S. Abubakar and M.M Aliyu**
Department of Physics, Kaduna State University.
**jtikbai@gmail.com

ABSTRACT

This study presents a comparison of performance of two commercially available 130W Rubitec Solar photovoltaic modules (PV): PV-SC1102 (Monocrystalline) and PV-HX108B (Polycrystalline), in Kaduna, Nigeria. The experiment was carried out under outdoor conditions for one month (January, 2017). Maximum power output values were determined for each module and the effect of solar irradiance on these parameters was investigated. Module parameters showed strong dependence on the solar irradiance, both modules showed considerably better power performance under high irradiance conditions, and degraded output under low irradiance. This study has determined the average modules' powers as 87.73W and 61.05W, for the Monocrystalline and Polycrystalline, respectively. Similarly, the corresponding total energies generated by the panels for the month were estimated to be 676.96Wh and 476.95Wh, with a cost per Wh of ₦16.92 and ₦12.55for the Monocrystalline and Polycrystalline, respectively. Considering the respective costs for each module, it has been concluded that the Monocrystalline solar modules are the more economical type of Photovoltaic panels to be used under the Kaduna climatic conditions.

Keywords: *Mono- and polycrystalline solar modules, PV module power and energy*

Introduction

Today, one of the most significant requirements of developed and developing countries is sustainable energy supply and utilization. Even in developed economies enjoying various methods of energy production and consumption technologies, there is high premium on affordability. In Nigeria, as in most developing countries, the demand for energy is increasing due to population and developmental requirements (Otun *et al*, 2012).Though the country is rich in oil and gas, the challenges in managing and exploiting these resources results in serious power inadequacies, leading to continuous demand for diversification by developing renewable energy sources.

Man has long relied on wood, coal and, more recently, petroleum, as the main sources of energy. However, the implications of these traditional energy sources for environmental degradation and global warming have now become a matter of great concern. In addition, it is now apparent that the fossil fuels could be depleted by about the year 2050 (Nehring, 2009), hence, compelling greater attention to alternative cleaner and renewable sources such as solar, wind and biomass. Solar energy stands out as one of the most flexible renewable sources for exploitation in different applications and power utilization levels. Photovoltaic modules provide safe, reliable, low maintenance, noiseless, and environmentally friendly source of power and the easiest energy technology in respect of design and installation (Parida *et al*, 2011).

In considering the different types of photovoltaic modules, the silicon-based technologists currently dominate the market. Silicon has several advantages such as abundance on Earth, low contamination rate, high durability, and the well-established experience in the microelectronics industry. The most widely used silicon cells are; Monocrystalline and polycrystalline, although many other technologies, such as thin-films and dye-sensitized are being developed.

Monocrystalline solar cells are made from a single crystal and are more efficient than polycrystalline. Monocrystalline silicon is the oldest semiconductor technology in the market and it has the highest conversion efficiency of around 25.6%, which is clearly superior to the cheaper and more popularly used polycrystalline, with the lower peak efficiencies of about 20.8% (Verlindan, *et al*, 2014).

As solar photovoltaic energy continues to find applications in wider areas of socio-economic life, it becomes more essential to critically examine and characterize the energy yields of the \available solar PV modules for designing applications and installations. This study is undertaken to investigate and compare the performances of Monocrystalline and polycrystalline silicon solar panels at outdoor conditions to obtain an accurate estimates of relative power performances of commercial PV modules under climatic conditions of Kaduna, Nigeria. The rated performance of PV modules provided by the manufacturer are based on the standard test conditions (i.e., irradiance 1000 W/m^2,at module temperature 25°C, and AM 1.5) which may often differ substantially from practical outdoor conditions at system installation sites. The model adopted to determine the maximum power involves the measurements of open circuit voltages, V_{oc}, and short circuit currents, I_{sc}, taking into consideration the estimated fill- factor, for the ambient temperature.

MODELING THE MODULE PERFORMANCE CHARACTERISTICS

The complex physics of the PV cell can be represented by the equivalent electrical circuit shown in Figure. 1 below.

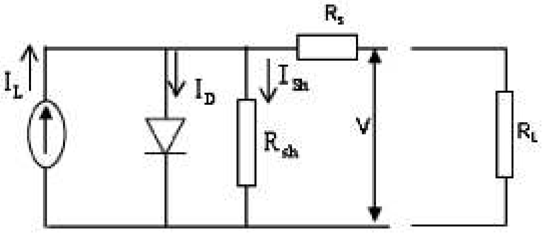

Figure : A PV cell equivalent electrical circuits (Duffie & Beckman, 2006)

The current I at the output terminals is equal to the light-generated current (I_L) less the diode current (I_D) and the shunt-leakage current (I_{sh}). The series resistance R_s represents the internal resistance to the current flow, and depends on the p-n junction depth, impurities, and contact resistance. The shunt resistance R_{sh} is inversely related to the leakage current to the ground. The general expression for the current of the solar cell, based on the circuit of Fig.1, is

$$I = I_L - I_L[exp\left(\frac{V + IR_s}{nkT/q}\right) -1] - \frac{V + IR_s}{R_{sh}} \qquad 1$$

Where *n* is the non-ideality factor, and *k*, *T*, and *q* are the Boltzmann's constant, cell temperature, and electronic charge, respectively. In ideal case, and most practical considerations: $Rs \rightarrow 0$, and $R_{sh} \rightarrow \infty$

A real solar cell can be characterized by the following fundamental parameters, which are also sketched in Figure 2, below:

*(a)*Short circuit current (Point M, Fig.2): [$I_{SC} = I_L$]. It is the greatest value of the current generated by a cell. It is produced under short circuit conditions: *V=0.*

(b) Open circuit voltage, [*Voc*] (Point S, Fig.2): corresponds to the voltage drop across the diode (p-n junction), when it is traversed by the photocurrent I_L(namely[$I_D = I_L$]), namely when the generated current is $I = 0$. It reflects the voltage of the cell in the night and it can be mathematically expressed as:

$$Voc = V_t ln\left[\frac{I_{sc}}{I_0} + 1\right] \qquad 2$$

Where $V_t = nkT/q$ is known as thermal voltage and T is the absolute cell temperature.

(c) Maximum power point: is the operating point A(V_{max}, I_{max}) in Figure 2, at which the power dissipated in the resistive load is maximum: [$P_{max} = I_{max}, V_{max}$]

(d) Fill factor: is the ratio of the maximum power that can be delivered to the load and the product of I_{sc} and V_{oc}:

$$FF = \frac{P_{max}}{V_{oc}I_{sc}} = \frac{I_{max}V_{max}}{V_{oc}I_{sc}} \leftrightarrow P_{max} = FF, (VocIsc) \qquad 3$$

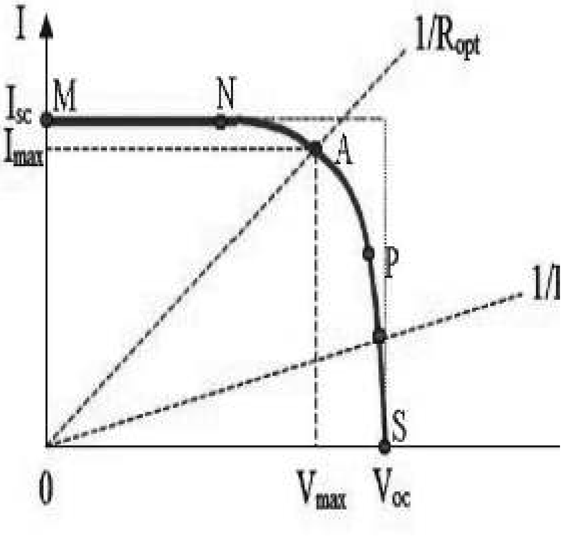

Figure : I-V Characteristics of a PV cell (Anca et al, 2000)

The optimized value of fill factor leads to the more squareness of the I-V characteristic curve of solar PV module. Consequently, it causes to the maximized efficiency (Haschk e*t al*, 2011) of solar PV power generating system. The maximum theoretical FF from a solar cell can be determined by differentiating the power from a solar cell with respect to voltage and equating the derivative to zero.

$$\frac{dIV}{dV} = 0 \qquad 4$$

which gives,

$$V_{mp} = V_{OC} - V_t ln\left(\frac{V_{mp}}{V_t} + 1\right) \qquad 5$$

$$I_{mp} = I_{SC}(1\text{-}\frac{V_t}{V_{OC}}) \qquad 6$$

As shown by Green (1982), the above expressions lead to the following approximate empirical formula for Fill Factor (Hacke &Meier, 2002; Qaing *et al*, 2011), that has been found to apply for wide range of solar cells:

$$FF = \frac{Voc - ln(Voc + 0.72)}{Voc + 1} \qquad 7$$

This whole expression is the function of open circuit voltage (V_{OC}). It means that the optimized value of this function will yield to ensure the extraction of maximum power from solar PV system to the load at any instant of time throughout the day. The above mathematical description of fill factor reflects that at the point of maximum power (at *dI/dv* = 0), the fill factor will be having a maximized efficiency of solar PV system. The efficiency (?) and fill factor (FF) are related as

$$?^{=}{}_{0} \qquad 8$$

MATERIALS AND METHODS

In this study, the power performances of Monocrystalline and Polycrystalline solar panels are experimentally determined under outdoor meteorological conditions of Kaduna North, Kaduna State of Nigeria (10.5°N latitude and 7.4°E longitude). The experiments were conducted in the month of January 2017, from 08:00 to 17:00 h. The PV panels' were place far from the shade of trees or buildings throughout the experiment.

In the testing system, The Monocrystalline Solar Panel (PV-SC1102) costing ? 40,000 about ($111.00) and A Polycrystalline solar panel (PV-HX108B) costing ? 38,000 (about $105.00) procured in Kaduna (November 2016), each rated 130W were used for the project. The Multimeter (VC-9805A) was used to measure Short circuit current, I_{SC}, Open circuit voltage, $V_{OC,}$ and module surface temperature, T. The readings were recorded at hourly interval from 8:00am to 5:00pm. To estimate solar input power, table of values of measured irradiance was collected from Nigerian Metrological Agency (NIMET), located in Kaduna, at a distance of 20km from experimental site. In order to capture the maximum amount of sunshine, the panels were positioned on flat surface but tilted 20^0, Southward (Turhan & Cetiner, 2012). All calculations were carried out using Microsoft Excel.

Figure : Setup of modules for the Current-Voltage measurement

RESULTS AND ANALYSIS

Current and Voltage

The average result shows that the open circuit voltage of polycrystalline solar panel is always higher than the Monocrystalline solar panel while the short circuit current of Monocrystalline solar panel is always higher than that of polycrystalline solar panel. Figure 4 and Figure 5 present the current and voltage result

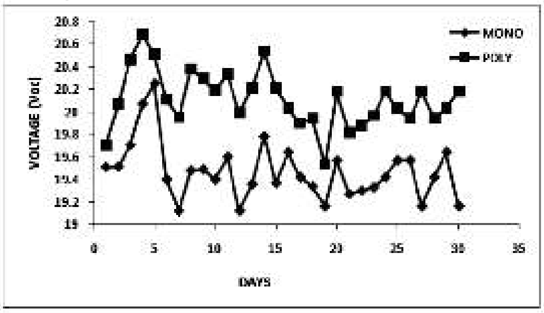

Figure 4: Average voltage of the month

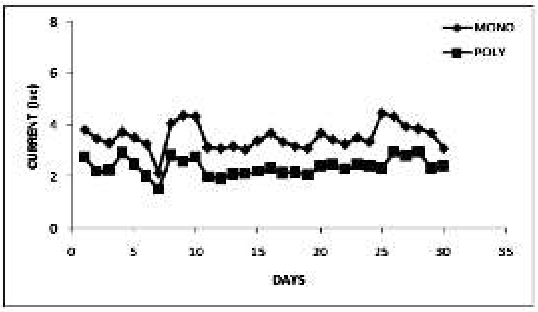

Figure 5: Average current of the month

Average Power

The tests was performed between 08:00 and 17:00 daily, the instantaneous Maximum power generation of 87.73 W had been realized by the Monocrystalline panel and of 61.05 W had been realized by the polycrystalline panel. It was determined that Monocrystalline solar panel generates 26.68W more instantaneous power than the Polycrystalline solar panel shows in Figure 6.

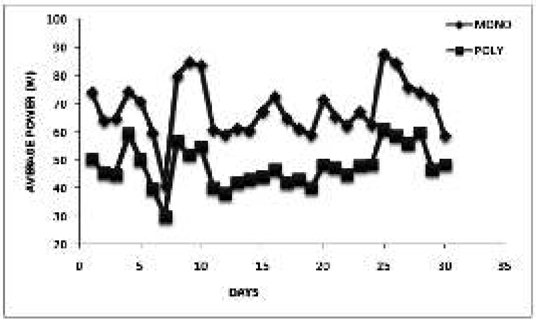

Figure 6: Average Power of the month

Average Power and Irradiance

Module parameters showed strong dependence on the solar irradiance, both modules showed considerably better power performance under high irradiance conditions and degraded output under low irradiance. Figure 7(b) show that the higher the irradiance the higher the power and the lower the irradiance the lower the power output. Figure 7(a) shows the average irradiance result of the month.

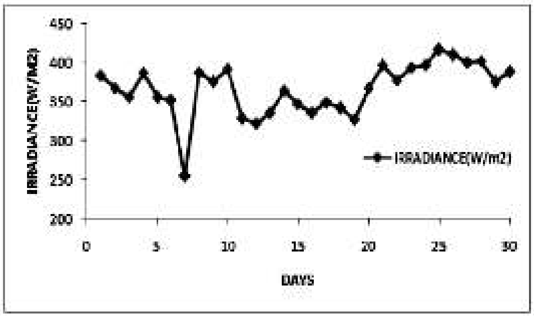

Figure 7(a): Average irradiance of the month

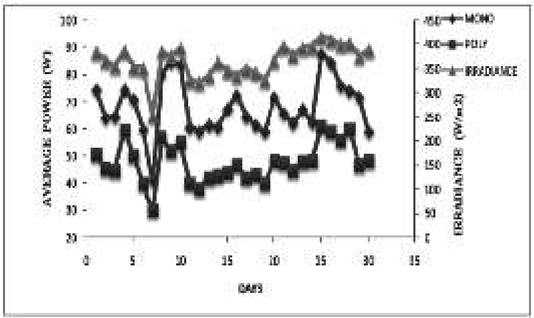

Figure 7(b): Average Power and irradiance

Average Energy for the Month

Figure 8 presents the daily average energy production performance of panels. Depending on the radiation intensity to the panel surface, differences are observed between energy generations. The average energy performances of the Monocrystalline and Polycrystalline are 676.96Wh and 476.95Wh, respectively.

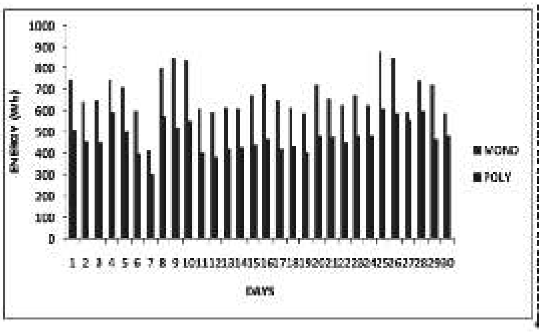

Figure 8: Average Energy of the month

Panels Efficiencies Ratio

Figure 9 shows the bar graph for average module efficiency for each solar panel in this experiment. The average conversion efficiencies of Monocrystalline and Polycrystalline are 15% and 11%.

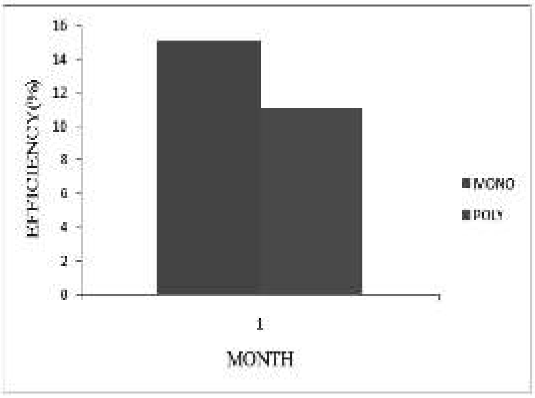

Figure 9: Efficiency of the Panels

SUMMARY, DISCUSSION AND CONCLUSIONS

Summary

The data recorded from the monthly experiment, the open circuit voltage of polycrystalline solar panel has higher value than the Monocrystalline solar panel, while Monocrystalline solar panel has higher current yield. The power generations show the Monocrystalline solar panel has the consequently higher energy generation within the period of measurements. Monocrystalline solar panel has higher efficiency than polycrystalline solar panel. Table 2 shows Average power cost analysis and efficiency of the two panels

Table 2: Average power, cost analysis and efficiency of the two panels

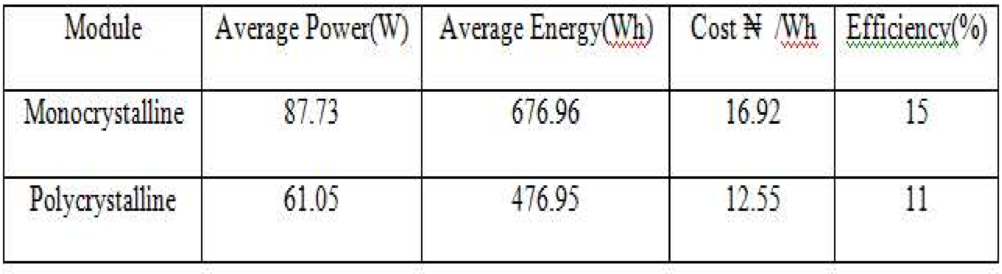

Module	Average Power(W)	Average Energy(Wh)	Cost ₦ /Wh	Efficiency(%)
Monocrystalline	87.73	676.96	16.92	15
Polycrystalline	61.05	476.95	12.55	11

Discussion The aim of this research is to experimentally investigate and compare the performance of Monocrystalline and polycrystalline solar panels, to identify which one gives better energy and economic advantage. From the results obtained, it is clear that Monocrystalline solar panels performed better than Polycrystalline solar panels for the same power input as can be observed in table 2. In terms of the cost, there seen to be very little between the two solar panels. Monocrystalline solar panels 130W costing ? 40,000 (about $111.00) while the Polycrystalline solar panel 130W ? 38,000 (about $105.00) at same location, 2016. The difference is ? 2,000 (about $6.00) only.

Conclusions

The geographical location of Kaduna North Strip at 10.5°N latitude and 7.4°E longitude makes it a relatively sun-rich region. This implies that solar energy systems would be very efficient in this part of country. Developing a clean and renewable energy reduces environmental degradation as well as helps energy independence in Nigeria. PV Solar energy from polycrystalline and Monocrystalline panels is most commonly used with different characteristic while the two technologies are similar, in several ways they differ in terms of cost, surface area, as well as efficiency.

In this study, it has been shown that the average photovoltaic panel power for PV module was 87.73W and 61.05W, the total energy generated by the panels for the month is 676.96Wh and 476.95Wh and the daily average photovoltaic panel efficiency was 15% and 11% for the Monocrystalline (PV-SC1102) and polycrystalline (PV-HX108B), respectively. In terms of economy Monocrystalline show better performance by having a lower value of ? /16.92Wh compare to polycrystalline solar panel ? /12.55Wh

A study by Ghazali, M. A and Abdul Rahman, A. M. (2012). Showed that a polycrystalline panel has higher power output when compared to a Monocrystalline panel. Thus additional investigations are needed in order to determine which specific climate conditions favour the different kind of panel to perform better.

REFERENCES

Anca, D. Hansen, P. Sørensen, L. Hansen H. & Henrik, B. (2000). Models for a Stand-Alone PV System.Riso national laboratory, Roskilde.

Duffie, J., & Beckman, W. (2006). "*Solar Engineering of Thermal Processes*". 3rd ed. New Jersey: John Wiley and Sons, Inc.

Green, A. M. 1982. "Solar Cells: Operating Principles, Technology and System Applications". Prentice-Hall: Englewood Cliffs, NJ

Ghazali, M. A & Abdul Rahman, A. M. (2012). "*The performance of three different solar panels for solar electricity applying solar* *tracking device under the Malaysian climate condition,” Energy and Environment Research*, vol. 2, no. 1, pp. 235–243. .

Hacke, P. &Meier, D.L.,(2002) “Analysis of fill factor losses using current-voltage curves obtained under dark and illuminated conditions” proceedings of *29th IEEE Photovoltaic Specialists Conference*, 2002 , pp.462,464.

Haschke, J.; Mingirulli, N.; Gogolin, R.; Ferrè, R.; Schulze, T.F.; Du?terho?t, J.; Harder, N.-P.; Korte, L., (2011) "Interdigitated Back-Contacted Silicon Heterojunction Solar Cells With Improved Fill Factor and Efficiency," *IEEE Journal of Photovoltaics*, **1(2)**, pp.130,134..

Nogueira, B. J, Niedzialkoski, R. K., de Souza, S. N.M. & das Neves J. C. M. (2015) “Performance of monocrystalline and polycrystalline solar panels in a water pumping system in Brazil,” *Renewable and Sustainable Energy Reviews*, vol. 51, pp. 1610–1616.

Nehring, R. (2009), Philos Trans R Soc Lond B Biol Sci. 2009 Oct 27; 364(1532): 3067–3079 .

Otun, J. A., Onemano, J. I., & Alayande, A. W. (2012). Assessment of the Hydropower Potential of Kangimi Reservoir in Kaduna State Nigeria. *Nigerian Journal of Technology (NIJOTE-CH)*, Vol.31(3), pp. 300-307.

Parida, B. Iniyan, S. & Goic, R. (2011) “A review of solar photovoltaic technologies,” *Renewable and Sustainable Energy Reviews*, vol. 15, no. 3, pp. 1625–1636.

Qiang M., Mingwei, S., Liying, L., Guerrero, J.M.,(2011) "A Novel Improved Variable Step-Size Incremental-Resistance MPPT Method for PV Systems," *IEEE Transactions on Industrial Electronics*, **58(6)** pp.2427-2434.

Turhan, S. & Çetiner, I. (2012) “Performance evaluation of photovoltaic systems,” in *Proceedings of the National Roof & Wall Symposium*, vol. 6, Bursa, Turkey.

Verlindan, P., Deng, W., Zhang, X., Yang, Y., Xu, J., Shu, Y., Sheng, J., Zhan, S., Bau, J., Ping, F., Zhang, Y., & Feng, Z (2014).” Strategy development and mass production of high efficiency crystalline Si PV modules”, paper 4sM$_{o}$O.1.4, 6th world conference on pv energy conversion, Kyoto.

INFLUENCE OF SiO_2 NANO-PARTICLES ON THE ELECTRICAL CONDUCTION OF NEEM VEGETABLE OIL

B. Yusuf[1], A.A. Abdelmalik[2], U. Sadiq[3]
[1,2,3]Department Of Physics, Ahmadu Bello University, Zaria
Email: bashiryusuf506@gmail.com

ABSTRACT

Effort has being on around the world to find alternative fluid for insulation application. Vegetable oil seems to be a perfect alternative but the use of most of the vegetable oil as feedstock posed a challenge to its use for insulation purpose. This paper investigates the influence of SiO_2 nanoparticles on the dielectrics and rheological properties of neem oil. The crude neem was purified and nanoparticles were dispersed in the purified oil with concentration ranging from 0.2% to 1.0% in 0.2% interval. Fourier Transform Infrared spectra (FTIR) as well as scanning electron microscopy analysis (SEM) ware used to examine the structures of the samples, The dielectric properties was studied at frequencies range of 20 Hz to 20000 kz to observe the charge transport phenomenon in the samples. The study shows that dipolar polarization and interfacial polarizations are the dominant polarization processes. Increase in temperature results to an increases in charge mobility in all the samples. Increase in temperature results in decrease in viscosity of all the studied samples, an indication that its heat transfer process has improved. The overall results indicate that small amount of SiO_2 nanoparticles in seed oil could improve the insulating properties of the fluid.

Keyword: *Neem oil, Nanoparticles, polarization*

Introduction

Mineral oils are the most widely used fluids for electrical insulation and heat transfer in equipment such as transformers, capacitors, bushings, drilling machines etc. Their technical characteristics have been optimized during the last century to fit the requirements of these applications. The main function of the oil electric power equipment is to dissipate the heat generated by the windings and core and to insulate between components at different potentials. For centuries, mineral oil product has been applied for insulation, however, it is known that this product will be eventually depleted in the future since it is a non-renewable source, also with the concern on the fire safety and environmental concerned, alternative fluids are currently being considered. Vegetable oil such as natural esters or synthetic esters are among the alternative fluids being considered. (Wang *et al.*, 2012)

Vegetable oils are renewable and potential source of energy with an energetic content close to diesel fuel. Oils derived from vegetable sources may in course of time become as important as petroleum and the coal tar products of the present time. Recent decrease in minerals oil prices and to the fear uncertainties concerning minerals oils availability renewed the interest in vegetable oil fluid for insulatingapplication. (Ganguli, 2002)

Neem (*Azadirachtaindica*) is a tree in the mahogany family which is abundantly grown in many parts of Nigeria. The Neem grows on almost all types of soils. Neem seed obtained from this tree are collected, de-pulped, sun dried and crushed for oil extraction. The seeds have 45% oil which makes it potential for the production of insulating fluid. [3] (Fazal*et al*., 2011).

Nanofluids can be used to enhance the performance of some electrical and mechanical insulating fluid. Most of the work in the field of nanofluids was done in national laboratories and academia and are at a stage beyond discovery research. Two-step method is the most widely used method for preparing nano-fluids. Nanofluid used in this method are first prepare as dry powders by chemical or physical methods. Then, the nanosized powder will be dispersed into a fluid in the second processing step with the help of intensive magnetic force agitation, ultrasonic agitation, and high-shear mixing. Two-step method is the most economic method to produce nanofluids in large scale, because nanopowder synthesis techniques have already been scaled up to industrial production levels. (Brajendra *et al.*,2006)

A dielectric material is an electric insulator that can be polarized by an applied electric field.When a dielectric is placed in an electric field, electric charges do not flow through a material as they do in the conductor, but only slightly shift from their average equilibrium positions causing dielectric polarization. Because of dielectric polarization positive charges are displaced toward the field and negative charges are shifted in anopposite's direction. This created an internal electric field that reduces the overall field within the dielectric itself. If the dielectric is composed of weakly bonded molecules, those molecules not only polarized but also reorient so that their symmetry axes align to the field. The study of dielectric properties concerns storage and dissipation of electric and magnetic energy in materials. Dielectrics are important for explaining various phenomena in electronics, optics and solid state physics.

MATERIALS AND METHOD

Chemicals

Stearic acid [CH_3 $(CH_2)_{16}$ CO_2H, 99% purity, 67-69?C M.P, and 183-184$^{?}$C B.P . BDH Limited poole, England], Sodium hydroxides [NaoH, Steven Moore Chemicals, Zaria, Nigeria], Acetone [CH_2 $(CH_2)_2$ O, . BDH Limited poole, England], Filter paper [12-5cm Grade Whatman, England], Activated carbon ,Silica hydrogel, Silicon oxides nano-particles [SkySpringNanomaterial,Inc USA], Crude Neem Vegetable oil (Nigerian Institute of Research and Chemical Technolog NIRCT. Zaria)

Equipment's

Hot plate magnetic stirrer [IKA CMAG HS10,], L.C.R Meter, Scanning electron microscopy machine, Fourier transform infrared FT-IT spectroscopy machine, Constructed cylindrical test cell

Preparation of Nanofluid Samples

In this research the two step method was used, in which the crudeNeem vegetable oil obtained from the Nigerian Institute for Research and Chemical Technology (NIRICT) Zaria purified using degumming process

200 ml of the Neem oil was measured using measuring cylinder, poured into a flask and then heated to 70°C, 1.5 ml citric acid was also measured and added to the heated oil sample and continuously heated and stirred for 15 minutes at 70°C,4 ml of 8 % NaoH (by dissolving 8 g NaoH in 100 ml of distilled water) was then add to the oil and continuously heated and stirred for another 15 minutes at 70°C, the mixture was then transferred to the

vacuum oven where it was heated at 85°C for 30 minutes, So also the mixture was taken back to hot magnetic stirrer and heated to 70°C after which a 2 g of silica hydrogel was added heated and stir for 30 minutes. Then the temperature was increase to 85°C and 4 g of activated carbon was then added to each 100 ml of the oil sample, heated and stir for 30 minutes. Then the mixture was separated using filter paper and obtained the pure sample. Then, the Nano-fluids of volume concentrations 0.2%, 0.8% and 1% of powdered SiO_2nano-particles and purified Neem oil were made respectively. To make the nano-particles more stable and remain more dispersed, each sample was stirred for 3 hours using magnetic stirrer. Samples are labelled for easy identification.

Morphological and Structural Analysis

The chemicals and functional group identifications were done via Fourier transform infrared (FT-IR) spectroscopy, distribution of the nano particles in the based fluid via Scanning Electron Microscope (SEM) Machine,

Dielectric Measurement

The dielectric measurements were performed using LCR meter. The measured parameters arecapacitance, resistance, and tandelta which allow the calculation of electrical conductivity and permittivity. All the calculations were carried out using Microsoft office excel 2007. The measuring cell is a parallel cylindrical conductivity test cell with platinum electrode of dimensions mentioned below.

The relative permittivity can be calculated as follows:

$$\varepsilon^{1}_{r} = \frac{Co}{C} \qquad 1$$

Where $$Co = \frac{2\pi L\varepsilon_0}{in\left(r_1/r_2\right)}$$

and L is the length of cylindrical test cell=4.6×10^{-2} m, ε_o is the permittivity of free space =8.854×10^{-12} F/m, $r_1$is the inner radius of outer cylinder=2.34×10^{-2}m, $r_2$is the outer radius of inner cylinder=1.33×10^{-2}m, C is the capacitance of the fluid in the cell at frequencies ranges from 20 Hz to 200 khz in LCR Meter.

The dielectric loss can be expressed as

$$\tan\delta = \frac{\varepsilon_r^{11}}{\varepsilon_r^{1}} \qquad 2$$

where ε_r^{11} is the imaginary part of dielectric constant and ε_r^{1} is the real part of the dielectric constant.

To separate the AC conductivity component from the total conductivity measured (DC and AC) tha following relationship was applied (park et al., 2003):

$$\sigma_{a.c} = \omega\varepsilon_0\varepsilon^{11} \qquad 3$$

By substituting equation (1) and (2) in to equation (3) get

$$\sigma_{a.c} = \omega\varepsilon\frac{C}{Co}\tan\delta \qquad 4$$

Similarly, substitute $$Co = \frac{2\pi L\varepsilon_0}{in\left(r_1/r_2\right)}$$

L and $\omega=2\pi f$ in equation (4) and simplify

$$\sigma_{a.c} = \frac{in\left(r_1/r_2\right)}{L} f\cdot c \tan\delta \qquad 5$$

Where f is the frequencies ranges from 20 Hz to 200 KHz, c and tan δ are the capacitance and loss tangent of the fluid respectively corresponds to f

RESULT

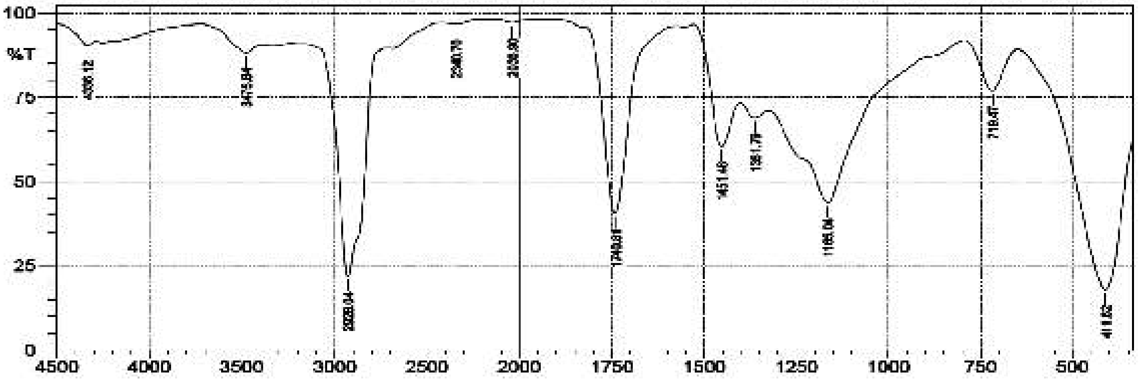

Fig.1.0: FT-IR Spectra of purified neem oil

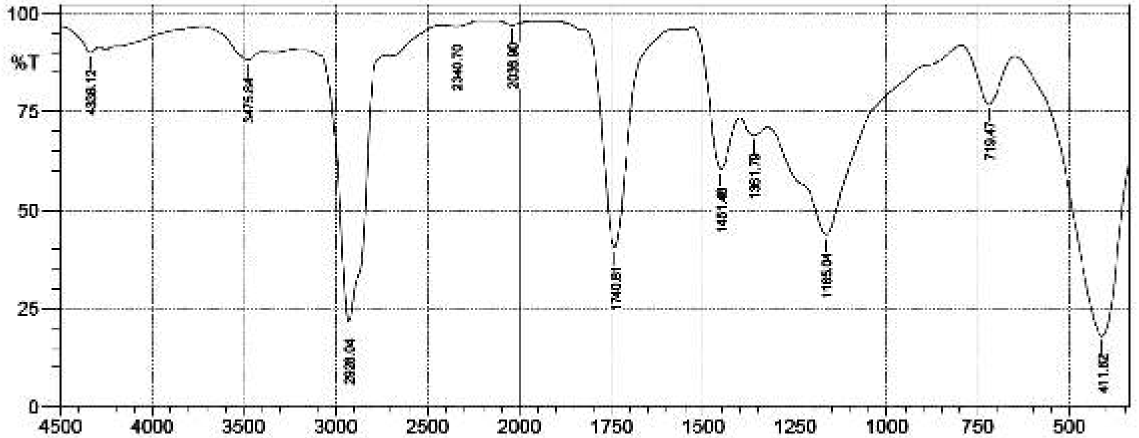

Fig.2.0: FT-IR Spectra of 0.2% nanoparticles concentration in neem oil (Sample A)

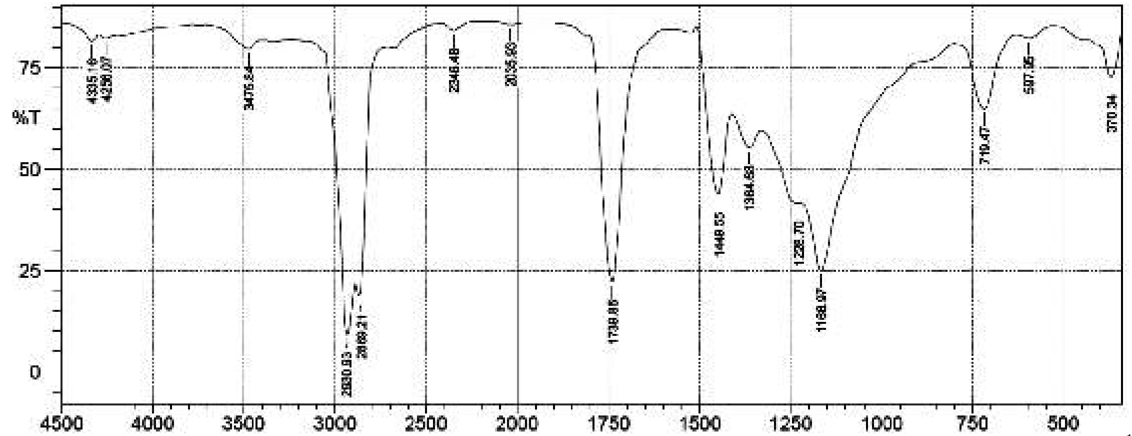

Fig.3.0: FT-IR Spectra of 0.8% nanoparticles concentration in neem oil (Sample D)

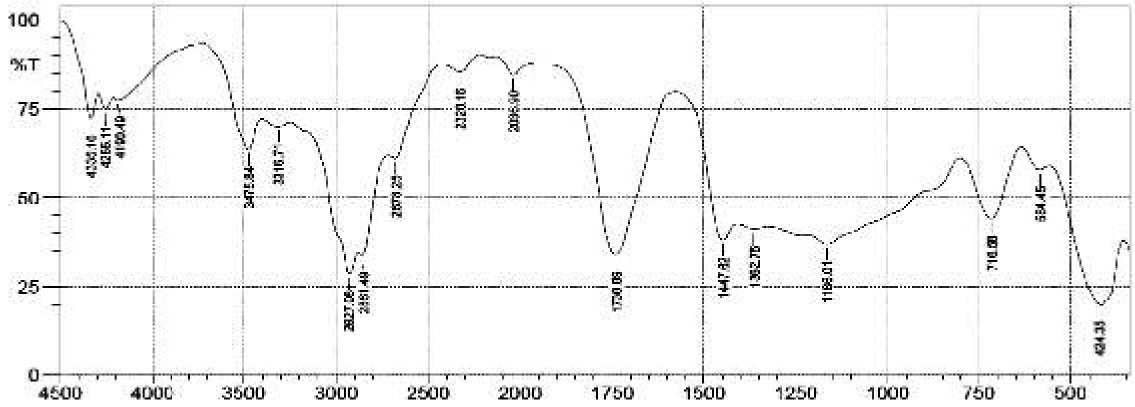

Fig.4.0: FT-IR Spectra of 1.0% nanoparticles concentration in neem oil (Sample E

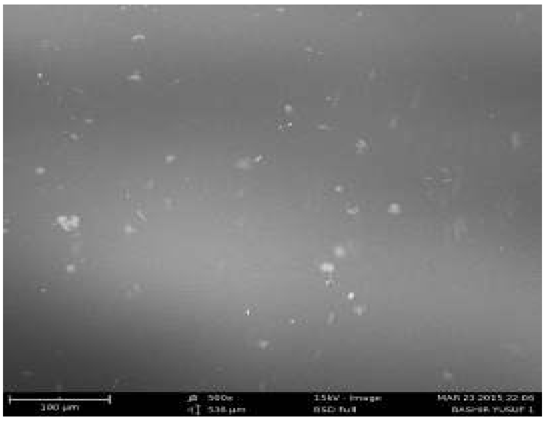

Plate I: SEM result of 1.0% silicon oxides nano-fluid

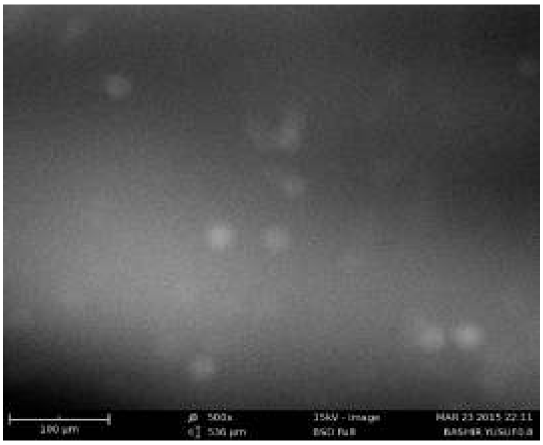

Plate II :SEM result of 0.8% silicon oxides nano-fluid

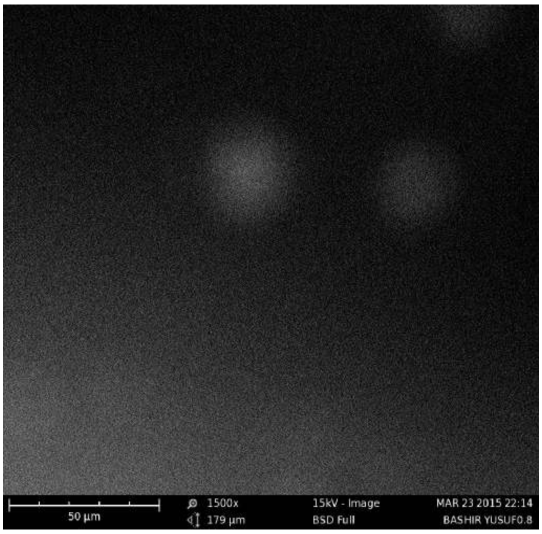

Plate III ; SEM result of 0.6 % **silicon oxides nano-fluid**

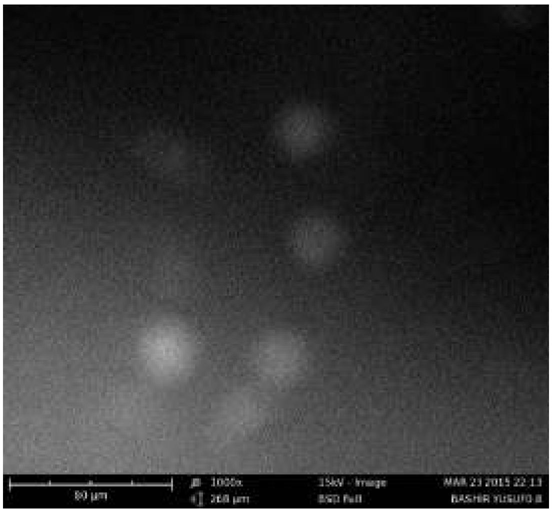

Plate IV ; SEM result of 0.4 % silicon oxides nano-fluid

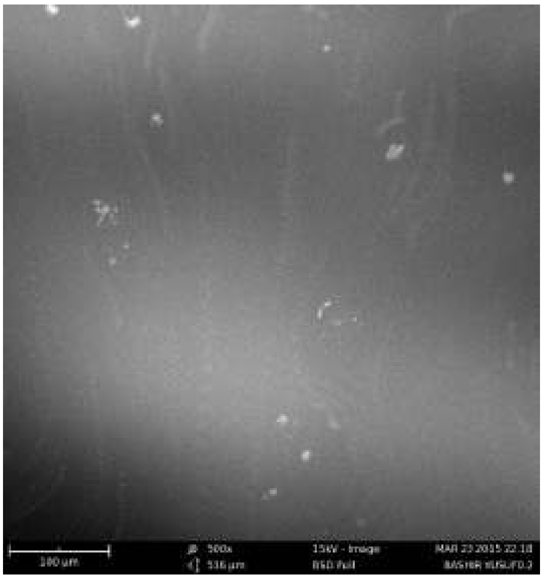

Plate V: SEM result of 0.2% silicon oxides nano-fluid

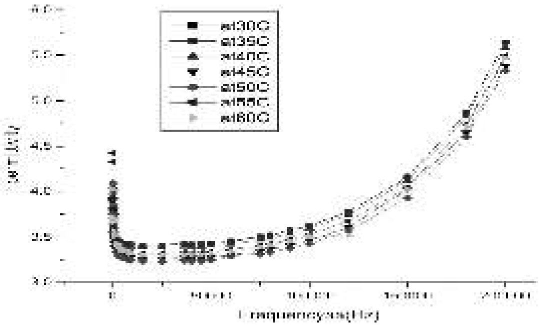

Fig.5.0 Relative permittivity versus frequency for 1.0% nanofluid

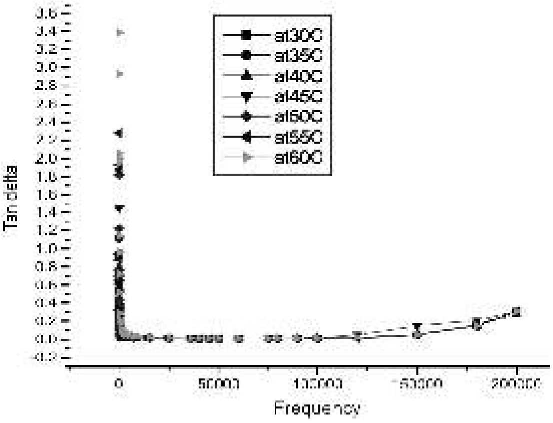

Fig. 6.0.Loss tangent versus frequency for 1.0% nanofluid

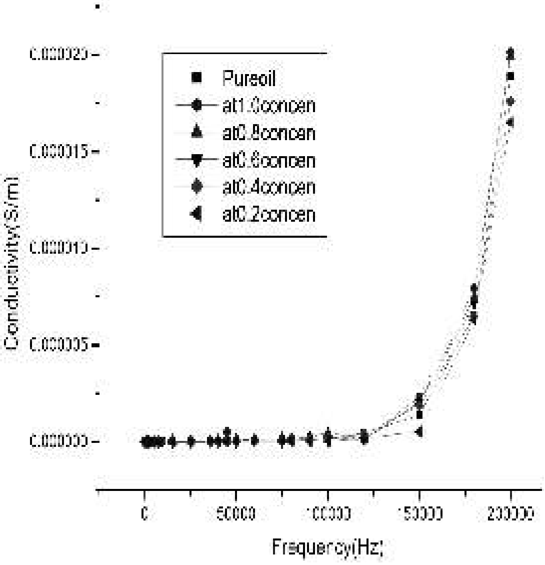

Fig.7.0. Conductivity versus frequency of the nanofluid at 30°C

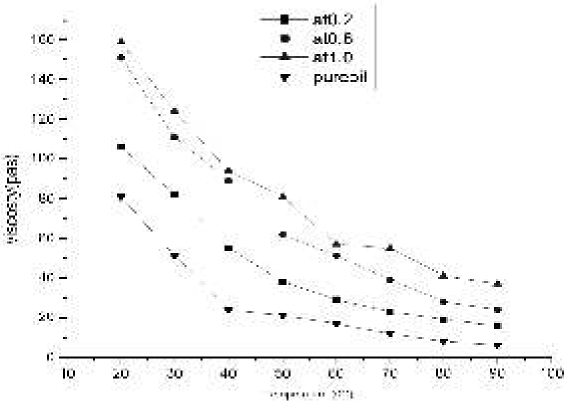

Fig. 8.0 viscosity vs temperature of the nanofluid

DISCUSSION

The FT-IR spectra as recorded using SHIMADZU FTIR-8400S in the region 3500-400 cm^{-1} reveals the structural characteristics of the samples as shown in Figs.(1 to 4).The presence of SiO_2nanoparticles in the nanofluid gave rise to a band on the spectra with a peak around 598 cm^{-1}. While the SiO_2 nanoparticle band was not visible in the nanofluid spectra when the concentration is 0.2% in the base fluid, while concentration above shows a fingerprint of the nanoparticles in the base fluid. The non-appearance of the nanoparticle band may have resulted from the low concentration of the nanoparticles. SEM images as shown in plate I-III shows the dispersion of the nanoparticles is relatively well distributed with some clustersin the samples. The presence of clusters may have resulted from the stirring process.

The dielectric constant (relative permittivity, ε?) decreases as a function of frequency at low frequency region (20 Hz to 400 Hz) as shown in Fig 5.0. The decrease in dielectric constant with frequency may have resulted from dipole orientation and interfacial effect within the frequency range. The dipoles begin to lag behind the field leading to a decrease in ε?. Fig. 6.0 shows the variation of dielectric loss (tan δ) as a function of frequency at different concentration. It is evidence from the figure that tan δ has a decreasing trend as frequencies increases. The decrease in loss tangent at low frequencies shows the presence of space charge polarization which arises due to the accumulation of space charges at grain boundaries and electrode interface under the application of external electric field. Within mid-frequency region, frequency appears to have no significant effect on the dielectric constant of the samples and loss tangent is stable within the mid-frequency. The low tan δ value at wide low frequency range makes the samples useful in low frequency device applications. Beyond 5kHz, dielectric constant began to increase. This may have resulted from orientation (dipolar) polarization in the fluid. This effect decrease with an increase in frequency as the response time decreases.The spectra of the real permittivity and tan δ are assumed to be due to the effects of transport of ions in the liquid. The impurities present in the oil sample may also have permanent dipoles.

The dielectric constant and loss of the SiO_2based nanofluid was investigated as a function of nanoparticle concentration, frequency and temperature. Addition of 0.2% lead to a reduction in dielectric constant. Increasing the concentration of the nanoparticles beyond 0.4% resulted in increase in dielectric constant. This is an indication increasing the concentration of the nanoparticles beyond 0.4% lead to an increase in energy storage capability of the nanofluid. The increment in the dielectric constant tend to be towards saturation after 0.8% concentration. Dielectric loss also reduce with the addition of 0.2% SiO_2nanoparticles. Further increase in the concentration of SiO_2 nanoparticles resulted in increase in dielectric loss. The increment appears to have linear relation with concentration within the range of studied.A.C conductivity of the samples was evaluated from the obtained results. Fig. 7.0 shows the variation of conductivity of fluid samples as a function of frequency, nanoparticle concentration and temperature respectively. Electrical conduction in purified neem oil as shown in Fig.7.0 may have resulted from ionic impurities and the polar nature of the oil.

The dispersion over a wider frequency range may have resulted from the different mobility's of the ionic impurities. The particles may also have different sizes with different values of radius contributing to the overall conductivity. Neem oil can be described as fluid with low concentration of dispersed polar molecules, making it a weak polar liquid. The increase in the conductivity of the fluid with percentage increases in concentration is as a result of the increase in ionic polarization. Below0.4% concentration, the ionic polarization is lower compare to one occurs above 0.4% concentration therefore the conductivity is higher with the percentage increase in the nanoparticles.

Temperature has no significant effect on the relative permittivity of the samples but seems to have significant impact on the ac conductivity of the samples. The increase in conductivity with temperature may be associated with the enhancement of mobility of charged carriers as a result of decrease in viscosity.

Low loss in seed based oil does not imply low concentration of charge particles in the oil. It may be that viscosity has a significant impact on the mobility of ions in the liquid and only few charged particles were mobile due to the viscosity of the oil. The conduction loss is contributed by only the mobile charges. Mobility of ions is influenced by the dynamic viscosity of the liquid (Abdelmalik, 2013).

Cooling equipment in industries are mainly governed by convection, so it is necessary to have a low viscosity for that application. The lower the viscosity, the better the cooling and friction reduction. The viscosity of pure neem oil at 40°C is 24mpa.s ($2.69\text{x}10^{-5}m^2/s$) which is lower than the specified value of 65mpa.s of a standard motor oil given by society of automotive engineers and higher than the specified value of $1.3\text{x}10^{-5}m^2/s$ of standard transformer oil at 40°C. However, for nano-neem oil, the viscosities of 0.2%, 0.8% and 1% nanoparticles concentration are 55mpa.s ($6.15\text{x}10^{-5}m^2/s$), 89mpa.s ($9.97 \times 10^{-5}m^2/s$), and 94mpa.s ($10.5 \times 10^{-5}m^2/s$), respectively. The 0.2% is close to the value given by SAE while 0.8% to above are greater than the values. So also, all the values are above the value of standard transformer oil at 40°C

CONCLUSION

This preliminary study shows that the prepared vegetable oil based nanofluid has properties that make it useful for industrial application. The nanofluid with 0.2% SiO_2 appears to be more suitable for insulation as the sample was observed to have lowest dielectric loss and good dielectric constant. Increasing the concentration of SiO_2 nanoparticle was observed to have initiated an increase in dielectric loss and the corresponding a.c conductivity. This may make the fluid with higher nanoparticles suitable as a base fluid for conducting drilling fluid. To fully characterize the fluid for specific industrial application, more tests need to be performed on other relevant parameters.

REFERENCES

Abdelmalik A.A., “Investigation of Frequency and Temperature Effects on the Dielectric Constant of Some Nigerian Manufactured Vegetable Oils”, *M Sc. Thesis* (Unpublished) A.B.U. Zaria, Nigeria, 2005.

Brajendra K. Sahrma, Zengshe Liu, Atanu Adhvaryu, and Sevim Z. Erhan, One-Pot Synthesis of Chemically Modified Vegetable Oils, J. Agric. Food Chem., 3049-3056, 2006

Brantly, J.E. History of Petroleum Engineering. Cater, D.V., ed. Boyed Printing Co. Dallas,1961. pp. 277, 278

Dosunmu and Ogunrinde, "Development of Environmentally Friendly Oil Based Drilling Mud using Palm-oil and Groundnut-oil", SPE 140720, 2010

Ganguli, S. (2002) 'Neem: A therapeutic for all seasons', Current Science, Vol. 82, pp.1304.

Fazal, M.A, Haseeb A.S.M.A and Masjuki H.H. (2011) 'Biodiesel feasibility study: An evaluation of material compatibility; performance; emission and engine durability', Renew. Sustain. Engy Reviews, Vol.15,2, 1314-1324.

Wang, N., Roetzel, W., and Das, S. (2012). "Natural convection of nano-fluids."*Heat and Mass Transfer*, 39(8-9), 775-784.

ISOPACH MAPS SHOWING SUBSURFACE CHARACTERIZATION AT SELECTED POINTS WITHIN KAURA AREA OF KADUNA STATE, NORTH-WESTERN NIGERIA

Afuwai Gwazah Cyril
Department of Physics, Kaduna State University
cyafuwai@gmail.com

ABSTRACT

Vertical Electrical Soundings (VES) using Schlumberger array were carried out at different points along fifty one (51) profiles at Kaura area of Kaduna state. Terrameter SAS300 is the instruments used to acquire the resistivity data. This is an attempt to understand the variations in Depth to basement, Aquifer thickness and Topsoil resistivity values with a purpose of providing hydrogeological information of the area for future groundwater exploration and geotechnical work. The Depth to basement map shows that the basement topography is rugged or undulating being deeper at some points and shallower at other points. The depth to basement ranges from 10m to 90m. The map also reveals a linear structure which trends in the NW-SE direction. The Aquifer Thickness map shows the variation of aquifer thickness from one place to another. The aquifer thickness varies from 1 to 90m with an average of 28m. The resistivity values of the top soil vary between 50 to 1400 ohm-m. The higher resistivity values are noticed around Kaura town, Manchok and Fadan Atakar.

Keywords: *Resistivity, Sounding, Kaura*

Introduction

Kaura area lies between latitudes 9°30' N and 9°45'N and longitudes 8°20'E and 8°35'E. The area has an approximately landmass of 770 km^2 within the crystalline hydrogeological province of northern Nigeria (Figure1) belonging to the Younger Granite and Basement Complex suites. These rocks lack primary porosity where groundwater could accumulate for exploitation. For these rocks to store water there must exist in them secondary porosity, which invariably results from weathering and fracturing (Afuwai and Yusuf, 2018). However, the spatial distribution and depth of this kind of porosity vary from one location to another, hence the occurrence of groundwater in these rocks is sporadic and borehole siting for its abstraction in this geological terrain is often difficult (Alan and Aftab 2000). Vertical Electrical Soundings (VES) using Schlumberger array were carried out at different points along fifty one (51) profiles. Terrameter SAS300 is the instruments used to acquire the resistivity data. This is an attempt to understand the variations in Depth to basement, Aquifer thickness and Topsoil resistivity values with a purpose of providing hydrogeological information of the area for future groundwater exploration and geotechnical work.. The area is mainly accessible through the Jos –Kagoro Kaduna road that runs East-West. In the central part of the study area, Rail line traverses from Kafanchan-Kagoro to Jos Terminus in Plateau State.

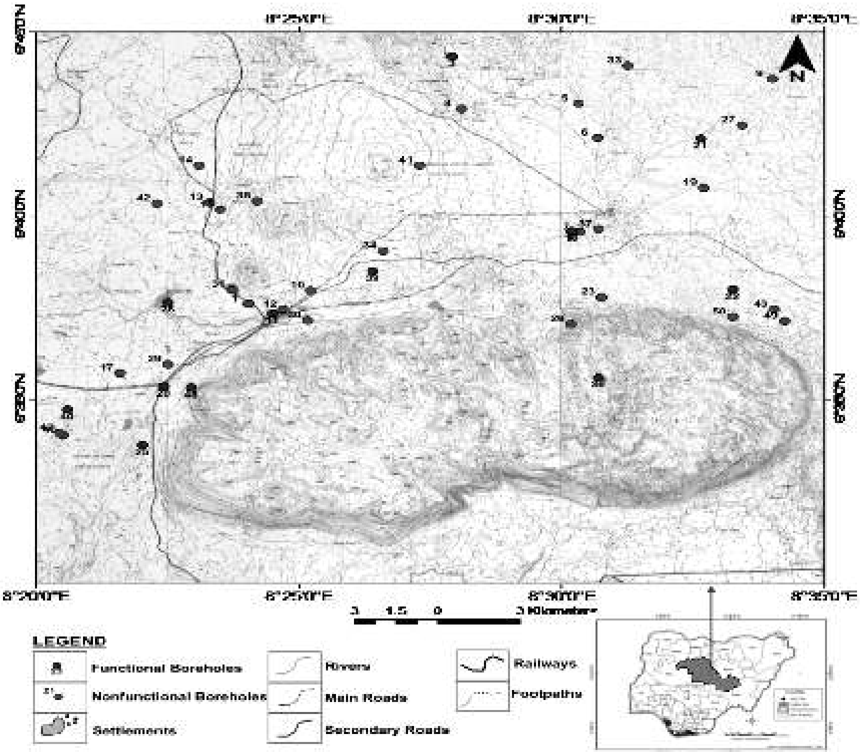

Figure 1. Map of Kaura showing the functional and non-functional boreholes

Source: Author

GEOLOGY OF THE SURVEY AREA

The study area is made up of the rocks of the Migmatite-Gneiss Complex, Gneiss, Younger Metasediments, Older Granites, Younger Granites and Newer Basalts. The distribution of the various rock types is as shown on the geological map of the area (Figure 2). Basement rocks that occur in the study area could be classified into: Newer Basalts, Younger Granites, Older Granites, Undifferentiated Schists, Migmatites-Gneiss Complex (Afuwai et al., 2014).

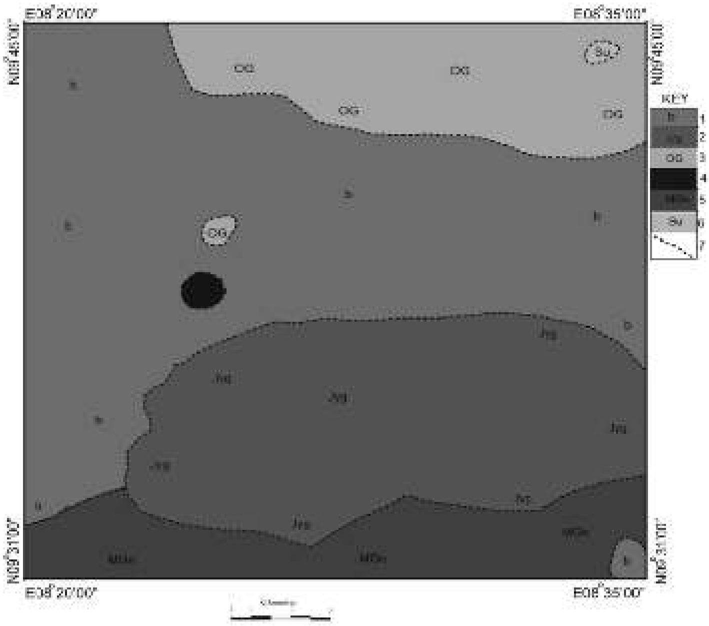

Newer basalts 2. Younger granites 3. Older granites 4. Gneisses 5. Migmatite-Gneisses 6. Undifferentiated Schists 7. Geologic boundary 8. River

Figure 2. Geological Map of the Kaura Area

CLIMATE, VEGETATION AND LAND USE

The study area is situated in the tropics within the Guinea Savannah region. Rainfall is seasonal and moderate with a mean annual amount of 1524 mm (Yanet, 2012). Rainfall usually commences in March and ends in October and for the rest of the year dry season prevails. Temperatures vary between less than 15^0C around December/ January and 32^0C in March and April with its annual mean between 24^0C and 28^0C. The relative humidity varies with the season with highest values in the rainy season and lowest values during the harmattan. The mean annual relative humidity is 57%. The vegetation consists of broad-leaved savannah woodland and when properly developed, the trees may attain heights of 10-15m. The dominant trees within are *Isoberlina doka* while *Khaya senegalensis*, *Danielia oliveri*, *Perkia* and *Ficus sycomotus* are common. There are abundant grasses with annual types dominating the uplands while the perennial type such as *Hyparrhenia spp* and *Andropogon spp* are also common. Sugarcane and other garden crops, mostly vegetable, are cultivated along streams courses. Dominant food crops found in the area include root crops e.g. yams and cassava while stem tubers include potatoes. These are sometime intercropped with millet and maize.

MATERIALS AND METHODS

Theory of the Electrical Resistivity Method

In the DC resistivity surveying, an electric current is passed into the ground through two outer electrodes (current electrodes), and the resultant potential difference is measured across two inner electrodes (potential electrodes) that are arranged in a straight line, symmetrically about a centre point. The ratio of the potential difference to the current is displayed by the Terrameter as resistance. A geometric factor ***k*** in metres is calculated as a function of the electrode spacing. The electrode spacing is progressively increased, keeping the centre point of the electrode array fixed. A and B are current electrodes through which current is supplied into the ground, **M** and **N** are two potential electrodes to measure the potential differences between the two electrodes and P is the VES station to be sounded. The potential difference between the two potential electrodes is measured. The apparent resistivity is given by

$$\rho_a = k\left(\frac{?V}{I}\right) \qquad 1$$

With K a geometric factor which only depends on electrode spacing and is given by

$$K = p\left(\frac{L^2}{2b} - \frac{b}{2}\right) \qquad 2$$

Electrical resistivity method is defined by their frequency of operation, the origin of the source signals and the manner by which the sources and receivers are coupled to the ground. The method is generally governed by Maxwell's equations of electromagnetism (Grant and West, 1965). In the direct-current (DC) frequency, the diffusion term is zero and the field is thus governed entirely by Poisson equation. Electrical methods of geophysical investigations are based on the resistivity (or its inverse, conductivity) contrasts of subsurface materials. The electrical resistance, ***R*** of a material is related to its physical dimension, cross-sectional area, ***A*** and length, ***l*** through the resistivity, r or its inverse, conductivity, s by

$$r = \frac{1}{s} = \frac{RA}{l} \qquad 3$$

Low-frequency alternating current is employed as source signals in the DC resistivity surveys in determining subsurface resistivity distributions. Thus, the magnetic properties of the materials can be ignored (Telford et al., 1990), so that Maxwell's equations of electromagnetism reduced to:

$$\nabla \cdot \vec{E} = \frac{1}{\varepsilon_o} q \qquad 4$$

$$\nabla \times \vec{E} = 0 \qquad 5$$

Where $\vec{E}$ is electric field in V/m, q is the charge density in C/m^3 and ε_o (8.854 X 10^{-12} F/m) is the permittivity of free space. These equations are applicable to continuous flow of direct current; however, they can be used to represent the effects of alternating currents at low frequencies such that the displacement currents and induction effects are negligible. Usually, a complete homogeneous and isotropic earth medium of uniform resistivity is assumed. For a continuous current flowing in an isotropic and homogeneous medium, the current density $\vec{J}$ is related to the electric field, $\vec{E}$ through Ohm's law

$$\vec{J} = \sigma \vec{E} \qquad 6$$

The electric field vector $\vec{E}$ can be represented as the gradient of the electric scalar potential,

$$\vec{E} = \nabla \phi \qquad 7$$

The apparent resistivity is the ratio of the potential obtained in-situ with a specific array and a specific injected current by the potential which will be obtained with the same array and current for a homogeneous and isotropic medium of 1Ω m resistivity. The apparent resistivity measurements give information about resistivity for a medium whose volume is proportional to the electrode spacing (Afuwai, 2013). Resistivity is affected more by water content and quality than the actual rock material in porous formations. While aquifers that are composed of unconsolidated materials their resistivity decreases with the degree of saturation and salinity of the groundwater (Afuwai and Lawal, 2013). Terrameter SAS300 was the instrument used to acquire the data, with a maximum current electrode spread of 200. IPI2Win Resistivity software was used for the data processing. The area predominantly, comprises of four layers i.e. the topsoil, weathered layer, fractured layer and the fresh basement layer. The K, A, H and HK sounding curves were mostly noticed at the survey area.

RESULTS AND DISCUSSIONS

Topsoil Resistivity Map

The map was produced by contouring the resistivity values of the top soil at fifty one (51) points along all the locations of the fifty one (51) profiles within the study area. The map is shown in figure (3). A contour interval of 50 ohm-m was used for the map. The resistivity values of the top soil vary between 50 to 1400 ohm-m. The higher resistivity values are noticed around Kaura town, Manchok and Fadan Atakar.

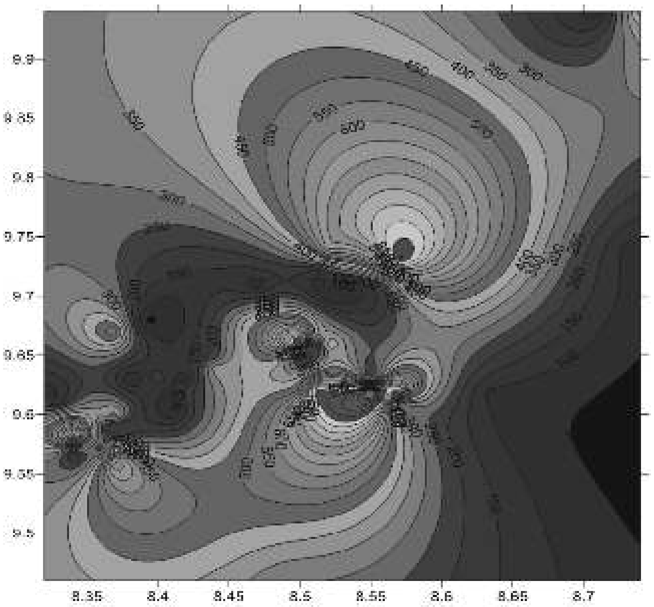

Figure3: Map of resistivity of topsoil (contour interval 50ohm-metres).

AQUIFER THICKNESS MAP

In the basement complex the main aquifer system include the weathered and the fractured rocks. However, other formations such as gravel layer may serve as underground water bearing layer. The aquifer thickness map was produced from the interpreted data of the weathered/fractured layer thicknesses at fifty one (51) points along all the locations of the fifty one (51) profiles within the study area at a contour interval of 5m. The map (Figure4) show the variation of aquifer thickness from one place to another. The aquifer thickness varies from 1 to 90m with an average of 28m.

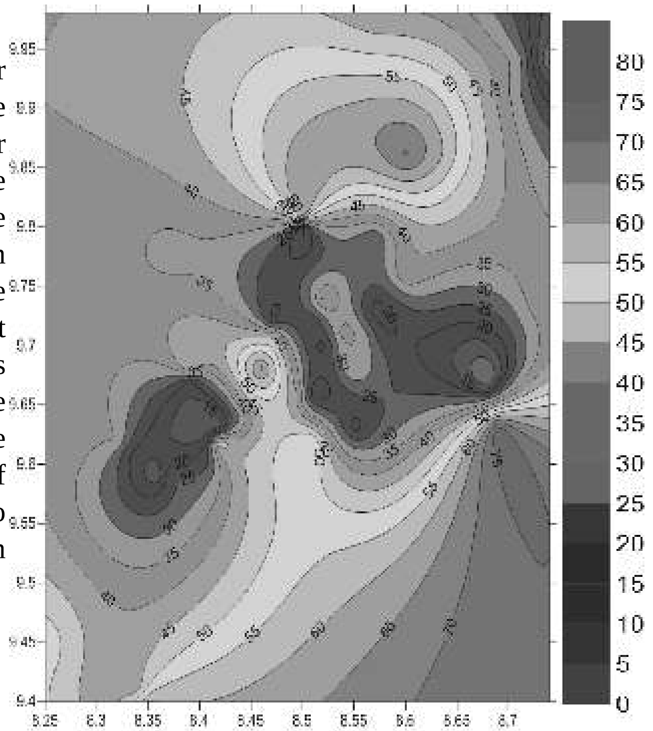

Figure4: Aquifer thickness map of the Area

DEPTH TO BASEMENT MAP

The depth to basement contour map for the study area is shown in Figure 5. The map was produced from the interpreted depth to fresh basement at fifty one (51) VES station along all the fifty one (51) profiles. This map gave a good picture of the basement topography in the area and the direction of groundwater flow. The map shows that the basement topography is rugged or undulating being deeper at some points and shallower at other points. The depth to basement ranges from 10m to 90m. The map also reveals a linear structure which trends in the NW-SE direction. This structure suggests a basement depression. The aquifer thickness and depth to basement maps correlate as the low thickness values correspond to areas of shallow basement. The larger thickness values correlate with the basement depressions.

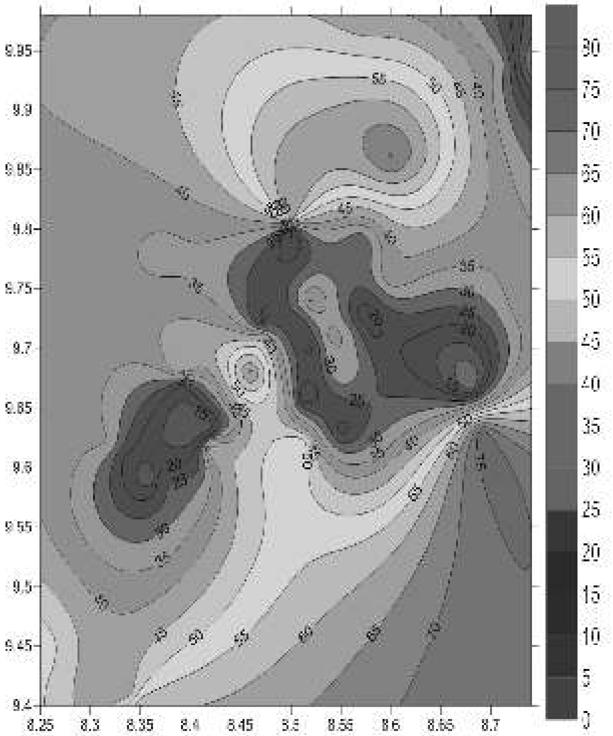

Figure5: Depth to basement map of the Area

CONCLUSION

The Depth to basement map shows that the basement topography is rugged or undulating being deeper at some points and shallower at other points. The depth to basement ranges from 10m to 90m. The map also reveals a linear structure which trends in the NW-SE direction. The Aquifer Thickness map shows the variation of aquifer thickness from one place to another. The aquifer thickness varies from 1 to 90m with an average of 28m. The resistivity values of the top soil vary between 50 to 1400 ohm-m. The higher resistivity values are noticed around Kaura town, Manchok and Fadan Atakar.

REFERENCES

Afuwai, G. C. (2013). Understanding the basics of Electrical Resistivity Geophysical Survey. Lambert Academic Publishing.

Afuwai G.C. and Lawal K.M. (2013). Interpretation of Vertical Electrical Sounding Points around two boreholes at Samaru College of Agriculture ABU, Zaria-Nigeria. Scholars Research Library, Archives of Physics Research. 4(5). 49-54.

Afuwai G. C. and Yusuf A. B (2018). Aeromagnetic Interpretation Showing Influence of Basalts to Borehole Failure over Kaura Area of Kaduna State, North-Western Nigeria. Journal of Nigerian Association of Mathematical Physics. Vol 44. January 2018. Pp 401-408

Alan E. M. And Aftab M. K. (2000). Looking into the Earth: An introduction to geological geophysics. *Cambridge University press*, 102-117.

Nuhu G.O. (2009). Geology and Mineral resources of Nigeria.

Grant FS, West GF (1965). Interpretation Theory in Applied Geophysics. McGraw-Hill, New York.

Telford, W.M., Geldart L.P., and Sheriff R.E. (1990). Applied Geophysic. Cambridge U.P., Cambridge. Pp 23-45.

Yanet, L.J. (2012). Assessment of groundwater potentials in Kaura and its Environs parts of Sheets 167 Se And 168 Sw Kaduna State Nigeria. Unpublished M.Sc thesis, Department of geology, Ahmadu Bello University, Zaria.

EFFECTS OF DAILY TEMPERATURE, SOLAR FLUX AND RELATIVE HUMIDITY ON THE PERFORMANCE OF CADMIUM TELLURIDE SOLAR CELL IN EDE TOWN OF OSUN STATE NIGERIA

ABSTRACT

This study investigates the effect of environmental parameters (temperature, solar flux and relative humidity) on the performance of the CdTe PV module in Ede, Osun State, Nigeria. A 3W cadmium telluride PV module solar cell was used. Solar flux, temperature, relative humidity, and current and voltage were measured using LX 9621 digital luxmeter, digital thermometer, HIH-4030 relative humidity sensor respectively. A 94% positive correlation between the solar flux and efficiency was obtained, which indicates that the efficiency of solar cell increases with increase in the solar flux. Meanwhile, a negative correlation of magnitude -0.38 was obtained between relative humidity and efficiency, showing how drastic it affects the performance of the cell. Results showed a decrease in the power output of the panel up to about 30% at high level of humidity. An increase in solar panel temperature from 31.26°C to 39.16°C corresponds to an increase in efficiency from 4% to 59%. Our results show that solar flux and solar panel temperature play a vital role in the performance of the efficiency of cadmium telluride solar cell, while a humid environment tends to reduce the efficiency drastically.

Introduction